UNIVERSIDADE FEDERAL DE SANTA CATARINA

CAMPUS FLORIANÓPOLIS / CAMPUS TECNOLÓGICO - CTC

PROGRAMA DE PÓS-GRADUAÇÃO EM CIÊNCIA E ENGENHARIA DE MATERIAIS

Heloisa Gonçalves Campos

Título: Effect of processing parameters on inverse alumina opal photonic crystals produced by atomic layer deposition

Florianópolis

2020

Heloisa Gonçalves Campos

Título: Effect of processing parameters on inverse alumina opal photonic crystals produced by atomic layer deposition

Dissertação/Tese submetida ao Programa de Pós Graduação em Ciência e Engenharia de Materiais da Universidade Federal de Santa Catarina para a obtenção do título de doutora em Ciência e Engenharia de Materiais

Orientador: Prof. Dr. Dachamir Hotza/UFSC

Coorientador: Kaline P. Furlan/ TUHH

Rolf Janssen/ TUHH

Florianópolis

2020

Ficha de identificação da obra elaborada pelo autor,
através do Programa de Geração Automática da Biblioteca Universitária da UFSC.

Campos, Heloisa
Effect of processing parameters on inverse alumina opal photonic crystals produced by atomic layer deposition / Heloisa Campos ; orientador, Dachamir Hotza, coorientador, Rolf Janssen, 2020.
97 p.

Tese (doutorado) - Universidade Federal de Santa Catarina, Centro Tecnológico, Programa de Pós-Graduação em Ciência e Engenharia de Materiais, Florianópolis, 2020.

Inclui referências.

1. Ciência e Engenharia de Materiais. 2. Cristal Fotônico Inverso. 3. Estabilidade Térmica. 4. ALD. 5. Alumina. I. Hotza, Dachamir. II. Janssen, Rolf. III. Universidade Federal de Santa Catarina. Programa de Pós Graduação em Ciência e Engenharia de Materiais. IV. Título.

Heloisa Gonçalves Campos

Título: Effect of processing parameters on inverse alumina opal photonic crystals produced by atomic layer deposition

O presente trabalho em nível de doutorado foi avaliado e aprovado por banca examinadora composta pelos seguintes membros:

Prof. Dr. Vânia Caldas de Sousa
Instituição UFRGS

Prof. Dr. Andre Avelino Pasa
Instituição UFSC

Prof. Dr. João Batista Rodrigues Neto
Instituição UFSC

Certificamos que esta é a **versão original e final** do trabalho de conclusão que foi julgado adequado para obtenção do título de doutor em Ciência e Engenharia de Materiais.

Documento assinado digitalmente
Guilherme Mariz de Oliveira Barra
Data: 11/08/2020 12:27:19-0300
CPF: 178.718.428-54

Coordenação do Programa de Pós-Graduação

Documento assinado digitalmente
Dachamir Hotza
Data: 03/08/2020 15:10:58-0300
CPF: 495.235.039-87

Prof. Dr. Dachamir Hotza
Orientador

Florianópolis, 2020.

Este trabalho é dedicado à minha amada família, e marido.

Acknowledgements

First and foremost, I would like to thank God for giving me the strength and encouragement especially during all the challenging moments in completing this thesis.

I would like to express my special appreciation and thanks to my advisors Prof. Dachamir Hotza, Dr Kaline P. Furlan and Dr. Rolf Janssen for their motivation, patience and immense knowledge that they kindly shared with me. Their guidance, suggestions and constructive criticism helped me in all the time of research and writing of this thesis.

I´m also grateful to the colleagues and the complete team of Hamburg University of Technology, TUHH (Technische Universität Hamburg-Harburg) for all help and support during the internship in the Institute of Advanced Ceramics at the Hamburg University of Technology, TUHH.

I would like to thank to the Brazilian funding agencies CAPES and to the Graduate Program on Materials Science and Engineering (PGMAT) for the financial support.

I am profoundly grateful to my family and friends for their continuous love and support that has been shown to me during my whole life. Without them none of this would be possible. They mean the world to me.

“One, remember to look up at the stars and not down at your feet. Two, never give up work. Work gives you meaning, and purpose and life is empty without it. Three, if you are lucky enough to find love, remember it is there and don't throw it away.”

Stephen Hawking

ABSTRACT

A correlation between the processing parameters and the structural thermal stability of inverse alumina opal photonic crystals produced by atomic layer deposition (ALD) was investigated. Polystyrene (PS) direct opals were deposited on sapphire through vertical colloidal deposition (VCD) using different combinations of parameters during self-assembly: polystyrene (PS) concentration, evaporation temperature and relative humidity. The templates formed by polystyrene direct opals (PS) were infiltrated with alumina by atomic layer deposition (ALD). The polymeric template was removed by heat treatment at 500 °C for 30 min (burn out) forming a macroporous alumina material. In order to investigate the structural thermal stability of the inverse alumina opals, the samples were thermally treated at 1400 °C for 4 h and 200 h. The characterization of the resulting samples was performed using Scanning Electron Microscopy (SEM), Transmission Electron Microscopy (TEM), Selected Area Electron Diffraction (SAED) Visible Ultraviolet Spectroscopy (UV-Vis) and image analysis (ImageJ). The combination: 1.5 mg/ml (PS concentration), 40 °C (evaporation temperature) and 70% (relative humidity) was the one that generated better results in the organizational sense and in the area occupied by unintentional defects. These conditions confered to these materials a vast number of potential applications as in solar cells, lasers and various optical and electronic equipment.

Keywords: VCD; Thermal stability; Inverse Photonic Crystal; ALD; Alumina, Processing parameters, Heat treatment

RESUMO

Uma correlação entre os parâmetros de processamento e a estabilidade térmica estrutural de opalas inversas de alumina produzidas por *atomic layer deposition* (ALD) foi investigada. Opalas de poliestireno (PS) foram depositadas em safira através de *vertical colloidal deposition* (VCD) utilizando diferentes combinações de parâmetros durante o *self-assembly*: concentração de poliestireno (PS), temperatura de evaporação e umidade relativa. Os *templates* formados pelas opalas de poliestireno (PS) foram infiltrados com alumina por meio da técnica *atomic layer deposition* (ALD). O *template* polimérico foi eliminado por tratamento térmico a 500 °C por 30 min (*burning out*) formando um material macroporoso de alumina. Com o objetivo de investigar a estabilidade térmica estrutural das opalas inversas de alumina, as amostras tratadas termicamente a 1400 °C por 4 h e 200 h. A caracterização das amostras resultantes foi realizada através das técnicas de Microscopia Eletrônica de Varredura (SEM), Microscopia Eletrônica de Transmissão (TEM), difração de área selecionada (SAED), espectroscopia Visível Ultravioleta (UV-Vis) e análise de imagem (ImageJ). A combinação 1.5 mg/ml (concentração de PS), 40 °C (temperatura de evaporação) e 70% (umidade relativa) foi a que gerou melhores resultados no sentido organizacional e de área ocupada por defeitos não intencionais. Essas condições conferem a esses materiais um vasto número de potenciais aplicações como em células solares, *lasers* e diversos equipamentos opticoeletrônicos.

***Palavras-Chave*:** VCD; Estabilidade térmica; Cristal Fotônico Inverso; ALD; Alumina, Parâmetros de processamento, Tratamento térmico.

RESUMO EXPANDIDO

Introdução

Uma correlação entre os parâmetros de processamento e a estabilidade térmica estrutural de opalas inversas de alumina produzidas por *atomic layer deposition* (ALD) foi investigada. Opalas de poliestireno (PS) foram depositadas em safira através de *vertical colloidal deposition* (VCD) utilizando diferentes combinações de parâmetros durante o *self-assembly*: concentração de poliestireno (PS), temperatura de evaporação e umidade relativa. Os *templates* formados pelas opalas de poliestireno (PS) foram infiltrados com alumina por meio da técnica *atomic layer deposition* (ALD). O *template* polimérico foi eliminado por tratamento térmico a 500 ° C por 30 min (*burning out*) formando um material macroporoso de alumina. Com o objetivo de investigar a estabilidade térmica estrutural das opalas inversas de alumina, as amostras tratadas termicamente a 1400 °C por 4 h e 200 h. A caracterização das amostras resultantes foi realizada através das técnicas de Microscopia Eletrônica de Varredura (SEM), Microscopia Eletrônica de Transmissão (TEM), difração de área selecionada (SAED), espectroscopia Visível Ultravioleta (UV-Vis) e análise de imagem (ImageJ). A combinação 1.5 mg/ml (concentração de PS), 40 °C (temperatura de evaporação) e 70% (umidade relativa) foi a que gerou melhores resultados no sentido organizacional e de área ocupada por defeitos não intencionais. Essas condições conferem a esses materiais um vasto número de potenciais aplicações como em células solares, lasers e diversos equipamentos optoeletrônicos.

Objetivos

O objetivo principal desta tese foi analisar e compreender os efeitos dos parâmetros de processamento na qualidade de cristais fotônicos tridimensionais formados por opalas inversas de alumina.

O processo de fabricação escolhido como objeto de estudo foi *atomic layer deposition* (ALD) devido à alta flexibilidade, e inúmeros benefícios já descritos na literatura. Diversas aplicações tecnológicas para cristais fotônicos tridimensionais formados por opalas inversas de alumina são possíveis apenas após tratamento térmico a altas temperaturas. Por esse motivo, dentre os objetivos deste trabalho está, também, a análise das propriedades físicas e mecânicas dos cristais fotônicos tridimensionais formados por opalas inversas de alumina produzidos em relação a temperatura e tempo de sinterização.

Metodologia

Partículas monodispersas de poliestireno (PS) (Microparticles GmbH), com diâmetro de 0,76±0,02 μm, foram depositadas em substratos de safira (25×30×0,53 mm, Crystec GmbH). A deposição das opalas de poliestireno foi realizada através do método de *Vertical Convective Self-Assembly* (VCSA) em uma câmara de umidade controlada (HCP 108, Memmert GmbH) por 120 h, ou até a evaporação completa do solvente usando béqueres de Teflon contendo suspensões PS em água deionizada. O ângulo entre o substrato e a base do copo foi entre 84° e 81°.

Os filmes finos de cristais coloidais foram obtidos por evaporação controlada (temperatura e umidade relativa) do solvente de diferentes concentrações de suspensões de PS (1 mg/ml, 1,5 mg/ml, 2

mg/ml), temperatura (40 °C, 55 °C, 80 °C) e umidade relativa (RH - 45%, 70%, 90%).

Após a deposição dos filmes por *self-assembly*, a espessura e estrutura dos cristais fotônicos foram avaliadas através de microscopia eletrônica de varredura (MEV, Leo-1530). Os defeitos estruturais foram analisados através de um programa de imagem (ImageJ, 1.51p22). Pelo menos 20 imagens de MEV (aumento de 500×) foram utilizadas para a análise de cada amostra. Para a eliminação do ruído (derivados das áreas escuras entre as esferas) foi utilizado filtro gaussiano. Após a binarização, os defeitos foram avaliados usando a ferramenta de *threshold*.

A infiltração de alumina nos substratos de safira (previamente depositados com opalas de poliestireno) foi realizada através do método *Atomic Layer Deposition* (ALD) usando os precursores trimetilalumínio (TMA, Sigma Aldrich) e água deionizada em um reator (Savannah 100, Ultratech, Cambridge Nanotech) a 95 °C. O ciclo foi realizado no modo de exposição (0,2/60/90 s) com nitrogênio como gás de purga (30 cm^3/min). Após ALD, o molde polimérico foi calcinado ao ar a 500 °C por 30 min, gerando a estrutura de cristal fotônico de opala inversa.

A resposta óptica dos cristais fotônicos de opala direta e inversa foi avaliada por medições de refletância especular (espectrômetro UV-vis-NIR, Perkin-Elmer, Lambda 1050) de 900 a 1850 nm e em um ângulo de incidência de 8°.

Após ALD, o molde polimérico foi queimado ao ar em um forno mufla a 500 °C por 30 min, produzindo cristais fotônicos de alumina inversa. As opalas inversas foram tratadas termicamente no ar em um forno mufla a uma taxa de aquecimento de 5 °C/min até que a temperatura e o tempo de permanência desejados fossem alcançados. O processo de sinterização foi executado a 1400 °C por 4 e 200 h. Após cada tratamento térmico, as morfologias das estruturas 3D resultantes foram examinadas por microscopia eletrônica de varredura (SEM, Zeiss Supra 55VP). Para as amostras tratadas a 1400 °C por 200 h e a estrutura 3D produzida com 55 °C e 70% (temperatura de evaporação e umidade relativa respectivamente) e tratadas termicamente a 1400 °C por 4 h, partes das amostras foram trituradas e dispersas em etanol por ultrassom e transferidos para uma grade revestida de carbono para geração de imagens TEM e área de tração eletrônica (SAED) (TEM, Jeol JEM-2000FX-II). Além disso, para essas amostras, as imagens TEM foram usadas para estimar o tamanho dos grãos.

Resultados e Discussão

Cristais fotônicos de opalas diretas de poliestireno foram *self-assembled* em substratos de safira por deposição vertical. A quantidade de defeitos nos cristais fotônicos diretos aumentou com a concentração de PS e a temperatura de evaporação e reduziu com a umidade relativa até um valor limite no qual o *self-assembly* falhou. A espessura também foi afetada por esses parâmetros. A capacidade de refletância resultante dos cristais fotônicos de opala direta e inversa foi essencialmente afetada pelos parâmetros de *self-assembly*. Embora o ALD e a sinterização do molde polimérico realizados a 500 °C tenham introduzido alguns defeitos adicionais e/ou defeitos preexistentes ampliados nas estruturas, o processo de *self-assembly* pode ser considerado o fator-chave que influencia o intervalo de banda fotônica resultante e a capacidade de refletância. Em relação ao desempenho dos cristais fotônicos de opala inversa de cerâmica, os parâmetros ótimos para a

automontagem relacionados à menor densidade de defeitos e à adesão do substrato foram 40 °C, 70% de UR e 1,5 mg/ml de concentração inicial da suspensão.

Os cristais fotônicos de opala inversa de alumina produzidos em todas as condições de *self-assembly* testadas são termicamente estáveis a altas temperaturas, como 1400 ° C por pelo menos 4 h, mas não após 200 h. Os parâmetros de processamento não parecem ter uma forte influência sobre a estabilidade térmica, como o material escolhido, neste caso, a alumina. No entanto, os efeitos dos parâmetros de *self-assembly* pareceram ampliados pelo tratamento térmico. As amostras produzidas abaixo de 40 °C, 45% e 1,5 mg/ml e 80 °C, 70% e 1,5 mg/ml levaram a cristais fotônicos mais defeituosos quando comparadas com aquelas fabricadas sob 40 °C, 70% e 1,5 mg/ml e 55 °C, 70% e 1,5 mg/ml, esse efeito pode ser mais claro após o tratamento térmico a 1400 °C por 4 h. No entanto, após 200 h de sinterização a 1400 °C, todas as amostras colapsaram, o que significa que as amostras 3D resultantes não têm mais as propriedades estruturais que possuíam antes do tratamento térmico. Além disso, foram comparadas as vistas superior e cruzada, e observadas discrepâncias, principalmente nos cristais fotônicos produzidos a 40 °C, 70% e 1,5 mg/ml (parâmetros de *self-assembly*). Esse efeito pode ser explicado pela transmissão de calor em materiais altamente porosos que, após um certo tempo de sinterização, leva a uma temperatura mais alta na superfície da amostra do que em seu interior; porém, esse fenômeno exige mais investigações. O tamanho de grão dos cristais fotônicos de opala de alumina inversa obtidos também foi estimado usando TEM e aplicando o software ImageJ para medir os grãos: 1,0±0,2 μm foi a média para as amostras tratadas termicamente até 1400 °C por 4 h; e 1,6±0,3 μm após 200 h. Nesse caso, o material (alumina) e o tempo de espera por sinterização (4 e 200 h) mostraram ter uma forte influência, mas não os parâmetros de processamento testados. A cristalinidade das amostras produzidas com 55 °C, 70% e 1,5 mg/ml e sinterizadas a 1400 °C por 4 h e aquelas fabricadas com todos os parâmetros de processamento testados (40 °C, 45%, 1,5 mg/ml; 40 °C, 70%; 1,5 mg/ml a 55 °C, 70%, 1,5 mg/ml e 80 °C, 70%, 1,5 mg/ml) tratados termicamente a 1400 °C por 200 h tiveram sua cristalinidade avaliada por SAED técnica e aplicação de software (CrysTBox 1.10). Todas as amostras apresentaram uma única estrutura cristalina com padrões típicos de α-alumina SAED, independentemente de parâmetros de processamento ou tempo de sinterização.

Considerações finais

As combinações dos parâmetros de processamento mostraram ter uma grande influência na ordem dos cristais fotônicos. A manipulação de parâmetros de automontagem pode ser usada para produzir não apenas cristais fotônicos, mas também vidros fotônicos, que também são materiais muito investigados, devido às suas possíveis aplicações.

O estudo da estabilidade térmica a altas temperaturas foi realizado para cristais fotônicos de opalas inversas de alumina. Por um curto período (4 h), as estruturas permaneceram estáveis, mas não por um longo período (200 h). Com o objetivo de obter cristais fotônicos 3D com maior estabilidade térmica, novos materiais devem ser testados. Compósitos com alumina e céria ou titânia, devido às suas propriedades mecânicas, podem ser algumas opções. Além disso, temperaturas mais altas podem ser testadas e possibilitar um número maior de aplicações para esses materiais.

Considera-se ainda o potencial demonstrado pelos resultados da nanoindentação, ao avaliar a estabilidade mecânica das estruturas 3D inversas para correlacioná-la com os parâmetros de

processamento. No entanto, seria importante uma investigação adicional dos dados. Uma modelagem matemática que permita obter resultados teóricos para essas propriedades e parâmetros pode ser feita com o objetivo de fornecer resultados mais precisos e permitir o projeto de estruturas 3D com um comportamento mecânico específico.

Palavras-Chave: *Self-assembly*, materiais fotônicos, estruturas tridimensionais, estabilidade térmica, alumina, ALD, propriedades ópticas.

LIST OF TABLES

LIST OF EQUATIONS

LIST OF FIGURES

LIST OF ABBREVIATIONS

ALD	=	Atomic Layer Deposition
CVD	=	Chemical Vapor Deposition
DOM	=	Three-Dimensional Macroporous
FIB		Focused Ion Beam
GI	=	Grazing Incidence
HTPS		High Temperature Photonic Structure
JCPDS	=	Joint Committee on Powder Diffraction
PBG	=	Photonic Bandgap
PMMA	=	Polymethylmethacrylate
PS	=	Polystyrene
SAED		Selected Area Electron Diffraction
SEM	=	Scanning Electron Microscopy
TBC		Thermal Barrier Coating
TEM		Transmission Electron Microscopy
TMA	=	Trimethylaluminum
UV	=	Ultraviolet
XRD	=	X-Ray Diffraction

Summary

1 INTRODUCTION

An optimal design for high-temperature photonic structure is desired. Ceramic thermal barrier coatings for gas turbines, and selective emitters for thermophotovoltaic purposes, materials and fabrication methods have been investigated.[1,2] It has an ecological and practical motivation, the increase of efficiency and a significant improvement of lifetime of gas turbines. For such applications, photonic crystals are required to operate at temperatures up to 1000 °C or even higher.[1] Microstructural, chemical or phase changes may not occur in photonic crystals exposed to high temperatures for a prolonged period. [2]

For those applications, high quality photonic crystals are needed. It means that the influence of imperfections such as cracks, disordering and vacancies must be well understood. The production of multilayer photonic crystals can be very challenging in order to fabricate a defect free photonic crystal.[3–5] A wide number of photonic crystals fabrication methods are available, such as self-assembly, lithographic and holographic techniques. Self-assembly is the most feasible method, which can be reached by vertical deposition, spin coating, gravity sedimentation and many other ways. Due to the possibility of controlling the processing parameters, which may lead to a superior quality large scale photonic crystal, vertical deposition self-assembly is the most used technique.[6]

Taking this into account, polystyrene spheres were assembled on sapphire substrates via vertical deposition self-assembly. A systematic study of self-assembly parameters, namely polystyrene suspension concentration, evaporation temperature and relative humidity was carried out. Afterwards, the polystyrene opal photonic crystals were filled with amorphous alumina by atomic layer deposition (ALD) and the polymeric template was eliminated by a heat treatment (burn-out at 500 °C, 30 min). The 3D structures formed before and after the burn-out were evaluated and compared in the aim of finding a correlation of the ceramic inverse photonic crystals performance and the processing parameters used during the self-assembly of the polystyrene spheres.

Thermal stability at high temperatures, like previously cited, is a critical issue of photonic crystals design. The retention of the 3D mesostructures at high temperatures remains a significant challenge. Therefore, the 3D inverse alumina opal photonic crystals structural stability after elevated temperatures heat treatments for prolonged periods was also investigated.

1.1 Objectives

1.1.1 Main Objective

The main objective is to understand the effect of processing parameters on the three-dimensional (3D) inverse alumina opal photonic crystals produced by atomic layer deposition (ALD) before and after heat treatment.

1.1.2 Specific Objectives

The specific objectives of this work are:

- Explain the influence of self-assembly parameters, such as evaporation temperature, relative humidity, and polystyrene concentration, on the polystyrene direct photonic crystals and

inverse alumina opals photonic crystals.

- Find a correlation between self-assembly parameters and the thermal stability of the produced 3-D structures.

- Explain the influence of heat treatment time and temperature on the inverse alumina opals photonic crystals.

- Achieve 3D high quality inverse alumina opal photonic crystals design parameters with high thermal stability to use in gas turbines.

2 LITERATURE REVIEW

2.1 Photonic Crystals Concept

Synthetic photonic crystals have been widely investigated and produced based on materials that are available in nature such as natural opals.[7] These materials were first proposed by John and Yablonovitch in the aim of comprehending optical principles.[8–10] The light is confined in the bulk material and the spontaneous emission is not allowed in a wide range of frequencies. Concepts of solid state physics, such as Maxwell equations and Block´s theorem are used to understand the photonic materials operation.[11]

The photonic crystals are periodically structured and possess photonic band gaps, which are frequency ranges in which it is not possible to the light to propagate through the structure.[12] The photonic band gap formation is similar to the electronic band gap. The periodicity of electric potentials and dielectric constants is the driving force of the electric band gap and photonic band gap respectively.[12,13] These crystals, artificially structured, have the ability to act on photons in optical devices, just as semiconductors act on electrons in electronic devices [14,15] These photonic structures allow the manipulation of visible light and other forms of electromagnetic radiation.

Photonic crystals are classified by the dimension of periodicity. These materials can be one, two or three dimensional (1D, 2D or 3D) photonic crystals, that are schematically illustrated in **Figure 1.**

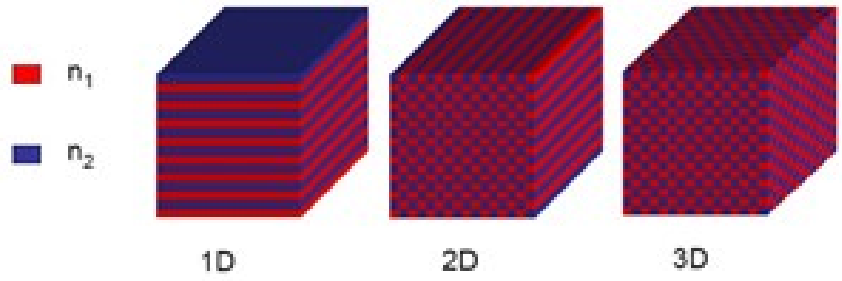

Figure 1. Schematic illustration of one, two and three-dimensional (1D, 2D and 3D) photonic crystals; n_1 and n_2 represent the different refractive indices of the constituent materials.[8]

One dimensional (1D) photonic crystal fabrication techniques are already well known and can be easily produced by alternated deposition of two materials. Besides, many assemblies and fabrication methods have been investigated for two and three-dimensional photonic crystals; nevertheless, these two last mentioned structures production remain a challenge.

Each of these types of photonic materials has specific photonic band gaps, which is a forbidden gap of photons. The light is not allowed to get inside the crystal and electrons cannot emit photons in

crystals interior.[16,17]

2.2 Photonic Crystals Applications

Due to their unique optical properties, photonic crystals have been deeply investigated in the past decades. Technological applications in numerous areas of science have been explored such as medicine, military defense, telecommunications, energy, agriculture, robotics, among others.

Celanovic et al.[18] investigated the optical characteristics of one and two-dimensional photonic crystals to be use as components of thermophotovoltaic (TPV) systems. One-dimensional photonic crystals were used as optical filters and two-dimensional ones were utilized as selective thermal emitters.

Cai et al.[19] investigated the progress that has been done in the development two-dimensional photonic crystals for chemical and biological detectors. Shen et al.[20] wrote a review about photonic crystals applications, one and 3D photonic crystals, more specifically. Due to its refractive index distribution in one direction, 1D photonic crystals are widely investigated and produced to be used as high-efficient refractor, chemical and physical sensors and so on. Shen et al.[20] also studied some typical 3D structures, fabrication methods and its remaining problems.

3D photonic crystals have refractive index periodicity in all three directions, and when these indexes are high enough, a full band gap can be formed. Moreover, the spontaneous emission and propagation of light can more easily controlled due to the photonic band gaps in three different directions. Because of this property, 3D photonic materials are considered one of the most potential materials for thermal barrier coatings (TBC), transfer of fuel energy into electricity and thermophotovoltaic cells (TPV).

The use of 3D photonic crystals has been studied for thermal barriers, which would be used in gas turbines. In this case, ceramic photonic crystals are specially considered due to ceramics properties such as chemical, physical, and thermal stability. Once the 3D photonic crystals would have to have a high thermal stability, these materials are called High Temperature Photonic Structures (HTPS).[1] Yablonovivitch et al.[21] studied silicon emitters of infrared radiation after their very first work with 3D photonic crystals. Nevertheless, the fabrication of defect free 3D photonic crystals with high thermal stability remains challenging.

2.3 Production Methods

Most of the studies done so far have been focused on one and two-dimensional photonic crystals, due to its easy production. Nevertheless, 1D and 2D photonic materials cannot exhibit a photonic band gap in a definite direction. Therefore, in the aim of producing an efficient and functional optical device using photonic crystals, 3D photonic crystals are required. [13,15,22] Besides, to enhance a 3D photonic band gap, ceramic materials like aluminum and titanium dioxide have been proposed as constituent materials for 3D photonic crystals by some researchers such as Dyachenko et al.[2], Furlan et al.[5], and Sung Park et al.[23]. In those works, a method has been proposed, in which, these a polymeric template is filled by ceramic materials layer by layer by atomic layer deposition (ALD). The objective of the authors was to combine the advantages of ALD and the ceramics properties leading to a material with high thermal stability and minimal thickness variation even after many

successive high temperature heat treatments. These are very important characteristics to produce thermal barriers coatings for gas turbines, one of the main objectives of this research. [2,5,23]

Self-assembly and etching are two of the most used manufacturing techniques of three-dimensional photonic crystals.[13,15,22,23] In the self-assembly method, a polymer-based template is produced, filled with a high refractive index material, normally done by chemical vapor deposition (CVD) or atomic layer deposition (ALD). Then, the polymeric template is eliminated by heat treatment or chemical etching.[6,24–26] In etching, a predetermined part is produced by a photo stimulated process; afterwards, an etching procedure is used to remove the unnecessary part. Chemical etching is normally used to fabricate 2D photonic crystals. In the aim of fabricating 3D photonic crystals, a complex process is applied, such as electron beam lithography, holography, multiple beam interference, wafer diffusion or two-photon polymerization.[23]

2.3.1 Self-assembly

Self-assembly can be defined as the spontaneous organization of materials by noncovalent interactions (Van der Waals forces, hydrogen bonding, electrostatic forces, and capillary forces). This self-organization of the materials normally results into periodic cubic (face cubic centered), hexagonal (hexagonal close packed) structures or a mixture of both.

Self-assembly is a widely used technique in the production of three-dimensional photonic crystals because of their relative simplicity of the process and the possibility to obtain a full photonic band gap. This method is based on assemble monodispersed size microspheres on a specific substrate by applying conditions and parameters in which these spheres will be able to arrange themselves periodically.

2.3.2 Vertical Deposition Self-Assembly

Dislocations, vacancies and stacking faults are typical defects present in photonic crystals structures. Nevertheless, it is well known that high quality crystals are necessary for optical and other technological applications such as thermal barrier coatings and thermal emitters.[1]

Self-assembly method is the most used route to produce two and three-dimensional photonic crystals. Gravity sedimentation, electrophoresis, spin coating, crystallization and vertical deposition are known as techniques to achieve the self-assembly.[6] Vertical deposition method is the most widely used in comparison to the other methods, due to the possibly of easy parameters controlling, which may lead to a superior quality and controllable thickness of photonic crystals produced by this process.[6,22,24] Besides, normally the vertical deposition technique leads to the formation of an FCC (face centered cubic) structure. However, even the morphology and geometry of the photonic material can be design by adjusting the self-assembly parameters.[6,25]

Further, in this thesis, the effect of some of self-assembly parameters – such as polymer concentration, humidity – on the photonic crystals' morphology, type and amount of unintentional defects will be investigated and discussed.

The vertical deposition method is based on a controlled evaporation of a suspension prepared with a specific concentration of polymers spheres, such as polystyrene. The evaporation control can be done by using a humidity chamber, in which the evaporation temperature and relative humidity can be set. In some chambers, it is also possible to control the system pressure. As long the suspension solvent is being evaporated the polymeric spheres are being deposited on the substrate. **(Figure 2)**

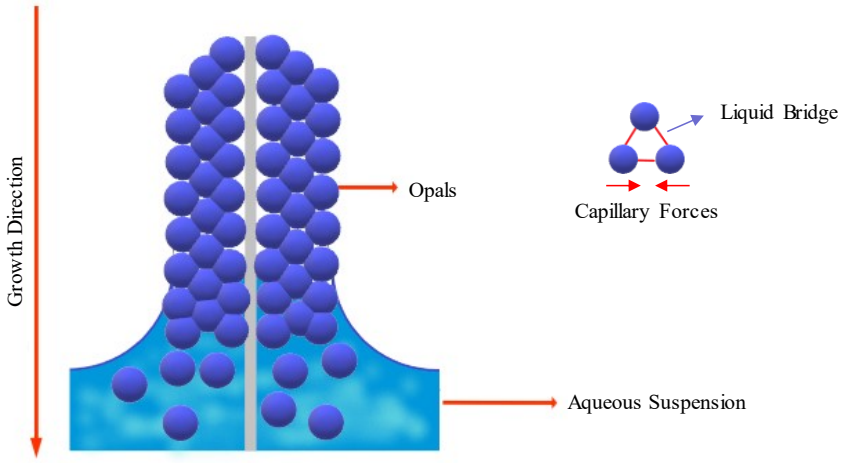

Figure 2. Schematic illustration of the vertical deposition technique for growth of opals. The spheres are assembled into FCC lattice at the interface formed between water-air-substrate. The capillary forces that occur between the polymer spheres and the liquid bridges formed among the spheres.

By adopting this technique, some defects may occur, stacking faults and macroscopic cracks, for example. Such imperfections disturb the light propagation through the photonic crystal.

Small differences between the free energy correspondent to the FCC and HCP geometries may lead to the formation of stacking faults. The appearance of macroscopic cracks, normally, is due to the contraction of the colloidal structure because of solvent evaporation. The evaporation rate of the suspension solvent is a well-known factor, which may lead to a high- or poor-quality photonic crystal. Some self-assembly parameters – such as evaporation temperature – showed to be a key factor for evaporation rate. Too high temperatures, because of the increase of particles kinetic energy, may cause a disordered structure instead a defect free photonic crystal. Contrariwise, too low temperature could affect the self-assembly process time, turning it extremely long. In addition, other self-assembly parameters – such as polymer concentration, relative humidity, substrate type and suspension solvent – seem to have influence on the photonic crystals' quality. It means that it is important to understand the changes that may occur in the structures of the photonic crystals according to the manipulation of such parameters in the aim of obtaining a defect free high-quality photonic crystal. In this thesis, some of these parameters influence on the photonic crystals morphology and thickness were evaluated with the objective of reaching an optimum design of 3D photonic crystals, which could be used as a thermal barrier coating for gas turbines.

2.3.3 Defects in Photonic Crystals Produced by Self-Assembly

Colloidal crystals formed by evaporation induced methods may present imperfections on two scales, micro and macro defects. Stacking faults, vacancies and dislocations are examples of micro defects, while cracks and void bands are classified as macro defects, which have origin in meniscus dynamics motion during the solvent evaporation.[12]

The self-assembly and photonic crystals growing process occurs at the meniscus region. Therefore, it is possible to say that the quality of the photonic crystals depends on the conditions at the meniscus area. There are two limitations of the meniscus region: the substrate and the liquid vapor phase. The liquid-vapor phase is deformable and moves as the solvent evaporates, depending on evaporation rate, while the substrate is solid and generally it is charged.[27] Capillary forces, which can be either repulsive or attractive depending on the colloids, are the driving forces of assembling the polymeric spheres together into FCC structure. This theory has been supported by Koh et al.[28], who studied the influence of the capillary forces by using aluminum and silicon substrates. They observed that more macroscopic defects were obtained using the aluminum substrate. However, these researches proved the influence of capillary forces on the formation of macro defects such as cracks. Another possible explanation has also been proposed: the divergence of thermal coefficient of the substrate and the photonic film deposited on it.[27,28] These cracks can be seen in the structure even with lower magnifications **(Figure 3).**

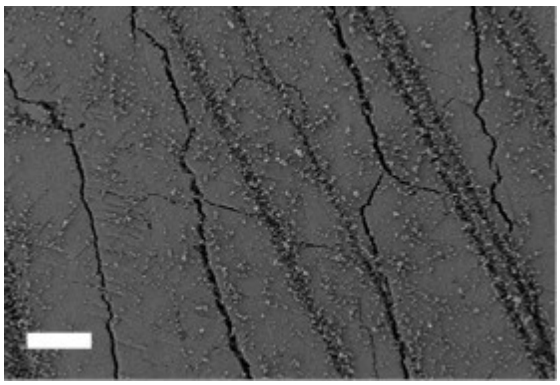

Figure 3. SEM image of cracks in a photonic crystal produced at 55 °C, 70%, 1.5 mg/ml (evaporation temperature, relative humidity and polystyrene concentration). The scale bar represents 10 μm.

Photonic crystals produced by induced evaporation self-assembly are generally composed by a structure with FCC configuration. Nevertheless, some micro defects such as stacking faults are present in almost every photonic crystal fabricated by self-assembly. These defects consist in the separation of the planes with FCC configuration by two planes hexagonal closed packed (HCP) and are considered a linear defect[29] (**Figure 4**). The results of Hilhorst et al.[29] have shown that the stacking faults are up to 5-10% of the photonic crystal structure. Therefore, it must be considered for future applications of self-assembled photonic crystals.

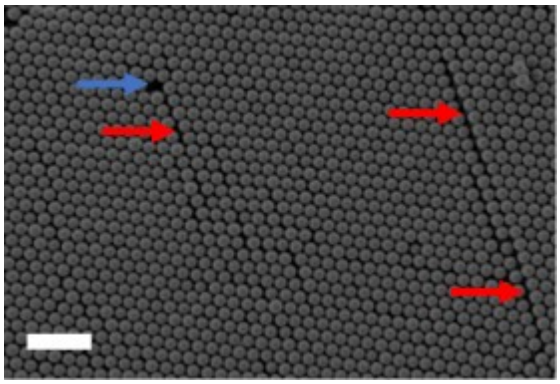

Figure 4. SEM image of stacking faults (pointed by red narrows) and vacancies (pointed by blue narrow) in a photonic crystal produced at 55 °C, 70%, 1.5 mg/ml (evaporation temperature, relative humidity, and polystyrene concentration). The scale bar represents 1 μm.

Another defect pointed in **Figure 4** is the vacancy. Classified as punctual defects, vacancies are the most common and studied defect in photonic crystals structures. It is thermodynamically expected (entropically favorable) to have some vacancies. [27]

$$C_v = A_o \exp\left(\frac{\Delta G_v}{kT}\right) \qquad \text{Equation 1}$$

As can be seen in $C_v = A_o \exp\left(\frac{\Delta G_v}{kT}\right)$ Equation 1 the concentration of vacancies has an exponential dependence on the temperature. C_v represents the vacancies concentration; A_o is a constant; ΔG_v is the vacancies formation energy; T is the evaporation temperature; and k is the rate constant.

The presence of some microscopic defects like vacancies and dislocations cannot be completely eliminated, because as previously analyzed, it is a thermodynamic issue. Dislocations (**Figure 5**) are also microscopic linear defects. The origin of such imperfections is during evaporation and they can lead to considerable damage on PBG, compromising the use of the material.[28]

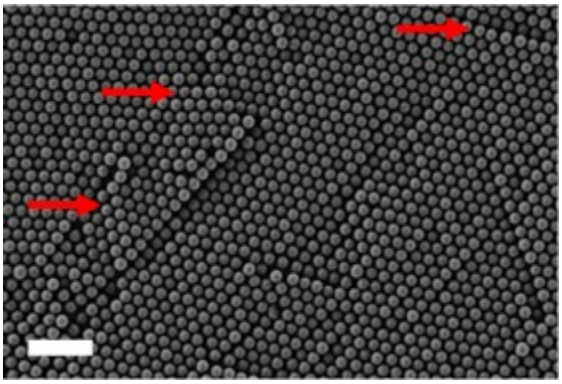

Figure 5. SEM image of dislocations in a photonic crystal produced at 80°C, 70%, 1.5 mg/ml (evaporation temperature, relative humidity, and polystyrene concentration). The scale bar represents 1 μm.

Therefore, to obtain applicable photonic bandgap materials, the effect of the defects on the PBG must be deeply investigated. Taking this into account, in this thesis, the effect of self-assembly parameters – such as evaporation temperature, relative humidity and polymer concentration – on the photonic crystals quality is studied in order to develop a self-assembly parameters combination, with which it is possible to achieve a high quality, thermal resistant photonic crystals.

2.3.4 Direct and Inverse Opals

To achieve photonic crystals with a full bandgap in a specific spectral region remains a considerable challenge. The major factors that establish a photonic bandgap are the refractive index contrast (ratio between the refractive indices of the constituent materials) and the filling fraction (percentage volume occupied by voids). Some methods are widely used to produce such materials, like lithographic techniques. Nevertheless, these approaches are expensive and time taking. Thick photonic crystals were not reachable so far.[30]

Self-assembly route is an alternative method to produce three-dimensional photonic structures with complete PBG. However, as it is possible to find in many researches, inverse opals present superior photonic bandgap (PBG) properties when compared to direct opals.[31–33] As inverse opals (

Figure 6c) are negative reproduction of direct opals (

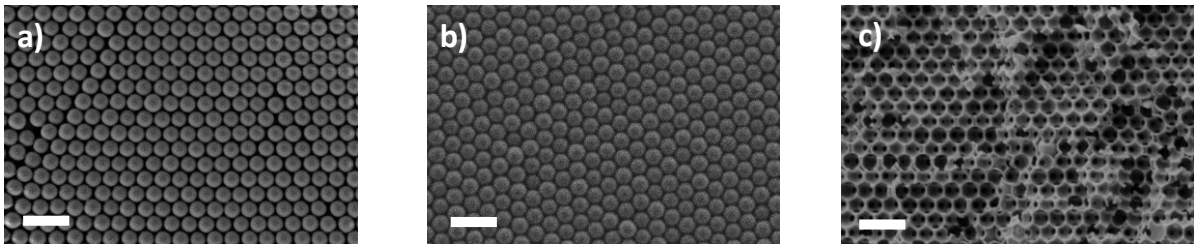

Figure 6a) with submicrometric voids bordered by high refractive index materials, such as alumina or titania. Because the inverse opals are the form that photonic crystals have their major technological applications, the production of such materials is a main goal of many researches.[30–33]

Figure 6. Images of (a) self-assembled polystyrene (PS) spheres on a sapphire substrate by vertical deposition self-assembly; (b) filled with alumina by atomic layer deposition (ALD); and (c) inverse alumina opal photonic crystal. The scale bars represent 1 μm.

Several approaches can be used to fabricate inverse opals. The direct opals template voids must be filled by a high refractive index material. Afterwards, the template must be removed by chemical etching or heat treatments. As filling techniques chemical vapor deposition (CVD)[34–36], atomic layer deposition (ALD)[5,23,37], floating or stacking[38,39] and spin coating[40] can be cited. Atomic layer

deposition is the most used, due to robustness and accurate thickness control of the produced photonic crystals. [5,23,37] ALD will be further discussed in more details in this thesis.

The last step of the inverse opals production is the template elimination. It can be performed using heat treatment or chemical etching. Chemical etching is normally used for metallic and silica templates. The problem about using this technique to polymeric templates is that chemical etching may increase the roughness of the structure and change the chemical constitution. By applying etching in polymeric templates, considerable modifications of the morphology and chemical properties of the structure may occur. Therefore, heat treatments are mostly applied for polymeric templates.[41]

Figure 6a presents a SEM image of self-assembled polystyrene (PS) spheres on a sapphire substrate via vertical deposition self-assembly. This PS template was filled with amorphous alumina by ALD (

Figure **6**-b). Afterwards, the polymeric template was eliminate using a heat treatment (burn-out at 500 °C, 30 min) leading to an inverse alumina opal photonic crystal. (

Figure 6c).

2.3.4.1 Atomic Layer Deposition

Atomic layer deposition (ALD) is a vapor phase method to layer thin films onto a substrate. The substrate is subjected to alternating precursors that do not overlap. The introduction of these materials is carried out sequentially. The ALD technique is based on saturated surface reactions, which means that in each alternate pulse, the precursor reacts with the surface until all reactive sites on the substrate have been saturated. A whole ALD cycle depends on the precursor surface interaction and nature. When a higher layer is required, multiple ALD cycles can be performed until the desired thickness have been reached.[42]

In Figure 7, a schematic illustration of an ALD cycle of alumina can be seen. In this case, the used precursors are trimethylaluminum (TMA) and water. TMA is dosed and adsorbed by reactive sites of the surface (step 1). Then, the excess of the precursor and the products of the reaction are purged out (step 2). Afterwards, a co-reactant, in this case water, is inserted into the chamber and reacts with TMA to form the desired material. In the situation presented in Figure 7, and in this thesis this material is alumina (step 3). Subsequently, the unreacted material and another reaction product are purged out (step 4).

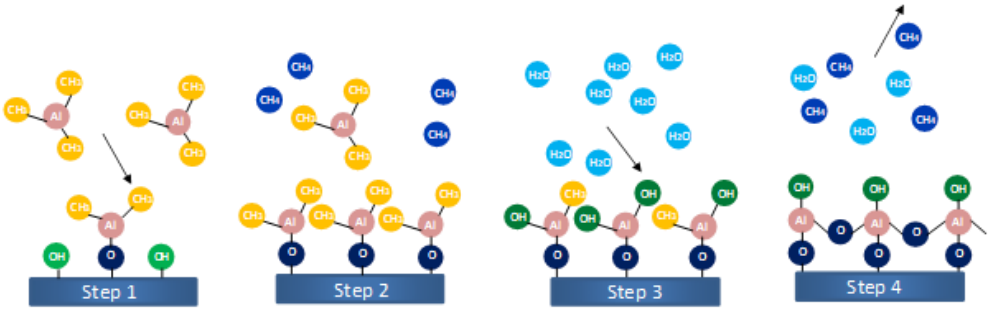

Figure 7. Schematic illustration of ALD technique procedure.

ALD has emerged as the main method for semiconductor micro and nanodevices such as tubes, and nanowires[120,121]. Atomic layer deposition is also the most adopted technology in complex nanostructured material surface modification.[120,122] These applications have similar demanding requirements, low gas permeability and poor electron leakage. Such requirements are accomplished due to ALD being a technique that leads to a continuous, pinhole free, and thickness controllable materials layers by means of self-limiting sequential surface reactions. [120–122]

In general, two self-limiting surface reactions occur sequentially depositing a binary compound film. As the surface sites number is limited, so is the number of surface species. The self-limiting characteristic of the two reactions allow the growth of numerous layers with an atomic scale level of control. This is one of ALD technique advantages; besides, it leads to an outstanding step coverage and conformal deposition on high aspect ratio structures due to the sensibility to the surface conditions .[120 123,124]

The ALD technique had its first studies published around 1970. Nevertheless, the terms used at that time were atomic layer epitaxy (ALE), molecular layering (ML), atomic layer chemical vapor deposition (ALCVD), or molecular layer epitaxy (MLE). ALD only started to be employed as a term during the 2000´s.[120–126] The fact of the layers growing not being epitaxial to the substrate, but adopting self-limiting sequential surface reactions made the ALE expression fall out of use. [127]

The pioneer of ALE was Tuomo Suntuola with a ZnS ALE system. His first patent regarding this subject came in 1977, and the first publication in 1980. Nevertheless, the first commercial ALE reactor was sold only in 1988.[120] Many previous reviews are focused on the use of ALD for nanotechnology and microelectronics[127–130]. Instead, in this review the intention is highlight the use of ALD on high performance photonic crystals production. Moreover, some key concepts and new directions of ALD technique are presented.

2.3.4.2 Photonic Crystals

Photonic crystals can be defined as structures with a periodic dielectric function modulated on a length scale according to the required wavelength of operation [131,132] The properties of the light can be modified by photonic crystals in the same way semiconductors can affect electrons. Photonic crystals can have what is called photonic band gaps (PBGs), which are frequency ranges where the light propagation is forbidden within the structure.[125,131,132] Plenty of devices that work making using

of this property have been identified such as semiconductors and photonic microdevices.

Light can travel within dielectric materials in a way greater velocity and carrying much more information than electrons do inside a metallic wire. Also, the bandwidth is significantly larger than in metals. A fiber-optic communication system is in an order of terahertz, while electronic systems of communications, such as telephone, are about just a few hundreds of kilohertz. In addition, the interaction between photons are poorer in relation of electrons´, which allows lower energy losses inside these systems.[126,131,132]

This property has been used in many devices' principles (waveguides, optical filters, drugs delivery system).[132,133] Nevertheless, the photonic crystals manufacturing remains a challenge. Many techniques such as lithography, layering and etching processes of photonic crystals fabrication have been explored to produce defective free two and three-dimensional photonic crystals in solid substrates. However, these are sophisticated techniques that requires expensive and large-scale equipment.[134,135] Atomic layer deposition (ALD), on the other hand, is a flexible and robust technique, which allows growth of a wide range of materials under extensive parameters combinations. [122,124,130,136]

Regarding to photonic crystals' manufacturing, it is well established that the photonic band gap is significantly affected by the quality of the void's infiltration with a higher dielectric constant material. ALD is a technique considered to have a high-filling fraction[136]. Therefore, ALD has been widely used in photonic crystals manufacturing.[130,137]

2.3.4.3 Alternative Manufacturing Techniques

Because of the development of technological applications in optical structures, thin film deposition methods have been widely studied and technologically advanced.[120,127,19]

All advanced applications – such as filters, lenses, anti-reflecting coatings, and drugs delivery – demand thin films with accurate thickness control, low defect density, and great adhesion with the substrate.[138–140] These mentioned properties rely on the chosen technique and the materials that are being deposited on the substrate.[140]

To be considered high quality thin films for nanophotonics, they must present high abrasion, thermal and chemical resistance, great adhesion and low defects density (cracks, holes)[141–143]. To manufacture optical coatings Physical Vapor Deposition (PVD) is widely used. This method is based on the deposition of a material in its vapor phase, result from its evaporation. PVD exhibits high deposition rate. Nevertheless, the previously mentioned desired properties are more likely to achieved using atomic layer deposition (ALD).[144–146]

ALD is one variation of chemical vapor deposition (CVD), which has been utilized in many applications. The main difference between these two techniques is that in ALD the precursor material pulses are led into the reactor once at time. Then some inert gas such as nitrogen or argon is used to purge the reactor chamber after each pulse of precursor material, which extracts from the chamber all the reaction´s by-products. The only materials that are left inside the reactor are the ones adsorbed on the substrate. Consequently, the film grows, and its thickness is determined by the number of

cycles, which is an extremely accurate control, in an atomic scale.

Another advantage of ALD method is that complex shaped high aspect ratio can be equally covered. The possibility of coating any sized and shaped structure employing ALD depends on the reactor chamber size only. ALD-Al_2O_3 [147]and ALD-TiO_2[148] were utilized to impregnate silica spheres. As a result of further investigations, the density of the produced films was higher when manufactured using ALD then other techniques. The hydrogen and H_2O fraction in these films were also lower comparing ALD to other methods.

In the current work, a 3D ALD-Al_2O_3 photonic crystal was produced and submitted to a heat treatment at 500 °C for 30 min (**Figure 8**). It was observed a continuous thickness, both in film and Al_2O_3 walls. What looks to be defects are, mostly, damages probably caused by the diamond pen, which was used to make the cut of the probe, so that it could be properly analyzed. These results also corroborate with the ones found on the literature. It was possible to observe a great uniformity on the 3D structure coverage and thickness.

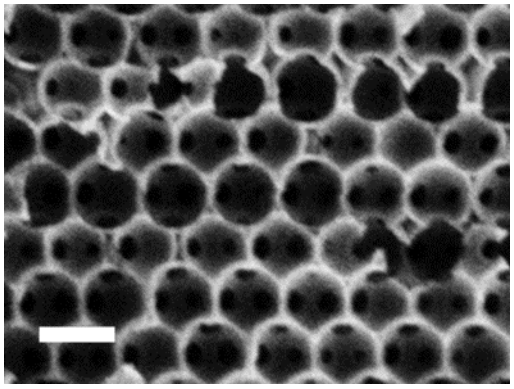

Figure 8. ALD-Al_2O_3 photonic crystals produced and submitted to a heat treatment at 500°C for 30 min. A PS spheres solution (1.5 mg/ml) dried at 55 °C, 70% and of RH was used to produce the direct opal photonic crystal. The scale bar represents 1 μm.

ALD-coated thin films have been playing a notable role in photonic crystals. This is because ALD promotes a low temperature growth, which is important, especially on polymer materials, to avoid their degradation during the filling process. Besides, ALD allows a wide range of precursor materials to be used. This gives the possibility to choose a material that is suitable with the substrate. Consequently, the structure will present better adhesion and low – or inexistent – damage to the substrate. The self-limiting reactions that occur during the ALD process confer a highly reproducible thickness after each ALD cycle.

2.3.4.4 ALD Temperature Increase

ALD cycles are performed under relative low temperatures (<350 °C). ALD temperature window is

a term used to refer to the appropriate temperature range for specific ALD processes.[149] Temperatures outside this window might result in slow reaction kinetics, which can lead to non-continuous material deposition on the substrate, poor growth rates, or even precursor condensation when the chosen temperature is lower than the recommended.[150–152] For higher temperatures than specified in the temperature window, a thermal decomposition or a fast desorption of the precursor may occur.[149] So, the ALD processes advantages can be achieved, so that it is appropriated to operate within the defined window temperature for each process. In the case of Al_2O_3-ALD, this range is between 180 and 200°C (**Figure 9**[153]).[127,149–151]

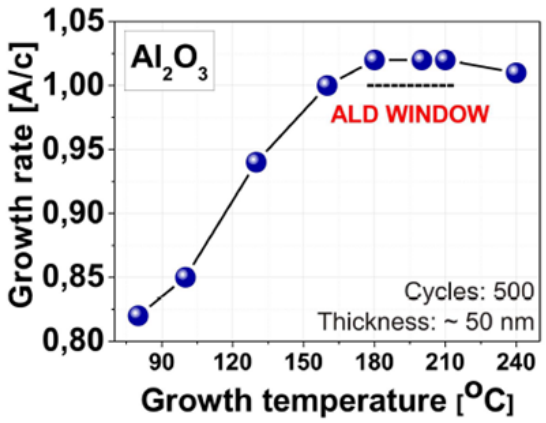

Figure 9. Graphic showing the experiment to define Al_2O_3-ALD temperature window. Adapted from Gierałtowska et al..[153]

Gierałtowska et al.[153] evaluate the role of some ALD parameters on the resulted thin film properties. As the temperature was pointed as one of the most crucial parameters in ALD processes, they performed numerous experiments to determine the ideal process temperature for Al_2O_3-ALD, as shown in Figure 2. According to Gierałtowska et al.[153], using the Al_2O_3-ALD window temperature (180–200 °C), they obtained a growth rate of 1.0 Å, against 0,8 Å in extreme low temperature (90°C).

2.3.4.5 Self-limiting Film Thickness

Another advantage of ALD is the thickness control and less interface roughness, when compared with different techniques such as CVD and PVD (ALD variations). The layer-by-layer deposition allows dictating the thin film thickness by the number of ALD cycles. The typical final thickness depends on the individual process. [120,122,124]

Because ALD has self-limiting reactions as a part of its process, the average roughness is, normally, lower than the observed in other methods. Nevertheless, due to different desired compositions, even ALD-coated thin films can present a higher or lower roughness. Moreover, the efficiency of the composition, roughness and thickness control relies on the volume and geometry of the reactor chamber. The higher the volume, the higher the time of precursors pulse and inert gases purge.[148,153]

It is possible to find in literature some experiments regarding ALD coated thin films. For the same

precursor and substrate, different results are likely to be observed.[154,155] This is due to the different reactors and parameters that were used. Besides, it was already published that when a very thin film is produced, its thickness and roughness are extremely hard to measure. Once again, the interaction between the produced film and the substrate plays a dominant role.[153]

Because of all mentioned ALD advantages, this method has been widely used in 2D and 3D photonic crystals production and has shown excellent results in technological applications such as catalysators[156], fuel cells[157], drug delivery[158], optical micro and nanodevices[159] among others.

2.3.4.6 Effect of Al_2O_3–ALD Coating on Photonic Applications

ALD can be performed using a wide range of materials. Nevertheless, ALD-Al_2O_3 photonic crystals have been one of the most extensively explored. There are some works in literature that emphasize the role of this material in photonic applications. In the sequence, there are the results of some of these researches with ALD-Al_2O_3 thin films for optical applications. Besides, because Al_2O_3 is a biomaterial, its use in biomedicine has been also deeply investigated.

Li, Cunin et al. [160] have studied ALD-Al_2O_3 thin films produced with different thickness and heat treated at diverse temperatures. Independent of the thickness, the roughness of the produced films was less than 1 nm. The effect of the films thickness on the refractive index was also evaluated by Li, Cunin et al. [160], and appeared to have a negative impact. Nonetheless, this effect seemed to disappear after all the tested heat treatments. This work features the possibility of using ALD parameters in order to obtain special materials for specific optical applications.

Low temperature (<33°C) ALD-Al_2O_3 growth in photonic crystals was studied by Groner, Fabreguette et al.[151] Despite the lower reaction kinetics, longer purge and pulses, this experiment highlights the use of lower temperatures to obtain films with even lower roughness. Such thin films can be used to avoid current, gases or any kind of leakage of other fluids, and for purposes where high dielectric constants are important, such as in fuel cells. Besides, it has shown to be an alternative method for thermally fragile materials. The films were tested and presented potential results for use in bottles insulation.

ALD-Al_2O_3 thin films were examined by Sechrist, Schwartz et al.[140] to evaluate the ALD- Al_2O_3 coating for photonic materials. To monitor the film, the wavelength of the Bragg peak reflection was used. It was observed a correlation between the film thickness and the Bragg peak wavelength. Sechrist, Schwartz et al.[140] and Li, Cunin et al. [160] works are highly comparable and seem to corroborate one with another, i.e., before annealing the ALD-Al_2O_3 thin films, their thickness increase seems to have a negative effect on the refractive index.

The main difference between the works of Sechrist, Schwartz et al.[140] and Li, Cunin et al. [160] is that the former compare the roughness presented by thin films coated using ALD technique and PECVD method, having a much lower roughness on the ALD- Al_2O_3 films.

Skoog, Elam et al. [161] wrote a review regarding the use of ALD coating for biomedical devices, biosensors, drug delivery devices and tissue engineering scaffold. The main reason of considering this technique for such purpose is its flexibility regarding precursor materials, process, temperature, and geometry. Biomaterials such as alumina and titania are between the most investigated for this kind of application.[162]

2.4 Heat Transfer in Porous Materials

Highly porous materials have attracted the attention for heat transfer controlling purposes, mostly as thermal barriers coatings for gas turbines or heat exchangers. For such applications, ceramics and metals are of more interest than polymers. Usually, polymers are unsuitable at extreme conditions, such as low or high temperatures, high gas pressures and irradiation fluxes. Nevertheless, even ceramic and metallic structures, under extreme environmental conditions, can have microstructural changes that may affect the heat transfer in the structure. Two parameters are of main importance: scale and the pores connectivity.

The scale factor is fundamental, because the permeability of the structure decreases in a more refined structure; on the other hand, the specific area for heat exchanges gets raised. Another point is that a finer microstructure may have a poorer stability under working conditions. High levels of stress can be induced by severe working conditions such as extreme temperature gradients and pressures. Thus, the mechanical properties of the porous structures are also an essential point of concern.

There are a few mechanisms of heat transferring in highly porous materials, such as conduction in gases and radiation. The conduction in gases depends on the pore's diameter. Larger pores have two effects, molecule-molecule, and molecule-wall, while smaller pores, majorly molecule-wall. (**Figure 10**). In the case of metallic templates, would also have heat conduction by electrons.

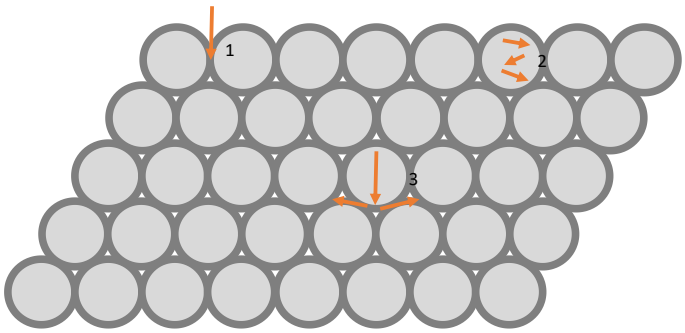

Figure 10. Mechanisms of heat transfer in ceramic porous materials. 1) Phonon conduction; 2) Gas conduction molecule-molecule; and 3) radiation scattering at interfaces.

Anyhow, the heat transfer in gases inside porous bodies is much lower than in free paths and solid bulks. The radiation is also affected by the porosity geometry, because radiation is basically scattered by interfaces and grain boundaries.

2.5 Sintering of Highly Porous Materials

Sintering is the one of the main steps in ceramic processing. The final characteristics of the ceramic material like strength, final shape and microstructure, which defines the mechanical properties of the material, are assign to it in this part of processing.[43]

There are numerous sintering mechanisms that occur concomitantly during this step of ceramic processing (**Figure 11**). Nevertheless, only surface diffusion and vapor transport result in particle coalescence and coarsening with no densification of the material. Atomic mobility is improved along surfaces due to less spatial constrictions. Therefore, the required activation energy is smaller in comparison to either grain boundary or lattice diffusion, which are the major densifying sintering mechanisms. Surface diffusion may designate migration of atoms and vacancies along several atomic layers. Since no shrinkage occurs during surface diffusion, only a microstructural toughening happens (the term "coarsening" is also used to name the process). Coarsening mechanism is enhanced, when vapor phase transport is arranged. [44,45]

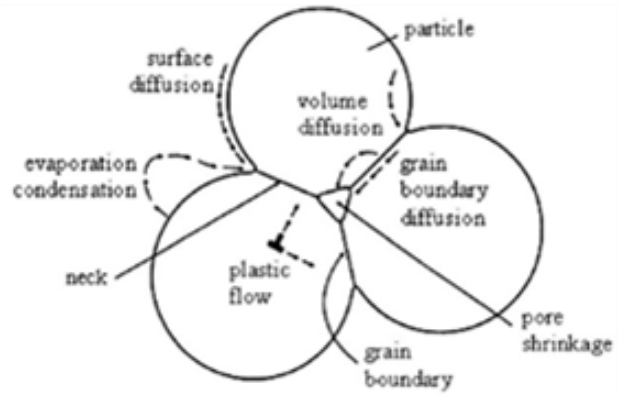

Figure 11. Mass transfer during sintering. (After Song et al.[46])

Vapor transport mechanism also leads to a neck and grain growth without shrinkage. Both mechanisms – surface diffusion and vapor transport – are quite similar. The mass transfer by vapor transport takes place via evaporation and recondensation. Besides, this mechanism has as driving force the energetically favorable surface area reduction. The achievement of such reduction occurs due to a partial pressure gradient along curved surfaces, leading to a mass transport from grains to necks in addition to from small to larger grains.[44,45]

The predominance of non-densifying mechanisms such as surface diffusion and vapor transport leads to the production of highly porous materials.[47] As one of the objectives of this research was to develop a design that would allow to fabricate a 3D defect-free high-temperature photonic structure, the chosen sintering parameters should lead to firing conditions, in which the non-densifying

mechanisms would be favored.

2.6 High Temperature Photonic Structure

High temperatures photonic structures (HTPS) are materials quite like ordinary photonic crystals. Nevertheless, HTPS have chemical and mechanical properties that allows these materials to work properly, without any damage at temperatures higher than 1000 K for significant periods. HTPS constituents must be chemically and mechanically stable. The substrate and the coating material have to be chosen in the way to avoid thermal stresses[48] (**Figure 12**).

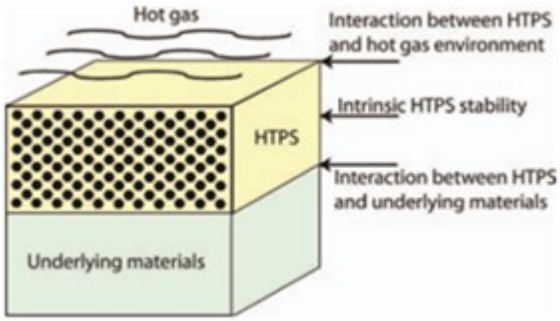

Figure 12. Schematic illustration of the system substrate-HTPS-hot gas and its interactions that should be considered to develop a proper HTPS design.

It means that their thermal expansion coefficient must be similar. Otherwise, a mechanical failure may happen. Also, the chemical stability is a critical factor, because once the photonic structure starts to react one with each other, the coating photonic properties can be compromised. Consequently, the thermal protection of the underlying material would be compromised, leading to a faster degradation of the protection coating and the underlying material. Thermal Barrier Coatings (TBC) are considered a potential application of photonic structures. In this case, the heat source would be a hot gas, about 1700-2000 K, originated from products of a combustion carried out in gas turbines. Regarding to the used fuel, the gas composition can vary. However, generally, NO_x, CO, CO_2, hydrocarbons that suffered an incomplete combustion and other residuals of such combustions are used. Besides, the gas can come already with some impurities (corrosive products, sulfur, vanadium, chloride and so on). For this reason, ceramic thermal barriers are preferred.[48,49] Many works have been done in the aim of obtaining an appropriate material and design of photonic structures to be used for such application.[48–50]

The photonic structure and thermal stability of yttria-stabilized zirconia (YSZ) coatings on IN100 superalloy substrates were evaluated by Scardi et al.[49] to verify the possibility of thermal engines applications for such material. Panwar et al.[50] did some practical experiments in the aim of evaluate the influence of YSZ thermal barrier coating thickness on its performance.

Taking in account the complexity of TBC's subject it is also possible to find in literature some reviews considering the application, functionality, and different approaches to develop these materials.

Padture et al.[51] wrote a review on numerous types of coatings used to protect structural engineering materials from erosion and corrosion, or to provide the use of the underlying materials (protected materials) in even more extreme environments in relation to the temperatures and pressures, like in aircrafts and gas turbines environments. The objective was to discuss the current limitations, future opportunities, and applications (e.g., gas-turbine engines). Shklover et al.[1] also did a review approaching theoretical issues and practical uses of these materials. A discussion regarding the evolution of the development techniques and applications of high thermal photonic structures (HTPS) was also given.

In this thesis, part of the current faults regarding to HTPS subject are also investigated. Besides, one of the main objectives is to develop a design for photonic structure that allows their use in the previously described extreme environments. Processing parameters were tested in the aim of provide a high ordered and defect free polymeric template and a correlation between the influence of such parameters and the thermal stability is also "investigated".

2.7 Characterization Techniques

2.7.1 Scanning Electron Microscopy –SEM

The scanning electron microscopy (SEM) is a powerful technique for detailed study of a specimen´s morphology and topography. When a specimen is irradiated with a high-energy electron beam, secondary electrons are emitted from the sample surface. These secondary electrons are detected and an image is acquired.[52,53]

SEM requires a source of electrons, a column with electromagnetic lenses, electron detector, sample chamber and a proper software to display the images (**Figure 13**).

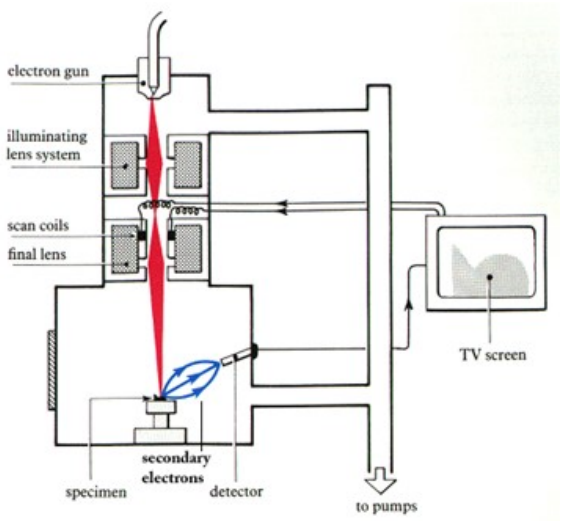

Figure 13. Scanning Electron Microscopy (SEM) equipment parts. [54]

Electrons are generated at the top of the column, emitted from tungsten or lanthanum hexaboride (LaB_6) thermionic emitters, accelerated through lenses and apertures to produce a focused beam of

electrons, which reaches the sample´s surface. Electron bombardment can produce a wide variety of emissions from the specimen, including backscattered electrons, secondary electrons, auger electrons, X-rays, visible photons and so on. The specimen is placed on a sample holder in the chamber area. Then both the column and the chamber are evacuated by pumps, producing vacuum on a level that depends on the equipment. [52,55] Secondary electrons are generated by collisions of incident electrons, formed at the column, with atoms that belongs to the sample's atoms. After each collision, new secondary electrons are formed, and the incident electron loses energy until not be able to dislodge new electrons. Some of these secondary electrons can be collected by the detector. As a direct result, secondary electron imaging is closely related to sample topography and morphology.[54,56,57]

The SEM systems employed in this work (Leo Gemini 1530 and a Zeiss Supra 55 VP) are shown in Figure 14. The observations were performed without covering with conductive metals, once we wanted to see highly porous 3D structures. The adopted way out to avoid the charging effect was to use a very low energy (EHT), about 2 kV.

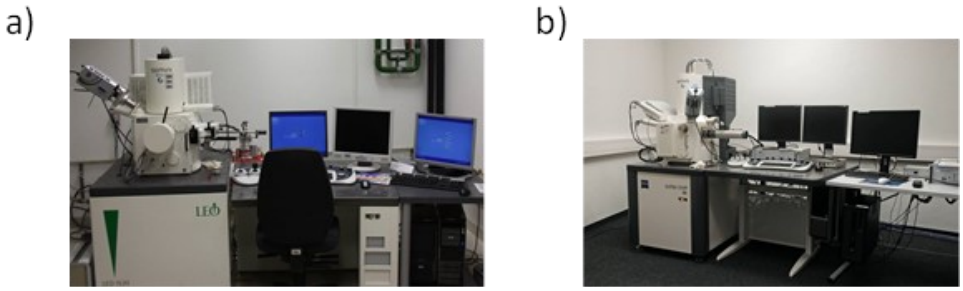

Figure 14. Scanning Electron Microscopy (SEM) systems employed in this work: a) Leo Gemini 1530; and b) Zeiss Supra 55 VP (Timmermann). [58]

2.7.2 X-Ray Diffraction

X-ray diffraction (XRD) is a versatile, non-destructive analytical method used to characterize crystalline materials such as minerals and determine their structure. In 1912, Bragg recognized a predictable relationship among several factors. The distance between adjacent planes in a mineral (d, interatomic spacing) is called the d-spacing and is measured in angstroms. The angle of diffraction is called the theta angle, measured in degrees. For geometrical reasons, a common diffractometer measures an angle twice that of the theta angle (Equation 2. The wavelength (λ) of the incident X-radiation, is correlated with d and θ expressed by the Bragg's law, in which n is a natural whole number (n=1,2,3…). [59,60]

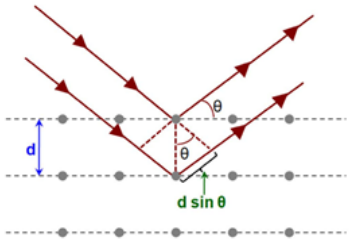

Figure 15. Bragg's law schematic representation.[59]

$$n\lambda = 2d\sin\theta \qquad \text{Equation 2}$$

From XRD, the crystallite size can be calculated by using Scherrer´s formula:

$$D = k\lambda\ \beta\cos\theta \qquad \text{Equation 3}$$

where D is the crystallite size; k is the shape factor; □ is the wavelength (1.54 Å); β is the full width of half maxima; θ is the diffraction angle.

In the aim to guarantee that the amorphous alumina used to cover the direct polystyrene photonic crystals were transformed in α-alumina, XRD diffractions were carried out (Brucker D8 Advance Eco X-ray diffractometer), Error! Reference source not found.after each heat treatment performed in this research.

Figure 16. Brucker D8 Advance Eco X-Ray diffractometer.[62]

2.7.3 UV-Vis Spectroscopy

UV-Vis spectroscopy is used to determine the absorption of the samples at different wavelengths. Absorbance is a measure of the light that does not pass through the sample and can be calculated using Lambert-Beers law (Equation 4).[63]

$$A = \log \frac{I_0}{I} = \varepsilon_\gamma cb$$ Equation 4

where A is the absorbance; ε_λ is the specific wavelength at the moment of the measurement; c is the concentration of species in the sample; and b is the path length of the light.[63]

Because of the correlation between defect density and photonic band profile, it was possible to use the optical properties as an indirect, but efficient tool to be able to compare the physical structure quality of the fabricated samples. [4,64,65]

UV-vis-NIR spectrometer (Perkin-Elmer, Lambda 1050), Figure 17, was used for characterization of the photonic crystals thin films deposited on sapphire substrates. The optical properties of the films were studied in the wavelength range of 900-1850 nm with the purpose of comparing the produced photonic crystals morphological structure.

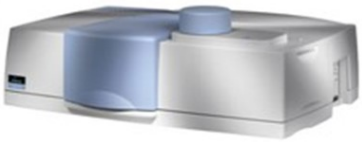

Figure 18. UV-vis-NIR spectrometer (Perkin-Elmer, Lambda 1050). [66]

2.7.4 Transmission Electron Microscopy (TEM) and Selected Area Electron Diffraction (SAED)

Transmission electron microscope (TEM) is an effective technique for characterization of nanoparticles, from few nanometers up to several hundreds, and their composites thin films with polymer. TEM principles are like those of scanning electron microscopy (SEM). The main difference between the two techniques is that TEM uses electrons instead of photons as energy source. When transmitting through thin samples, electrons can be absorbed (bright field image) or diffracted in a certain direction (dark field image). With different levels of electrons absorption, areas of the investigated material are displayed in the bright field image, while the structure crystallography is showed in the dark field image. The material crystallographic structure can be estimated from an electron diffraction pattern by Selected Area Electron Diffraction (SAED) analysis. An effective characterization and good contrast can be obtained for composite thin films with components having great variance in electron absorption.[67,68]

A transmission electron microscope (Jeol JEM-2000FX-II) (Figure 19) was applied to investigate the crystalline structure of the thin films after 1400 °C, 200 h heat treatments for all tested self-assembly samples. This technique was also used to study the crystallography of the samples produced with 1.5 mg/ml, 55 °C and 70% (polystyrene concentration, evaporation temperature and relative humidity) and heat treated at 1400 °C for 4 and 200 h. Afterwards, SEM was carried out with the objective of estimating the resultant 3D structures grain size by imaging software (ImageJ, 1.51p22).

Figure 20. Transmission Electron Microscope (TEM, Timmermann)[58].

2.7.5 Focused Ion Beam– FIB

Focused Ion Beam (FIB) principle is similar to SEM, but instead of electrons, ions beam is used. Accelerated heavy ions, normally gallium, reach the target material, sputtering its atoms. The efficiency of the sputtering process depends on the ion source, which should have a low melting point and vapor pressure. A Ga liquid metal ion source (LMIS) is composed of a small Ga reservoir connected to a tungsten needle. The solid Ga is heated to its melting point and the liquid Ga flows to the tip of the needle by surface tension thus wetting the tungsten needle. A strong electric field (108 V/cm) applied to the end of the tungsten tip causes the liquid Ga to form a point source of about 2–5 nm in diameter and extracts ions from that narrow tip. The Ga ions are accelerated in an electrical field (up to 30 keV). A continuous flow of liquid Ga to the tip replaces the extracted Ga+ ions resulting in a constant ion current, which is a basic requirement for an automated sputtering process.[69,70]

To obtain information about the internal structure of the photonic crystals after each heat treatment, including burning out, they were cross sectioned by FIB (FEI Helios NanoLab G3, DualBeam) and the sections were imaged by SEM. An epoxy resin infiltration was done to protect the structures during the FIB process. The typical beam current that has been used for cutting was 25 pA at an accelerating voltage of 2 kV.

2.7.6 Nanoindentation

Indentation is a well-known technique that can be applied to characterize thin films, polymers, metals, and composites. It can be used to measure mechanical properties on small scale, structures with no more than 100 nm and thin films smaller than 5 nm. The test methods may be applied for either comparative or qualitative analysis of hardness, wear resistance, thin film adhesion, and elastic modulus.[71]

The testing procedure begins with a tip pressuring the sample with an increasing load as long the tip penetrates the specimen. An impression is created on the sample, accordingly to the tips shape until the user predefined load or displacement value be achieved. Load and tip displacement are continually accompanied and measured throughout loading cycle. From the load-displacement data (**Figure 21**), it is possible to estimate the mechanical properties of the evaluated material. [71,72]

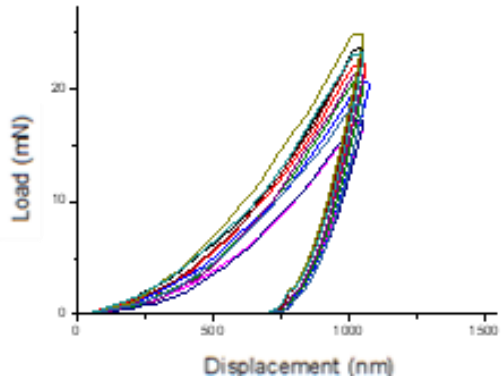

Figure 21. Load-Displacement curve of an inverse alumina photonic crystal produced at 55 °C, 70%, 1.5 mg/ml (evaporation temperature, relative humidity, and polystyrene concentration respectively) after burn-out (500 °C, 30 min).

Nanoindentation can also be performed combined with atomic force microscopy (AFM). In this case, the testing area and the indentation marks are defined and obtained respectively by AFM imaging.[71]

Mostly, nanoindentation has been applied in dense materials. Nevertheless, Chen et al.[72] proposed the use of this technique for measuring mechanical properties of porous thin films. The author investigated the effects of porosity in indentation hardness and elastic modulus applying the finite element analyses and concluded that nanoindentation is an applicable technique for evaluating the toughness of porous thin films if the indentation depths are sufficiently small to avoid substrate effect. Rosário et al.[73] applied nanoindentation in inverse titania opal photonic crystals with the objective of evaluating the stiffness of the produced structures as well as the structural efficiency.

In this thesis, we used nanoindentation with the purpose of evaluating the mechanical stability of inverse alumina opal photonic crystals structures after each heat treatment applied. A quantitative result was not expected, but a new way of comparing the fabricated structures mechanical stability. The nanoindentation test was performed (Nanoindenter XP) with a flat ended 60° conical diamond indenter adopting a displacement rate of 10 nm^{-1}, i.e., the same parameters employed by Rosário et al.[73] in inverse titania opal photonic crystals.

3 MATERIALS AND METHODS

3.1 Preparation of Direct Photonic Crystals

3.1.1 Vertical Colloidal Deposition

Monodisperse polystyrene (PS) particles (Microparticles GmbH), with diameter of 0.762 ± 0.023 µm were self-assembled onto single crystal sapphire substrates (25×30×0.53 mm, Crystec GmbH). Vertical colloidal deposition was performed in a humidity chamber (HCP 108, Memmert GmbH) using Teflon beakers containing PS suspensions in deionized filtered water (**Figure 22**).

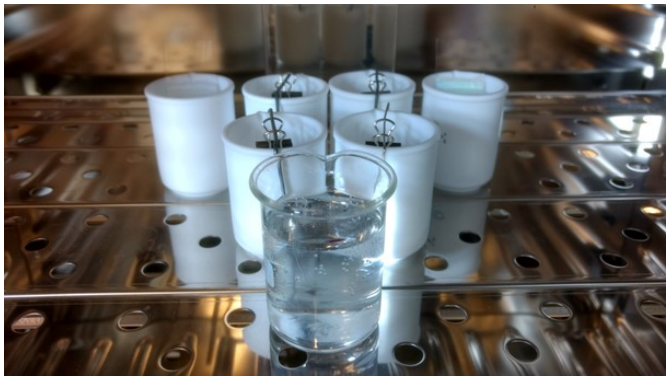

Figure 22. Image of the direct photonic crystals preparation.

The colloidal crystals films were obtained by controlled evaporation of the solvent. After 120 h, or the complete solvent evaporation, the self-assembly process was interrupted. The produced samples were then enclosed with a glass cover and placed in a laboratory fume hood for 24 h, resulting in direct polystyrene photonic crystals (**Figure 23**). In this step, different processing parameters were tested: polystyrene (PS) concentration (1, 1.5, or 2 mg/ml), evaporation temperature (40, 55, or 80°C) and relative humidity (45%, 70%, or 90%).

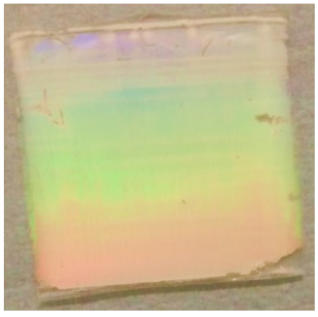

Figure 23. Image of polystyrene (PS) direct photonic crystal.

3.2 Filling of Direct Photonic Crystals

3.2.1 Atomic Layer Deposition

Atomic layer deposition (ALD) was performed in a reactor (SavannahTM 100, Ultratech/Cambridge Nanotech) for filling the direct photonic crystals (PS templates) with trimethylaluminum (TMA, Sigma Aldrich), at 95 °C to avoid structural changes or damage of the polymer templates. An average growth rate of 1.7 Å/cycle was achieved. The cycle was performed under exposure mode (0.2/60/90 s) with nitrogen as carrier gas (30 standard cm^3) using the precursors, TMA, and deionized water. (**Figure 24**)

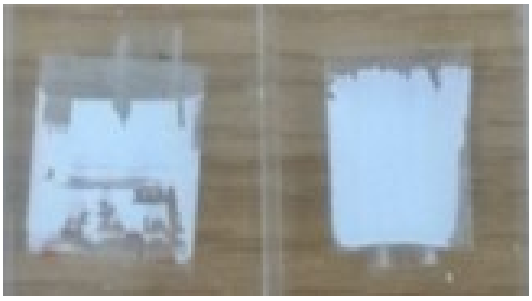

Figure 24. Image of polystyrene (PS) direct photonic crystals infiltrated by atomic layer deposition (ALD).

3.3 Heat Treatment of Inverse Alumina Opal Photonic Crystals

3.3.1 Burn Out

After ALD, the polymeric template was burned out in air at 500 °C for 30 min, generating the inverse photonic crystal structure.

3.3.2 Sintering

The inverse alumina opal photonic crystals were heat treated at 1400 °C for 4 h and 200 h in air in a muffle furnace.

3.4 Characterization of Direct and Inverse Opal Photonic Crystals

3.4.1 Visual analysis

About 20 pictures, in different angles, were taken from the direct opal photonic crystals samples to analyze possible visual defects and diffraction effects.

3.4.2 Scanning Electron Microscopy

Scanning Electron Microscopy (SEM) cross-section and top view images were done of the direct and indirect opal photonic crystals (Zeiss Supra VP 55) for morphological analysis.

3.4.3 UV-Vis

The optical response of both direct and inverse photonic crystals was evaluated by specular reflectance measurements (UV-vis-NIR spectrometer, Perkin-Elmer, Lambda 1050) from 900 to 1850 nm and incident angle of 8°.

3.4.4 X-Ray Diffraction

X-ray diffractometry (XRD) measurements of the inverse photonic crystals were carried out (Drucker D8, Advanced) using Cu Kα radiation with a wavelength of $\lambda\alpha_1$ = 1.5406 Å. The analysis ranged from 20 to 60º (2θ) with a step size of 0.01º and a measuring time of 5 s/step. Background noise and $K\alpha_2$ superimposition were subtracted from the patterns using analysis software for phase identification.

3.4.5 Transmission Electron Microscopy and Selected Area Electron Diffraction

For the inverse photonic crystals treated at 1400 °C for 200 h and for the inverse photonic crystal produced with 55 °C, 70% and 1.5 mg/ml (evaporation temperature, relative humidity and polystyrene concentration) heated to 1400 °C for 4 h, parts of the sample were crushed, dispersed in ethanol by ultrasonication and transferred to a carbon-coated grid for TEM imaging and selected-area electron diffraction (SAED, TEM, Jeol JEM-2000FX-II)

3.4.6 Focused Ion Beam

The resultant 3D structures of the photonic crystals after each heat treatment, including burning out, were investigated. The 3D structures were cross sectioned by FIB (FEI Helios NanoLab G3, DualBeam), and the sections were imaged by SEM. An epoxy resin infiltration was done to protect the structures during the FIB process. The typical beam current that has been used for cutting was 25 pA at an accelerating voltage of 2 kV.

3.4.7 Nanoindentation

A nanoindenter (XP) equipped with a flat ended 60° conical diamond tip was used to provide a new comparison method of the mechanical stability of the produced inverse alumina opal photonic crystals after each performed heat treatment. The depth was fixed (2000 nm) and a displacement constant in (1 1 1) direction was also predetermined (10 $nm \cdot s^{-1}$). As the nanoindenter is also equipped with AFM, the areas that would be tested were previously selected and checked to avoid cracks and edges.

3.4.8 Image Analysis

A dedicated software (Image J, version 1.51p22) was used to estimate structural properties.

3.4.8.1 Thickness Measurement

The SEM cross-section images of the direct opal photonic crystals were analyzed (Image J, version 1.51p22) in the aim of a thickness estimative. About 10 images of each sample were measured.

3.4.8.2 Defective Area Estimation

The direct opal photonic crystals defects were evaluated by image analysis (ImageJ, 1.51p22) of a minimum of 20 SEM images taken at lower magnification. For elimination of noise (coming from the shadowing in between the spheres) a Gaussian filter was applied, with no loss of information concerning the defects. After binarization, the defects area was analyzed by automated threshold definition.

3.4.8.3 Grain Size Estimation

TEM bright field images were taken from the inverse photonic crystals treated at 1400 °C for 200 h and for the inverse photonic crystal produced with 55 °C, 70% and 1.5 mg/ml (evaporation temperature, relative humidity and polystyrene concentration) heated to 1400°C for 4 h were analyzed in Image J. The average grain size was estimated.

4 RESULTS AND DISCUSSION

4.1 Polystyrene Direct Opal Photonic Crystals

4.1.1 Visual characterization

The direct polystyrene photonic crystals fabricated by vertical deposition self-assembly showed an angle dependent reflectance behavior when interacting with visible light, which was expected. As shown in Figure 25. Photo (a) and SEM image (b) of a PS direct photonic crystal self-assembled on a sapphire substrate at 55 °C and 70% RH using a PS suspension concentration of 1.5 mg/ml. Scale bars represent 8 mm and 2 µm, respectively. reflected light changes from blue-green to red as consequence of the incident angle.[25]

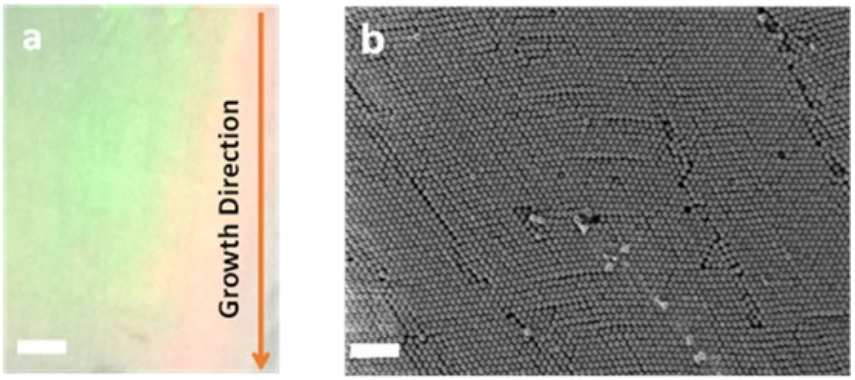

Figure 25. Photo (a) and SEM image (b) of a PS direct photonic crystal self-assembled on a sapphire substrate at 55 °C and 70% RH using a PS suspension concentration of 1.5 mg/ml. Scale bars represent 8 mm and 2 µm, respectively.

All the produced samples showed also characteristic self-assembly stripes (Figure 26), which were expected from the vertical deposition and described elsewhere[74,75]. The orientation of the stripes is perpendicular to the growth direction of the crystalline layer and shows a characteristic periodicity. According to Yoldi et al.[75], the stripes are formed when the meniscus draws back with a discontinuous velocity, with the surface tension embracing the meniscus. When the tension turns to be too elevated, there is the film rupture and a new meniscus starts to grow, generating the stripes.

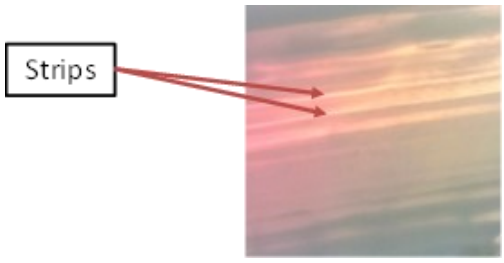

Figure 26. Vertical colloidal deposition typical strips.

4.1.2 Influence of suspension concentration

The polymer concentration plays an important role in the opals film growth. Solvent evaporation out of the thin meniscus leads to a constant solution influx, which draws the colloid into the area of film formation[26]. The suspension concentration controls the particles flux, and consequently the thickness of the crystals films[76].

As shown in Figure 27. Top view and cross section SEM images of PS direct photonic crystals produced at 55 °C and 70% RH for PS concentrations of 1 (a,b), 1.5 (c,d) and 2 mg/ml (e,f). The scale bars are equivalent to 2 µm (a,c,e), 1 µm (b), 2 µm (d), and 3 µm (f). In the inserts, the scale bars are equivalent to 2 µm. and Figure 28, the thickness of the produced films increases with the suspension concentration. Although a higher thickness is desired for a probable higher reflectance, a higher fraction of defects was observed.

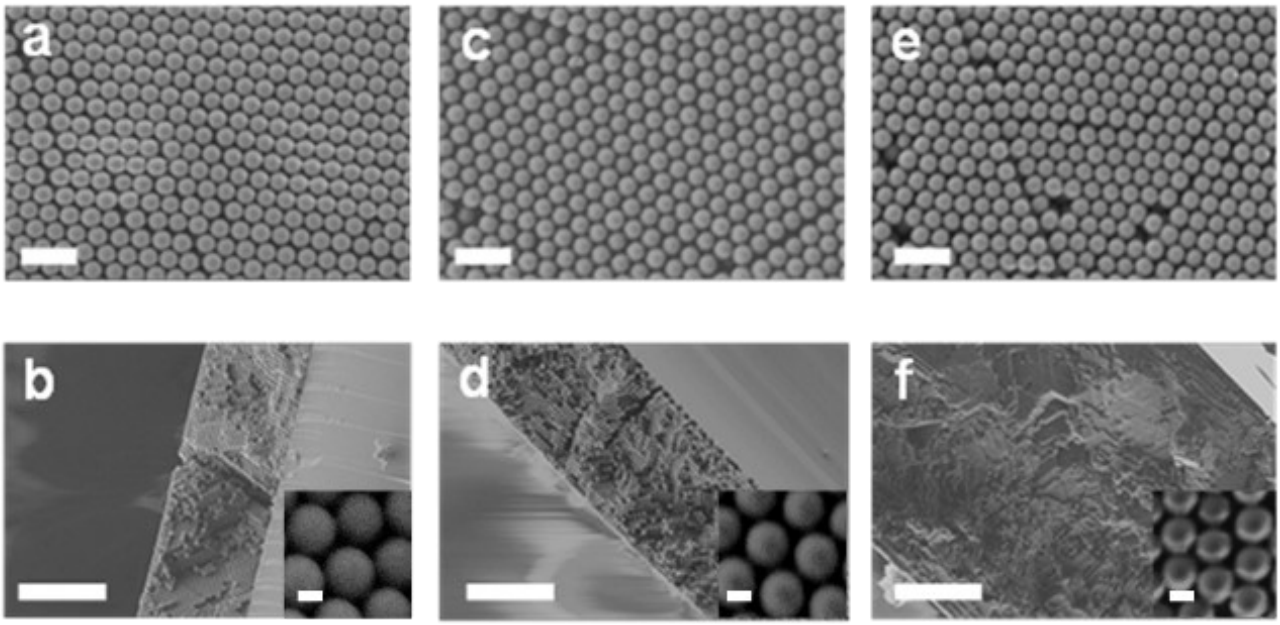

Figure 27. Top view and cross section SEM images of PS direct photonic crystals produced at 55 °C and 70% RH for PS concentrations of 1 (a,b), 1.5 (c,d) and 2 mg/ml (e,f). The scale bars are equivalent to 2 µm (a,c,e), 1 µm (b), 2 µm (d), and 3 µm (f). In the inserts, the scale bars are equivalent to 2 µm.

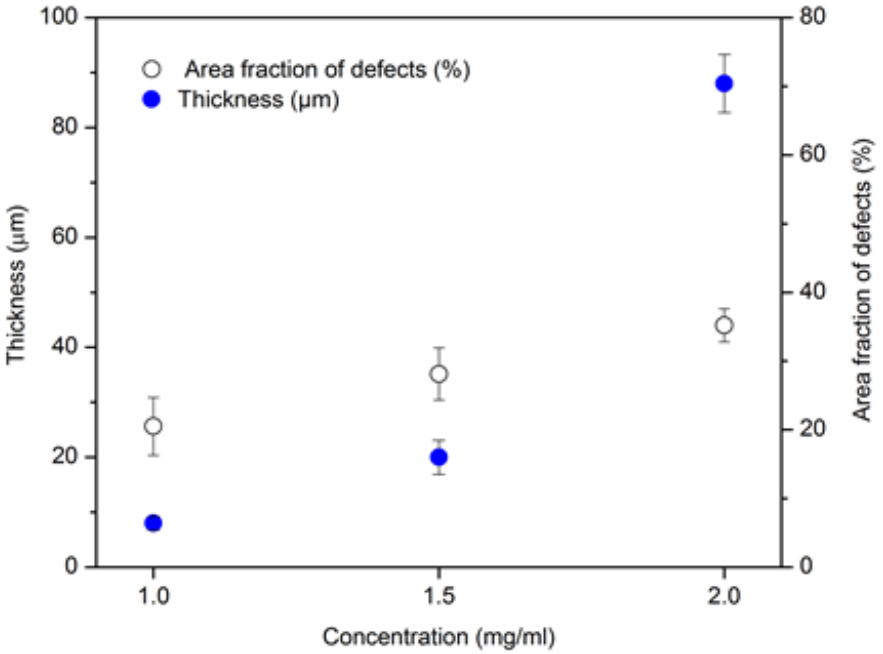

Figure 28. Effect of suspension concentration on the direct photonic crystals' thickness and area fraction of defects.

These results are in agreement with the results presented by Yan et al.[76], which modified the total volume of the solvent. The increase in the thickness by variation of the suspension concentration was also reported by McLachlan et al.[77], for direct polystyrene photonic crystals (volume variation of 1 to 5%) and by Zhang et al.[6] No quantification of the defects density was presented, though.

Bormashenko et al.[24] also found that the concentration of the solution exerts a decisive influence on the mesoscopic cell characteristic dimension. Cell dimensions grow linearly with the polymer solution concentration for all kinds of tested polymers, solvents, and substrates. The dependence could be explained by a physical mechanism, based on the mass transport instability occurring under the intensive evaporation of the solvent. Bormashenko et al.[24] demonstrated that the variation of the polymer solution concentration can supply such qualitative data and shed some light on the physical mechanisms responsible for the patterning in evaporated polymer films.

In this work, the increment in the direct photonic crystals' thickness generated a higher density of cracks and the adhesion to the substrate was compromised, which was also observed by Liu et al.[78], but not quantified. Although the thickness jumped from 8 to 88 µm (100%) for the concentration increase from 1.5 to 2.0 mg/ml, the increase in the defects' density kept a linear relation to the concentration. This indicates that the majority of the defects are possibly generated and guided by the particles' interactions, either between the substrate or the already assembled layers, and the free particles still in suspension. The possible defects of polymeric direct photonic crystals (self-assembled templates) are drying cracks, vacancies, screw dislocations and Frenkel defects (Figure 29), here characterized and named as defects density.[79] This linear dependence with concentration was also observed elsewhere.[80 - 81]

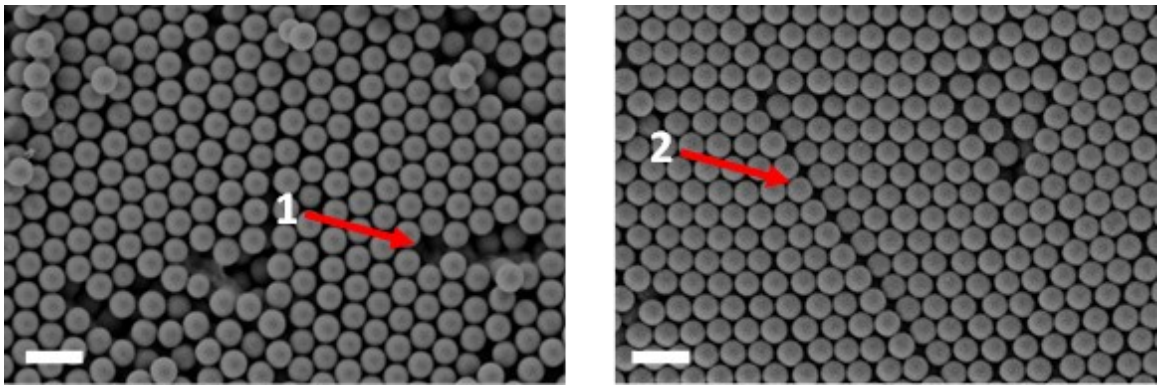

Figure 29. Defects such as 1) vacancies and 2) dislocations on a direct polystyrene photonic crystal produced with 2 mg/ml, 55 °C and 70% (polystyrene concentration, evaporation temperature and relative humidity respectively). The scale bars represent 2 µm.

In this research, the reflectance was measured to support the defects analysis of the direct photonic crystals. Many works such as those from Liau et al.[81] and Zhou et al.[82] affirm that the reflectance gets lower when the defects amount increases, which was not observed in this work (**Figure 30**). This behavior is most likely associated to the higher number of assembled layers for higher suspension concentration, supported by other authors.[82, 81 - 83]

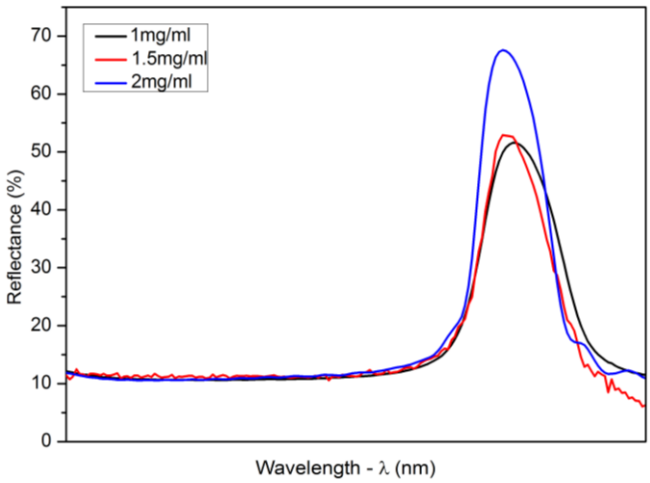

Figure 30. Specular reflectance measurements of the PS direct photonic crystals according to the PS suspensions initial concentration (1, 1.5 and 2.0 mg/ml).

4.1.3 Influence of Temperature

It was found that the self-assembly temperature is one of the most important parameters, a key point for solvent evaporation, in the self-assembly of colloidal particles.[84] More elevated temperatures raise the evaporation rate and tensile stresses created into the films are increased. These tensile stresses are generated during the drying step, in which the distance between two particles increases and cracks are formed. This phenomenon is quite common during vertical deposition process. Vacancies are also produced when the evaporation speed is too high, and the particles do not have enough time to move to the optimal lattice before its deposition on the substrate. [85]

According to Mastai et al.[86], The et al. [87] and Bogue [88] these vacancies and cracks can compromise photonic crystals applications because the periodicity is interrupted by the defects. Ahmed et al.[89] investigated the influence of the defects on the photonic crystals structures, by comparing the photonic bandgap (PBG) of a perfect 1D and 2D photonic crystal and of a defective 1D and 2D photonic crystal. According to Ahmed et al.[89], there is a difference between the PBG of the perfects and the defectives ones. The PBG of the defectives samples was partially destroyed.

In this work, the effect of the evaporation temperature was evaluated, while the suspension concentration and the relative humidity were kept at 1.5 mg/ml and 70%, respectively. The thickness and defects amount have a clear correlation with the evaporation temperature, being increased by the temperature raise (**Figure 31**).

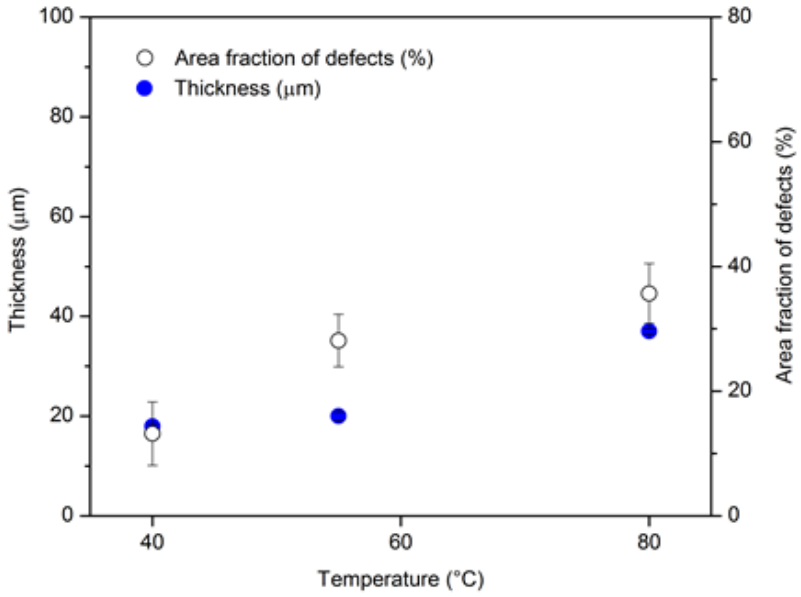

Figure 31. Effect of the evaporation temperature on the film thickness and area fraction of defects.

It is important to point out that the self-assembly process was interrupted either after 96 h or after total evaporation of the solvent. For the process performed at 80 °C, the process time was 40% faster than the ones performed at 55 and 40 °C. Although the amount of defects was higher for this condition (36% against 28% for the process at 55 °C), the higher thickness obtained at reduced time could be an advantage of such high temperature self-assembly process, if the colloidal film mechanical stability and photonic response are still considered acceptable (**Figure 32**).

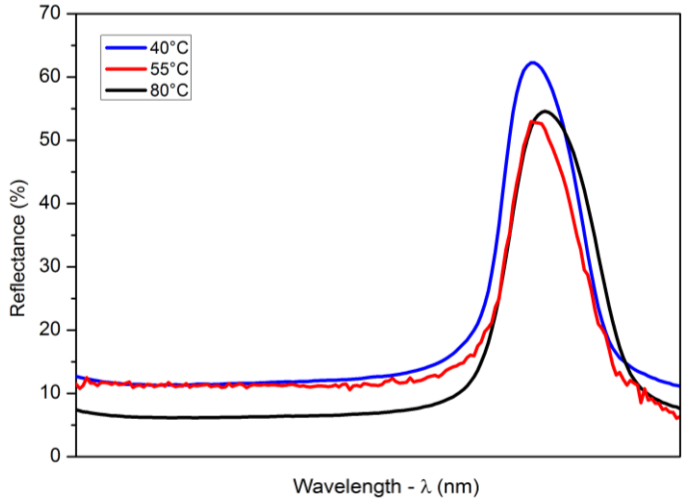

Figure 32. Specular reflectance measurements of the PS direct photonic crystals according to different process temperatures (40, 55, 80 °C).

The direct photonic crystals produced at 55 and 80 °C as evaporation temperature, showed more defects such as cracks and vacancies (**Figure 33**) than those fabricated at 40 °C.

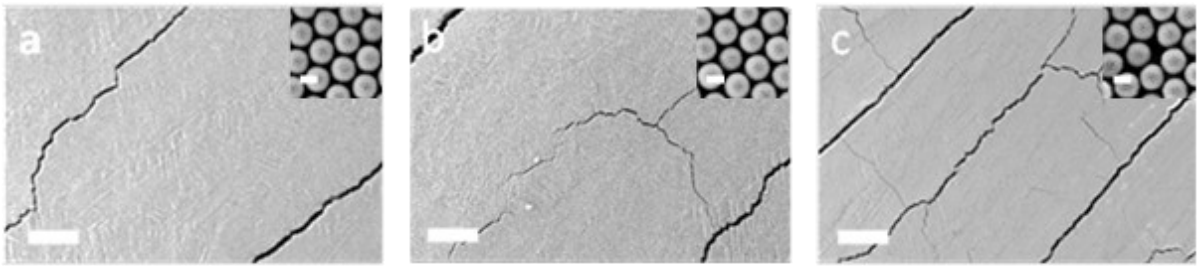

Figure 33. Top view SEM images of PS direct photonic crystals showing the self-assembly cracks according to the process temperature (40, 55 and 80 °C) using PS suspensions concentration of 1.5 mg/ml, and RH kept at 70%. The scale bars in the figures represent 10 µm. In the insets, the scale bars represent 0.15 µm.

The reflectance measurements support the structural evaluation of the direct photonic crystals quality (Figure 32), as the samples produced at 40°C presented higher reflectance than those fabricated at 55 and 80°C, even though the thickness was smaller (18 to 20 and 37 µm, respectively). This relationship between colloidal films quality (direct photonic crystals in our work) and evaporation

temperature has been also discussed qualitatively elsewhere[90-91]. Chun et al.[92] compared the morphology of colloidal crystals obtained at evaporation temperatures of 45, 60 and 70°C, with constant humidity (90%). High quality crystals with respect to ordering and reflectivity were obtained at 45 °C in 24 h, while poorly ordered structures (indicating a lot of defects) were produced at the other two temperatures, which also corroborate our results.

In contrast, Im & Park[84] observed that the quality of the formed crystals was increased from 30 to 60 °C, which was not observed in the current work, though. However, the samples prepared at 90 °C in their case also revealed significantly more defects, which is in good agreement with the trend we observed.

4.1.4 Influence of relative humidity

The influence of humidity on the ordering and defects of the direct photonic crystals can be even more critical than the pure temperature. Relative humidity influences the evaporation rate and the crystal formation.[78]

Figure 34 and **Figure 35** present the dependence of the film thickness, defects amount and structural ordering. The results showed that the higher the relative humidity (actively controlled by the humidity chamber), the thicker, more ordered and less defective the photonic crystals.

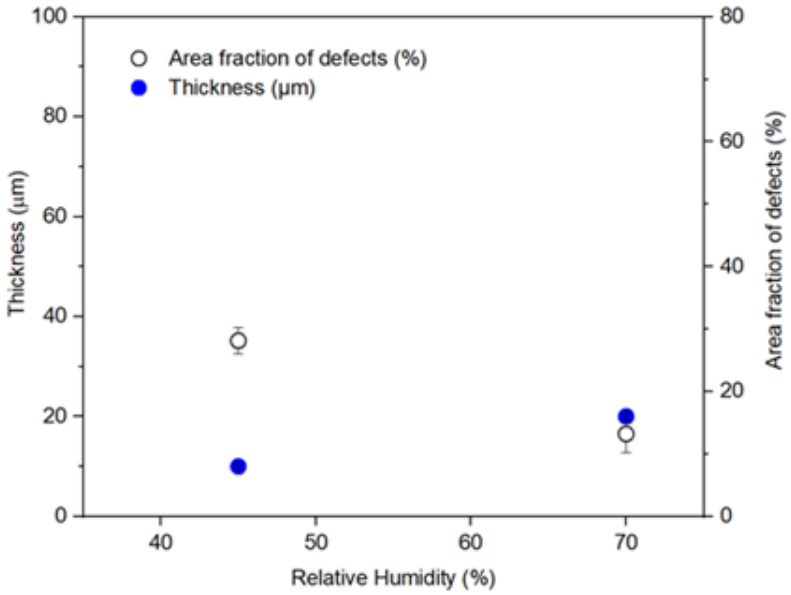

Figure 34. Effect of relative humidity on the film thickness and area fraction of defects.

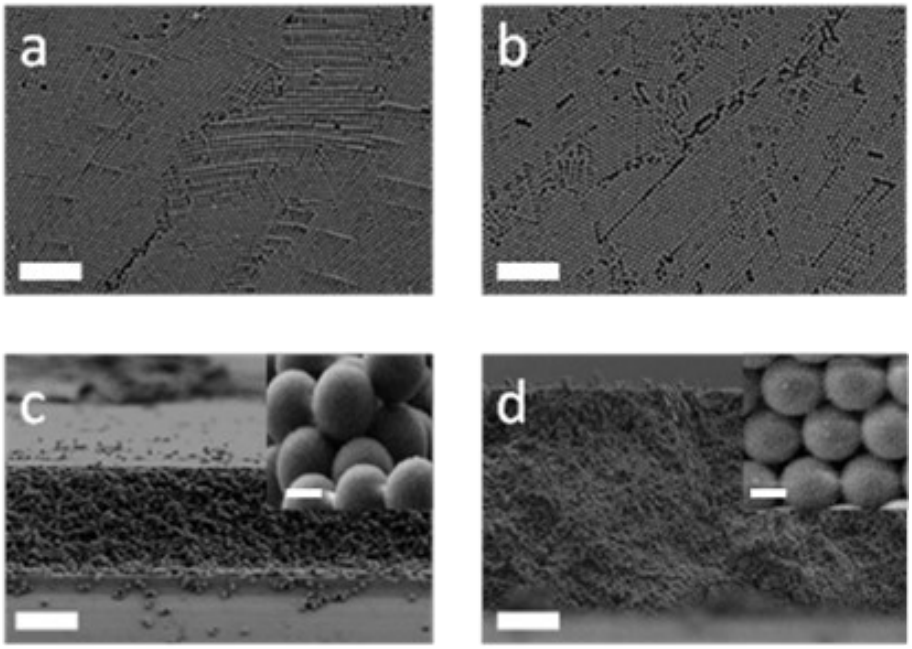

Figure 35. Top view and cross section SEM images of PS direct photonic crystals according to the relative humidity of 45% (a and c) and 70% (b and d), at 55°C and PS initial concentration of 1.5 mg/ml. In all images, the scale bars are equivalent to 2 µm. In the insets the scale bars are equivalent to 0.25 µm.

The samples fabricated at 70% RH presented a higher reflectance than those produced at 45% RH (**Figure 36**) strongly supporting our observation regarding suppressed defect at higher RH. The lack of ordering in the structure is clearly visible in the cross section analysis (**Figure 35c**), where the samples presented a more photonic-glass like appearance [93].

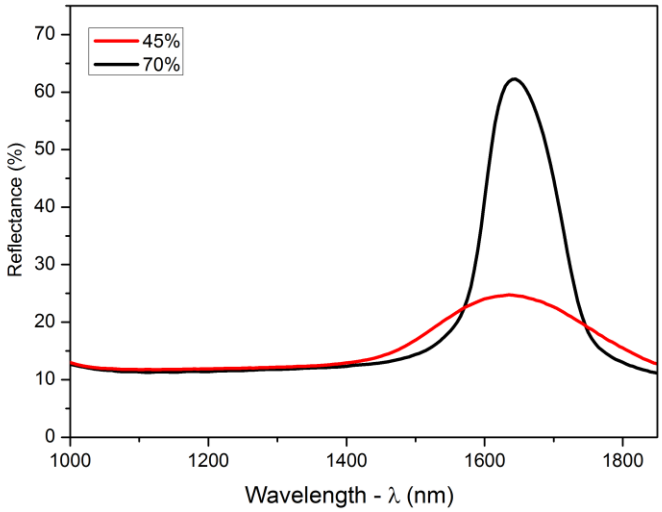

Figure 36. Specular reflectance measurements of the PS direct photonic crystals according to relative humidity (45%, 70%).

Please note, at 90% humidity, no self-assembly could be observed, in accordance to Kuai et al.,[4] who tested several RH values and found a decrease in the films thickness for values larger than 77%. Furthermore, Liu et al. [78] presented similar humidity values (40, 70 and 90%) as our work and observed that high or low RH values resulted in many vacancies and dislocations formation, indicating that there probably exist an optimum point around 70%. Specifically, a lower humidity promotes liquid evaporation, increasing the evaporation rate, and bringing additional internal stress, thus increasing the cracking and defects in the direct photonic crystals. However, higher RH – close to the optimum point the lateral capillary force and slower liquid evaporation – results in a better crystalline quality. Overcoming this point, a very low evaporation rate and too weak lateral force occur resulting in poor crystal quality. The fact that Liu et al. [78] could obtain samples even with a low quality, might be related with the chamber pressure. In that case, a pressure of 6 kPa was applied, while this work was performed always under atmospheric pressure.

4.2 Inverse Alumina Opal Photonic Crystals

After the ALD and polymer template burn-out, inverse opal photonic structures of Al_2O_3 were generated[5] (**Figure 37**). Reflectance measurements show a shift in the peak associated to the photonic band gap (**Figure 38**), which is related to the overall different structure and also to the different refractive indexes relationship between PS and air, and Al_2O_3 and air.[94]

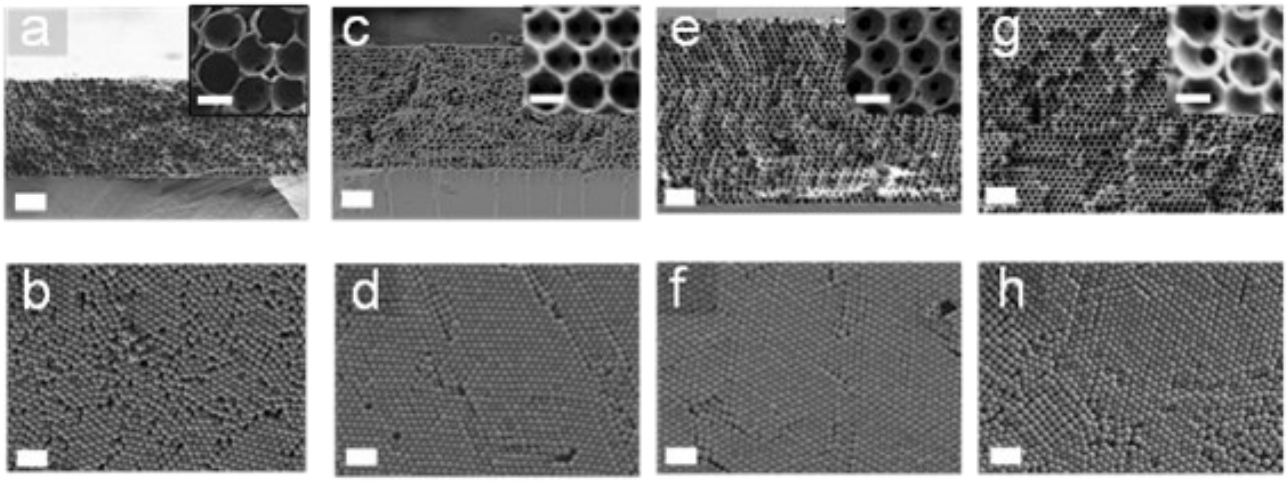

Figure 37. SEM images of cross section (a, c, e and g) and top view (b, d, f and h) of the produced alumina inverse opals. Temperature and relative humidity were respectively: 40 °C and 45% RH (a and b); 40 °C and 70% (c and d); 55 °C and 70% (e and f); 80 °C and 70 (g and h). Scale bars represent 5 μm in the full images and 1 μm in the insets.

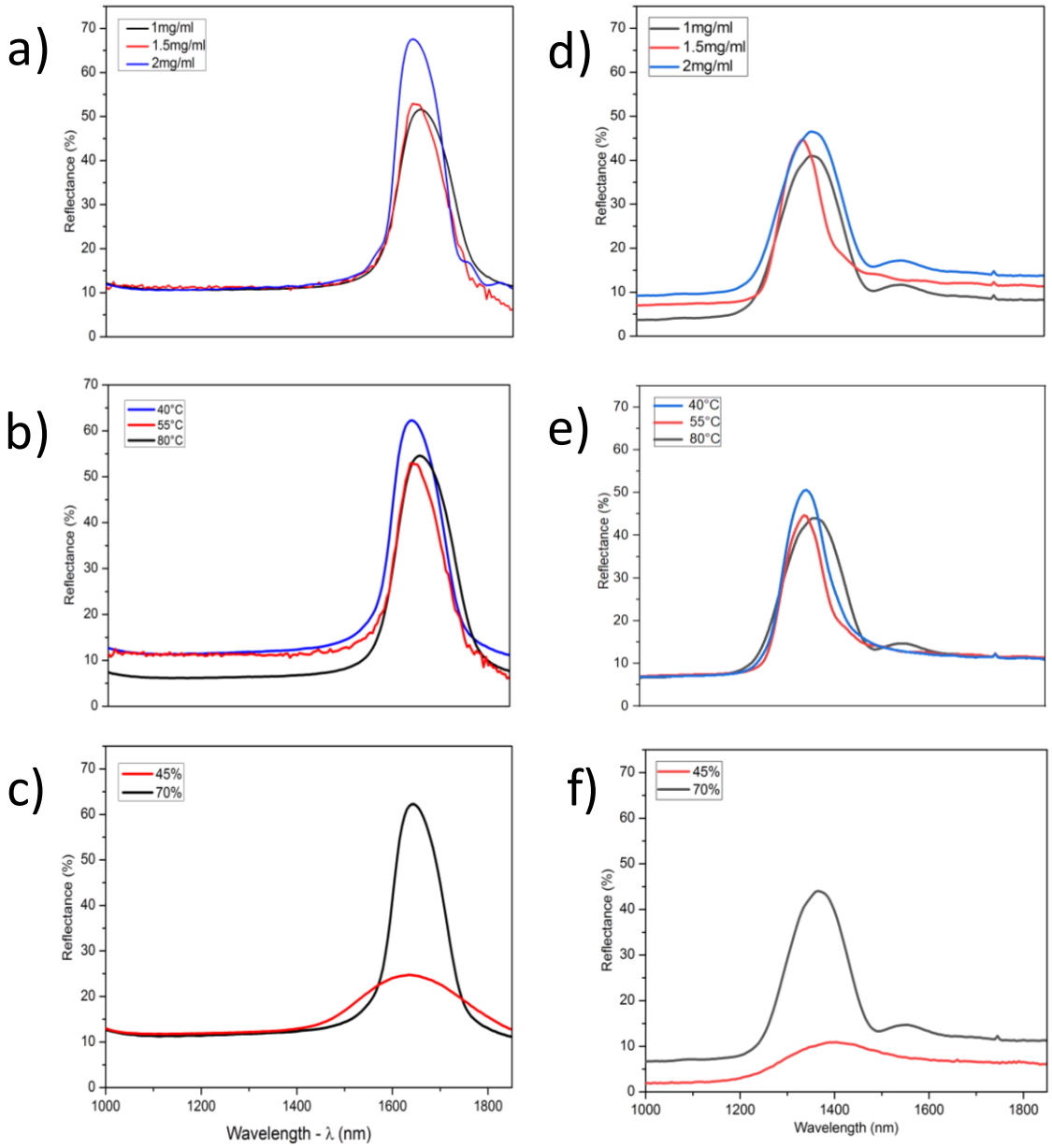

Figure 38. Specular reflectance measurements of the direct (a,b,c) and inverse (d,e,f) opal photonic crystals for different (a,d) PS suspensions initial concentration (1, 1.5 and 2.0 mg/ml) at 55 °C and 70% (RH); (b,e) process temperatures (40, 55 and 80 °C, at initial concentration of 1.5 mg /ml and 70% RH; (c,f) humidity conditions (45 and 70%) at 55 °C and PS initial concentration of 1.5 mg/ml.

Inverse opal photonic crystals present a more efficient scattering system than direct photonic crystals[95], due to a larger relationship between gap-to-midgap[94] ratio. Since the inverse opal photonic crystals produced in this work presented slightly lower values for the reflectance, one can assume that an additional small amount of defects, probably vacancies, faults and cracks (Figure 39) originated during the heat treatment (polystyrene burn out) were introduced during ALD and template burn-out. Zhang et al.[96] investigated metallic inverse opals produced by sol-gel infiltration. The author found that the defects that were already in the photonic crystal structure were magnified and other ones were added after infiltration and burn out procedures. Zhang et al.[96] localized the inverse opals structural defects and called them V, P and H defects. V defect is a pore that is bigger

than the others, P is related to deformed pores and H is coalesced pores. Although the used materials and the infiltration method being different from the adopted in this work, we also found H defects in the produced inverse alumina opals. The appearance of this kind of defects and the magnification of the already existent cracks and faults may be the cause of the reflectance suppression observed when the data obtained before ALD and burn out are compared to the ones accessed after these procedures.

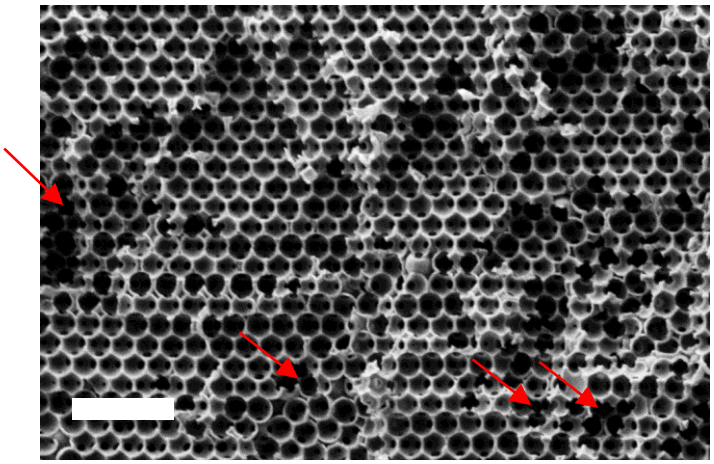

Figure 39. SEM image of an inverse alumina opal photonic crystal produced at 1.5 mg/ml, 55 °C, 70% (PS concentration, evaporation temperature and relative humidity). The arrows show "H" defects[96].

Liau et al. [81] and Zhou et al. [82] showed that an increase in the defects amount causes a decrease in the reflectance peak. However, these papers dealt with polymer-based direct photonic crystals, not with ceramic inverse opal photonic crystals. Nevertheless, a correlation between those behaviors can be made. It can be concluded that most defects originated during the self-assembly step remained in the structure even after ALD. However, the ALD infiltration followed by thermal handling (polymer burn-out) suppressed the reflectance, which might mean that the defects, already present in the structures, were magnified by these procedures. This means the reflectance capability of the ceramic oxide-based inverse opal photonic crystals is defined and greatly influenced by the initial polymeric template self-assembly parameters.

Besides, the application of focused ion beam (FIB) has been done with the objective of a better structural investigation of the inverse photonic crystals (**Figure 40**). FIB has been widely studied for nano-optical materials such as photonic crystals, mainly of these researches have been reported for gallium compounds.[97–99] In this work, gallium was applied as ions source; however, as can be seen in **Figure 40**, this technique showed to be too aggressive for the tested samples. Cryan et al.[99] used FIB for GaN two dimensional photonic crystals, Huyang et al[98] for silica 2D photonic crystals and Ridder et al.[97] for SiC or $LiNbO_3$. All these authors had high resolution images, which helped to make a detailed structural study. Nevertheless, Cryan et al.[99], Huyang et al.[98] and Ridder et al.[97] also reported problems with FIB induced optical damages. Differences among the results obtained in this

research and the ones found by Cryan et al.[99], Huyang et al.[98] and Ridder et al.[97] happened, probably, because different materials were used. Olea-Mejía et al.[100] investigated the FIB-SEM technique applications and found that for polymeric and other fragile materials, such as the ones we studied, FIB-SEM can bring heating damage, redeposition and curtain effect. Heating damage is the formation of cracks or deformed areas on the samples because of heat (**Figure 40**-a,1;b,2;c,4;d,6 and 7). Moreover, during milling the material from the surface is ejected in every direction and can be redeposited on the walls of the milled area (**Figure 40**-c,5). Finally, when material from the surface is ejected, some holes can be seen on the milled surface area (**Figure 40**-b,3).

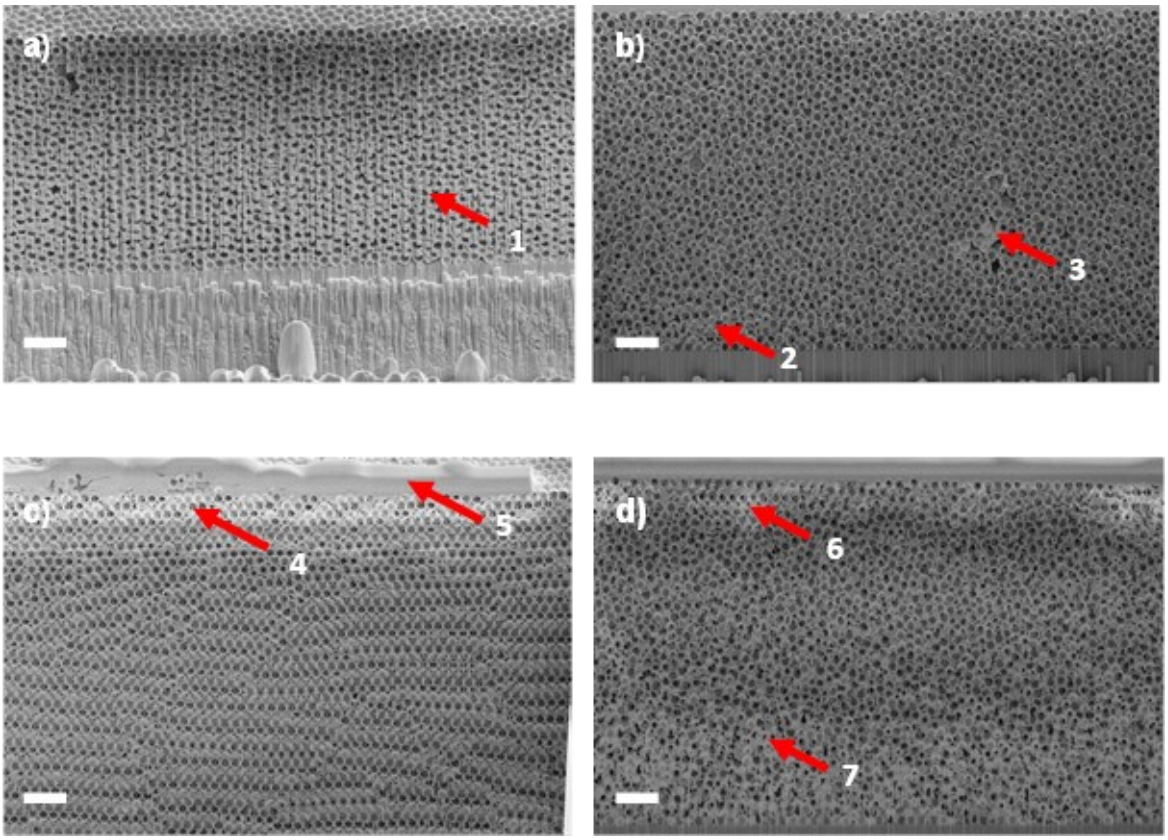

Figure 40. Focused Ion Beam (FIB) images of inverse alumina opal photonic crystals produced at a) 40°C, 45%, b) 40°C, 70%, c) 55°C, 70% and d) 80°C, 70% (evaporation temperature and relative humidity, respectively). The scale bars represent 1 µm. The numbered arrows 1, 2, 4, 6 and 7 present heat damaged areas of the tested samples; 3 and 5 show the curtain effect and redeposited material, respectively.

Considering that all FIB-SEM images showed a very damaged area, caused by FIB-SEM effects, a detailed investigation of the inverse opals structures was not possible by applying this technique.

4.3 Heat Treatment of Inverse Alumina Opal Photonic Crystals

4.3.1 Phase identification

XRD data were collected with angular sweeping from 2θ, 20° to 60° at 0.1◦/min (**Figure 41** and **Figure 42**) before and after high temperature heat treatment. Before sintering, it is possible to see

that the photonic crystal sample is covered by amorphous alumina. No crystalline phase can be identified from the diffractogram (**Figure 41**). As all produced samples were covered with the same material and presented amorphous phase, as shown in **Figure 41,** only the result from the sample prepared at 50°C and 70% (evaporation temperature and relative humidity) is represented in **Figure 41**, as a reference. The peak between 20° and 25° is typical of the sapphire substrate.[101]

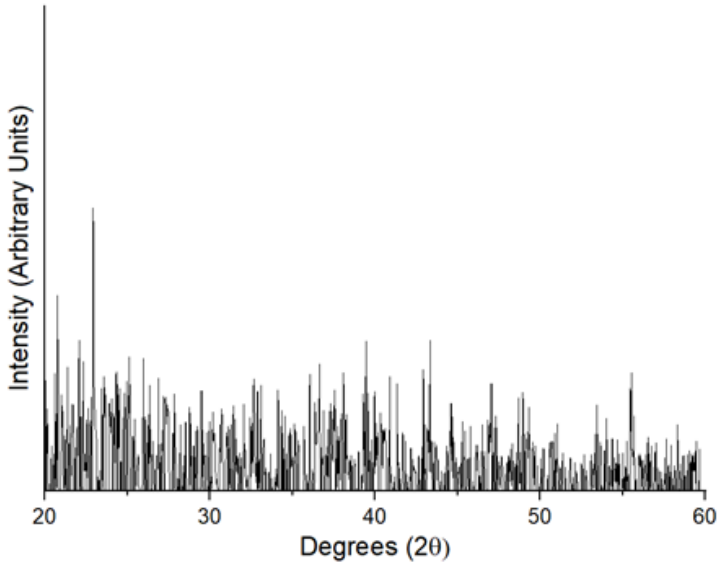

Figure 41. XRD diffractogram of an inverse alumina opal photonic crystal after burning out produced at 55 °C, 70% (evaporation temperature and relative humidity).

The phases, after both heat treatments, were identified by comparison with the ICDD (corundum, 00-010-0173). The XRD patterns of all samples do not show the high intensity and broad peaks of alumina in α-alumina phase. It may had occurred because of an overlap of corundum peaks with the peaks of the substrate (sapphire) and the other phases that are not evidently discernible [102] in the diffractogram, as the peaks between 42.5° and 45°.

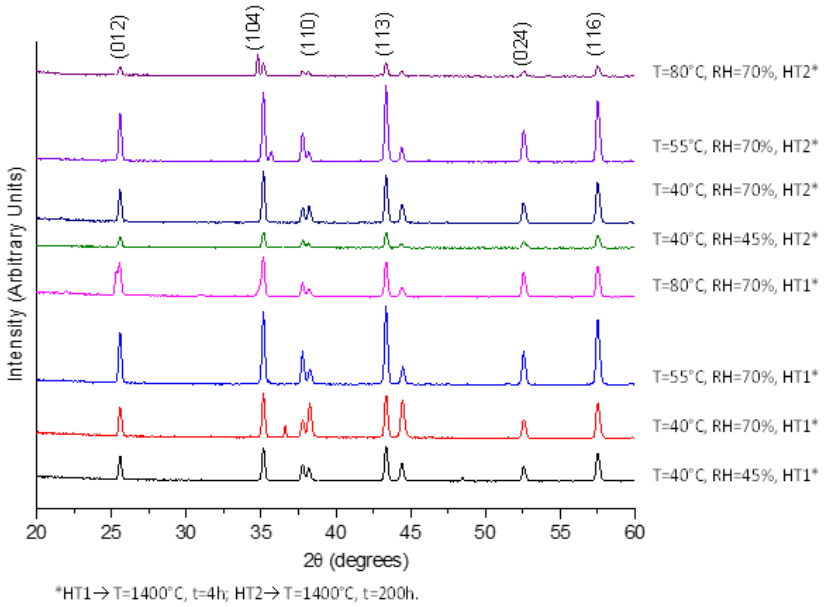

Figure 42. XRD diffractogram of heat-treated inverse alumina opal photonic crystals.

During high temperature treatment of alumina, various transition alumina phases are formed before reaching the most stable phase, α-Al_2O_3. [103–105] The thermal stability of porous transition alumina at high temperature is a crucial challenge for several applications.[104] The structural transformation of transition alumina into well crystallized α-Al_2O_3, which occurs at around 1200°C, is described by a nucleation and growth mechanism. [103] The samples produced during this research were heat treated at 1400 °C for 4 h and 200 h. As previously discussed by Rossignol et al.[103], Boumaza et al.[104] and Kumagai et al.[105], at this temperature alumina is already in α-Al_2O_3 phase, as can be seen in **Figure 42**.

4.3.2 Ordering and Structural Defects

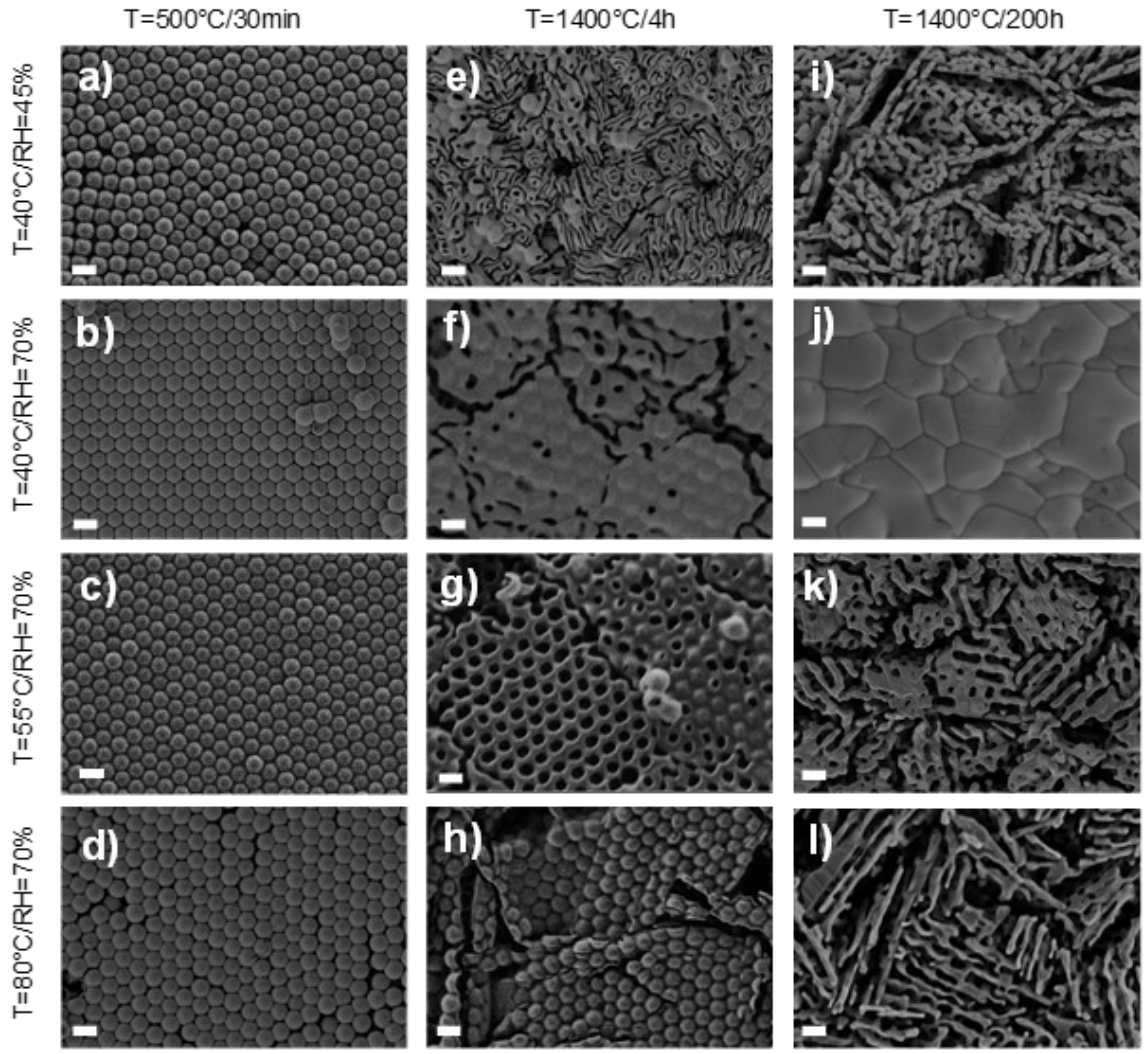

Figure 43. SEM top view images showing the structural evolution of the produced inverse alumina opal photonic crystals after each heat treatment. The scale bars represent 0.5 μm.

The evolution of the inverse alumina opals photonic crystals after each heat treatment was evaluated. SEM analysis (**Figure 43**) has been done in the aim to investigate the sintering effect on the 3D structures. As previously discussed, it was found that with the increase of the evaporation temperature, the colloidal crystal shows an increasing amount of defects due to the fast water evaporation rate.[106] As with RH, the evaporation temperature during vertical deposition also influences the solvent evaporation rate, and thus it is an important parameter during crystal growth.

Kuai et al.[4] and Ye et al.[106] produced high quality colloidal crystals from aqueous solutions with a vertical deposition technique. Both authors found that processing parameters have a strong influence on ordering and defects amount present in the resultant structures. **Figure 43** shows top view SEM

images of inverse alumina opals photonic crystals presenting this same tendency, i.e., the self-assembly parameters adopted on the direct polystyrene photonic crystals preparation kept their effects after each heat treatment performed in this work. Nonetheless, it is also possible to see that the self-assembly parameters structural influence is magnified with heat treatment.

In **Figure 43,** it is possible to observe that the dwell time and temperature had a significant influence on the final 3D structure. An increasing on structure degradation can be perceived, when the inverse alumina opals structures are compared after burning out, heated at 1400 °C for 4 h and 200 h. After burning out (**Figure 43**- a, b, c and d), the structures remained stable, i.e., thermal damages cannot be visually noted. However, after heating the samples to 1400 °C for 4 h, it is already possible to see some thermal damages. Finally, after 200 h at 1400 °C, the collapse of almost all 3D structures occurred. The sample produced at 40°C and 70% (evaporation temperature and relative humidity, respectively) showed a different behavior: its surface did not collapse but densified instead. The self-assembly tests were repeated in the aim to check the reproducibility of the results and it was confirmed.

Lin et al.[107] prepared inverse alumina opal photonic crystals and heated the samples at 1200 °C, 1 h and at 1400 °C, 1 h. Lin et al.[107] observed that until 1200 °C the inverse alumina opal photonic crystals remained without any significant degradation, contrasting with the ones that reached 1400 °C, which were damaged, presenting a vermicular structure. Furlan et al.[5] fabricated highly porous α-alumina and, as Lin et al.[107], heat treated the samples at 1200 °C, 1 h. Nevertheless, Furlan et al.[5] had already a vermicular structure at 1200 °C; subsequently, they heated the inverse alumina opal photonic crystals to 1400 °C, 4 h and also obtained a vermicular structure. These resultant structures from Furlan et al.´s[5] work presented the same vermicular structure as the ones heated to 1200 °C. In the current work, only the inverse opals produced at 55 °C, 70% (evaporation temperature, relative humidity) were heated to 1200 °C for 1 h and 4 h; the rest of the samples were heated to 1400 °C for 4 h and 200 h. The samples heat treated at 1200 °C for 1 h and 4 h had no several structural changes; the ones submitted to 1400 °C for 200 h completely collapsed, which was also found by Lin et al.[107] but not by Furlan et al.[5]. The difference between the results obtained can be explained by the discrepancy in the dwell time or the heating rate. Also, cross section SEM images (Figure 44) were performed to allow a deeper study of the resultant 3D structures.

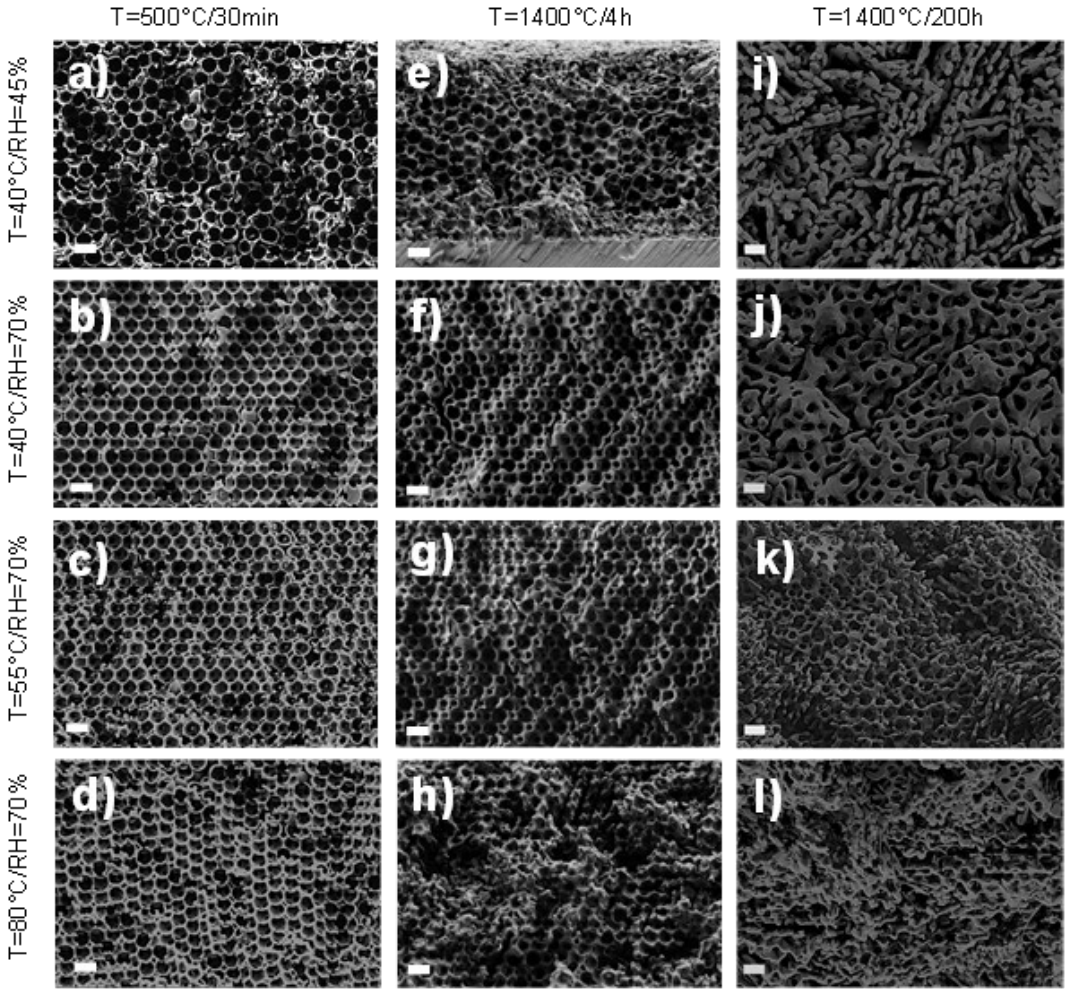

Figure 44. SEM cross section images showing the structural evolution of the produced inverse alumina opal photonic crystals after each heat treatment. The scale bars represent 0.5 µm.

Considering the principles of heat treatment on highly porous structures,[108,109] a possible explanation for the discrepancy between the top view (Figure 43) and cross section (Figure 44) SEM images can be elaborated. The inverse opals were sintered having electric resistances as a heating source, which may provide heat transfer by conduction, radiation, and convection on the material´s surface. However, in highly porous structures such as the ones showed in Figure 43, gas phase conduction, recirculatory convective gas flow and convective gas flow through interconnected porosity might happen.[110] Clyne et al.[110] analyzed how heat transfer takes place in porous materials of various types (Figure 45), including metals and ceramics. They found that the heat transfer in porous materials is slower than in bulk materials leading to a higher temperature on the surface than in the porous area of the samples.

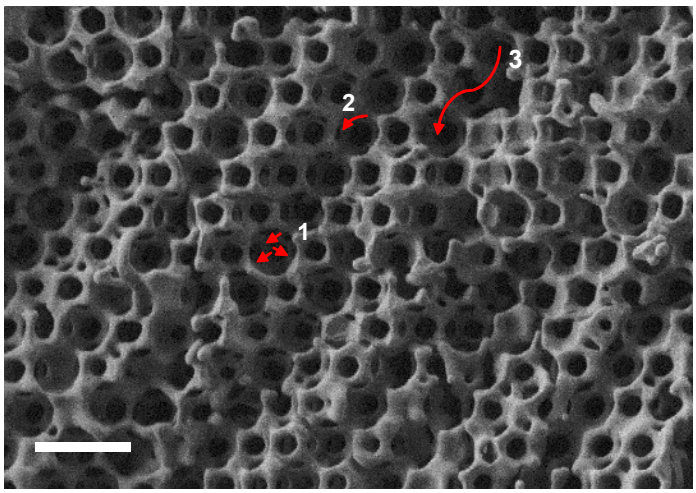

Figure 45. Typical porous structures heating transfer (1- gas phase conduction, 2- recirculatory convective gas flow, and 3- convective gas flow through interconnected porosity) showed in a SEM image of an inverse alumina opal photonic crystal produced at 55 °C and 70% (evaporation temperature and relative humidity) and heat treated at 1400 °C for 4 h. The scale bar represents 1 μm.

This difference, between the top view and cross section areas, is even more noticeable in **Figure 43**-j, in which is also possible to perceive a discrepancy between this, and the other structures showed in **Figure 43** as well. Lamouri et al.[111] studied the aptitude to sintering green bodies using γ-Al_2O_3 as raw powder. Lamouri et al.[111] focused on the influence of the heating rate on densification and microstructural evolution, and found that lower heating rates led to higher grain growth. Just as in this work, the alumina densification is based on grain growth and nucleation; consequently, at lower heating rates, it is possible to obtain more densified samples. Nonetheless, all samples produced in that case were sintered at the same heating rate (5 °C/min). Another observation of Lamouri et al.[111] is that the formation of a glassy phase – located in grain boundaries and triple points – facilitates alumina densification during sintering, which could be what happened with the structure presented in **Figure 43**-j. **Figure 46** shows the structure obtained by Lamouri et al.[111] (**Figure 46**-a) and in this work in a higher magnification than showed in Figure 43-j **(Figure 46**-b)

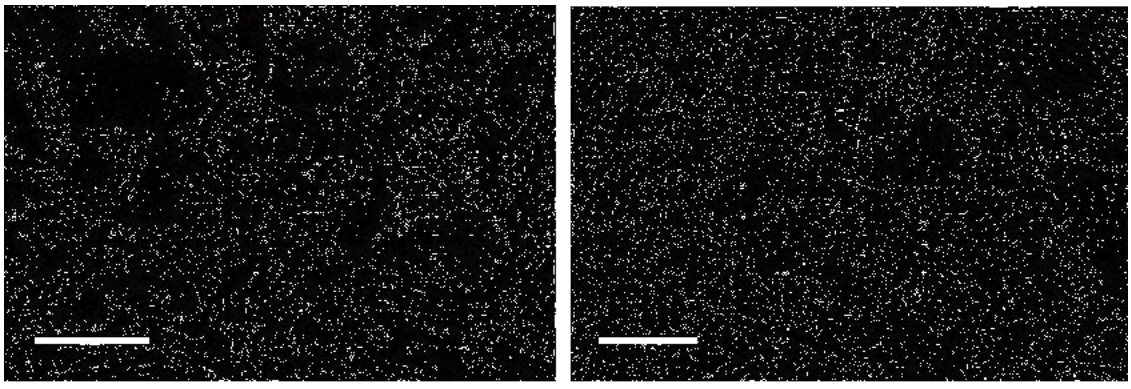

Figure 46. SEM images of a) inverse alumina opal photonic crystal produced with 40 °C, 70% (evaporation temperature and relative humidity) heat treated to 1400 °C for 4 h and b) alumina powder heat treated at 1700 °C for 2 h (Adapted from Lamouri et al[111]). Scale bars represent 1 μm.

The samples in **Figure 43** and **Figure 44** were prepared with different combinations of self-assembly parameters (polystyrene concentration, evaporation temperature and relative humidity). As previously discussed, these processing parameters have a strong influence on structure ordering. The inverse alumina photonic crystals produced at 40 °C, 70% (evaporation temperature and relative humidity, respectively) presented the most ordered structure, when compared with the ones fabricated using other self-assembly parameters combinations. A possibility is that because of the high organization order, the alumina shells, after atomic layer deposition (ALD), were closer than in other samples, facilitating the production of a more densified structure as showed in **Figure 43**-j. With the objective of making a comparison of the 3D structure produced in this research and the one obtained by Lamouri et al.,[111] the grain size of the structure showed in **Figure 43**-j was measured (Image J). The grain size was around 3.7±1.1 µm, which is similar to Lamouri et al.[111] result for the structure in **Figure 46**-b (3.2 µm), corroborating with the hypothesis that the same phenomenon had occurred in both structures. Thus, a high densification was related to grain growth, a typical behavior of alumina materials.

4.3.3 Crystallinity and Grain Size Estimation

To understand the structural characteristics of sintered inverse alumina opal photonic crystals, TEM investigations were carried out. TEM was also used to estimate inverse alumina opals grain size. TEM pictures were taken at two different magnifications (25k and 45k) to obtain information about the sample in general, plus a closer visualization of the grains. The estimative of the grain size analysis were performed using Image J (version 1.51 J8).

Figure 47 shows TEM images that were used in grain size estimative. At least 30 measurements of each sample were done.

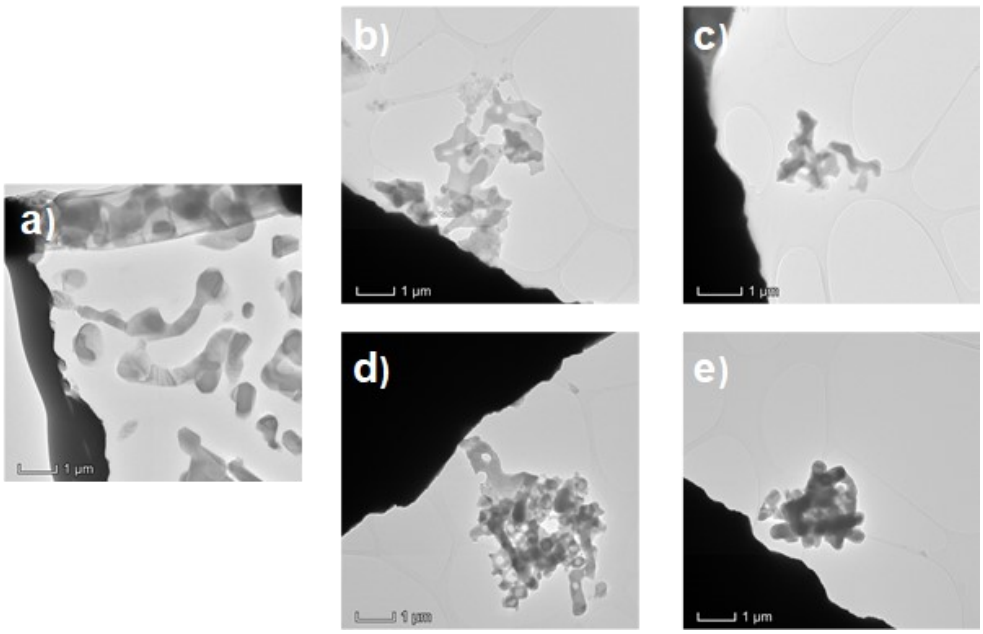

Figure 47. TEM images of inverse alumina opal photonic crystals produced at a) and d) 55 °C,

70%, b) 40 °C, 45%, c) 40 °C, 70% and e) 80 °C, 70%; heat treated at 1400 °C for 4 h (a) and 200 h (b,c,d,e).

TEM analysis reveals that the structures consist of single grain domains of up to 1.6 μm, each containing a randomly interconnected network of alumina ligaments that share a common crystalline orientation, suggesting a different mechanism of grain boundary migration during sintering. It was also found that the dwell time has influence on the alumina grain size. The inverse alumina opals produced at 55 °C and 70% (evaporation temperature and relative humidity, respectively) and sintered at 1400 °C for 4 h had the grain size of 1.0±0.2 μm. The samples, fabricated with the same conditions, but heat treated at 1400 °C for 200 h presented grain size of 1.6±0.3 μm. Thus, different processing parameters seemed to have a great influence on the structural ordering and defects, but not on the grain size. This aspect seemed to depend principally on the material, in this case, alumina.

Furlan et al.[5] applied TEM analysis to estimate grain size of 3D inverse alumina opals produced at 55 °C and 70% RH, and sintered at 1400 °C for 4 h. In that case, values of 3 μm were found for the structured grain size. TEM is often used to determine the size or distribution size of grains and particles. Nevertheless, this method is open to human errors, once finding and stipulating the grain boundaries depends on the person that is making the analysis; so it is possible to say that only a grain size estimation can be done rather than a determination.[112]

In the aim of having a more accurate grain size measurement many reasearchers[113–116] use XRD diffraction associated with TEM. For the samples investigated in this work, this was not possible because the grain size was over 1 μm, and the obtained XRD diffractograms had broad peaks with low counting, which hindered the application of the Rietveld method.[117]

Figure 48 shows the bright field TEM image of α-alumina single crystal and corresponding selected area electron diffraction (SAED) pattern, which confirm that the free-standing crystal presents single crystal characteristics. **Figure 48** shows SAED patterns of the inverse alumina opal photonic crystals heat treated at 1400 °C for 200 h and for the inverse alumina opal photonic crystals sintered at 1400 °C for 4 h of the sample produced at 55 °C and 70% RH, which were adopted as reference. The objective of applying TEM on these samples after the first and second sintering steps (1400 °C for 4 h and 200 h, respectively) was to verify if the single crystals characteristics would remain after 200 h of heat treatment, which seems to happen when comparing **Figure 48**(b and d).

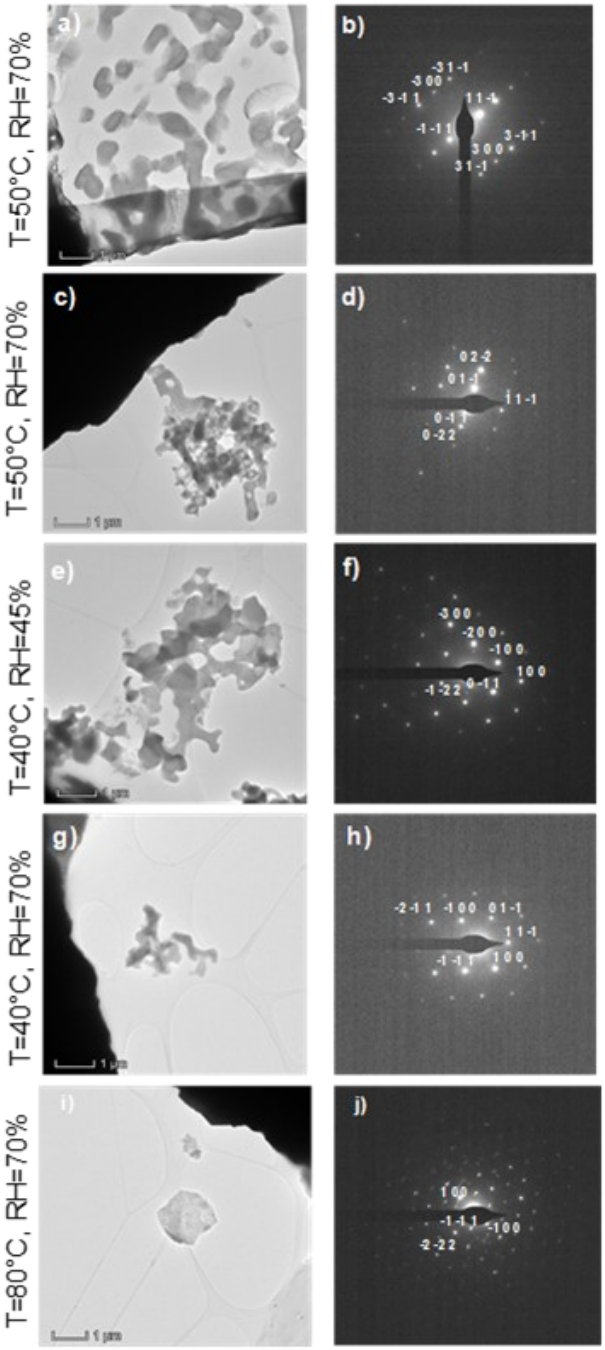

Figure 48. TEM images (a,c,e,g and i) and SAED patterns of inverse alumina opal photonic crystals heat treated at 1400 °C for 4 h (a and b) and 200 h (c,d,e,f,g,h,i and j). The used self-assembly parameters are on figures right side.

SAED patterns, including its diffraction indices, from inverse alumina opal photonic crystals are shown in **Figure 48**. Indexing this pattern proves the presence of pure α-alumina in these samples. SAED patterns were acquired from several areas in inverse alumina opal photonic crystals and only

α-alumina was detected in all of them. However, as SAED only probes the crystal structure locally[118,119], then the patterns were acquired from several areas in inverse alumina opal photonic crystals and the results were consistent in all the different areas.

4.3.4 Mechanical Stability Comparison

The produced photonic crystals, after each heat treatment, had their mechanical stability evaluated by the application of nanoindentation. A nanoindenter was used with a fixed depth (2000 nm) and displacement rate (10 $nm \cdot s^{-1}$). These parameters were based on the ones used by Rosário et al. [73], who measured mechanical properties of inverse titania opal photonic crystals applying this method.

Nevertheless, differently from Rosário et al.[73], here the nanoindentation test was applied with the objective of providing a comparison of mechanical stability. Our objective was not to measure a specific mechanical property, but perform and compare load-displacement curves (**Figure 49**). It is possible to see in this case that the load value varied widely along the same sample. The percent of the load divergence for each sample was calculated and it is shown in Table 1. Load percent divergence in relation to self-assembly and heat treatment parameters.

Table 1. Load percent divergence in relation to self-assembly and heat treatment parameters.

Heat treatment temperature, time	**Evaporation Temperature, Relative Humidity**			
	40 ºC, 45%	**40 ºC, 70%**	**55 ºC, 70%**	**80 ºC, 70%**
500 ºC, 30 min	33.0±8.5%	37.5±9.7%	32.0±9.4%	53±10%
1400 ºC, 4 h	33±17%	58±19%	59±20%	75±18%
1400 ºC, 4 h	-	75±21%	71±20%	80±19%

This high divergence between load values for the sample may be related to the defects present in the sample, such as cracks or faults. Besides, we can do a correlation with the defects evaluation that had been done. In this case, the evaporation temperature showed to be a key factor on the production of a high-quality photonic crystal. The photonic crystal produced at 80 °C, 70% RH presented higher percent divergence in load measurements and also standard deviation, which can lead to think that a more defective, and consequently more instable sample will have higher load divergence percentage and standard deviation values.

Nevertheless, performing nanoindentation in highly porous materials is quite challenging and demands special care. It depends heavily on the area to be analyzed and how instable the specimen is. The samples produced at 40 °C, 45% RH can lead to the idea that these samples are more stable than the others; however, they are in fact the most instable. After heat treatment at 1400 °C for 200 h, the film was completely removed from the substrate during the test. This was repeated three times with the same result. Keeping this fact in mind, we can say that this test has a tricky interpretation.

Another way to analyze the results is to observe the loading curve. Undulation with small amplitude

can be seen as nonuniformity or even collapse of the pores.[71] The samples were previously analyzed by SEM, so it is known that the samples are quite ordered, leading to the idea that this undulations can be related directly to the collapse of pores and an idea of mechanical stability comparison can be taken.

Analyzing the graphs visually (**Figure 49**), based on the concept that the undulation on the loading curve are related to the pores collapsing, it would be possible to say that the samples after burn-out produced at 50 °C, 70% RH are the most stable structure, followed by the fabricated at 40 °C, 70% RH and 80 °C, 70% RH, respectively. Moreover, the most instable structure is the one produced at 40 °C, 45% RH as self-assembly parameters.

After the heat treatment at 1400 °C for 4 and 200 h, the comparison is not that intuitive anymore. It seems that after sintering, the mechanical stability of all samples was decreased. Whilst after sintering the most stable structure seems to be the ones produced at 40 °C, 70% instead of 55 °C, 70%, followed by the one produced with 80 °C, 70%, we can say that the same tendency as after burn-out occurred. The most instable sample after heat treatment process kept being the one fabricated at 40 °C, 45% RH.

Considering that 40 °C, 70% and 55 °C, 70% are very similar (the polymer concentration was kept as 1.5 mg/ml for both cases) the obtained tendency to the mechanical stability of inverse opals after heat treatment at high temperatures even for long periods (200 h) match with the area fraction defects in relation of the tested self-assembly parameters, evaporation temperature and relative humidity. The lower the relative humidity, and the higher the evaporation temperature, the faster the solvent evaporation leading to more structural defects as already discussed in this thesis.

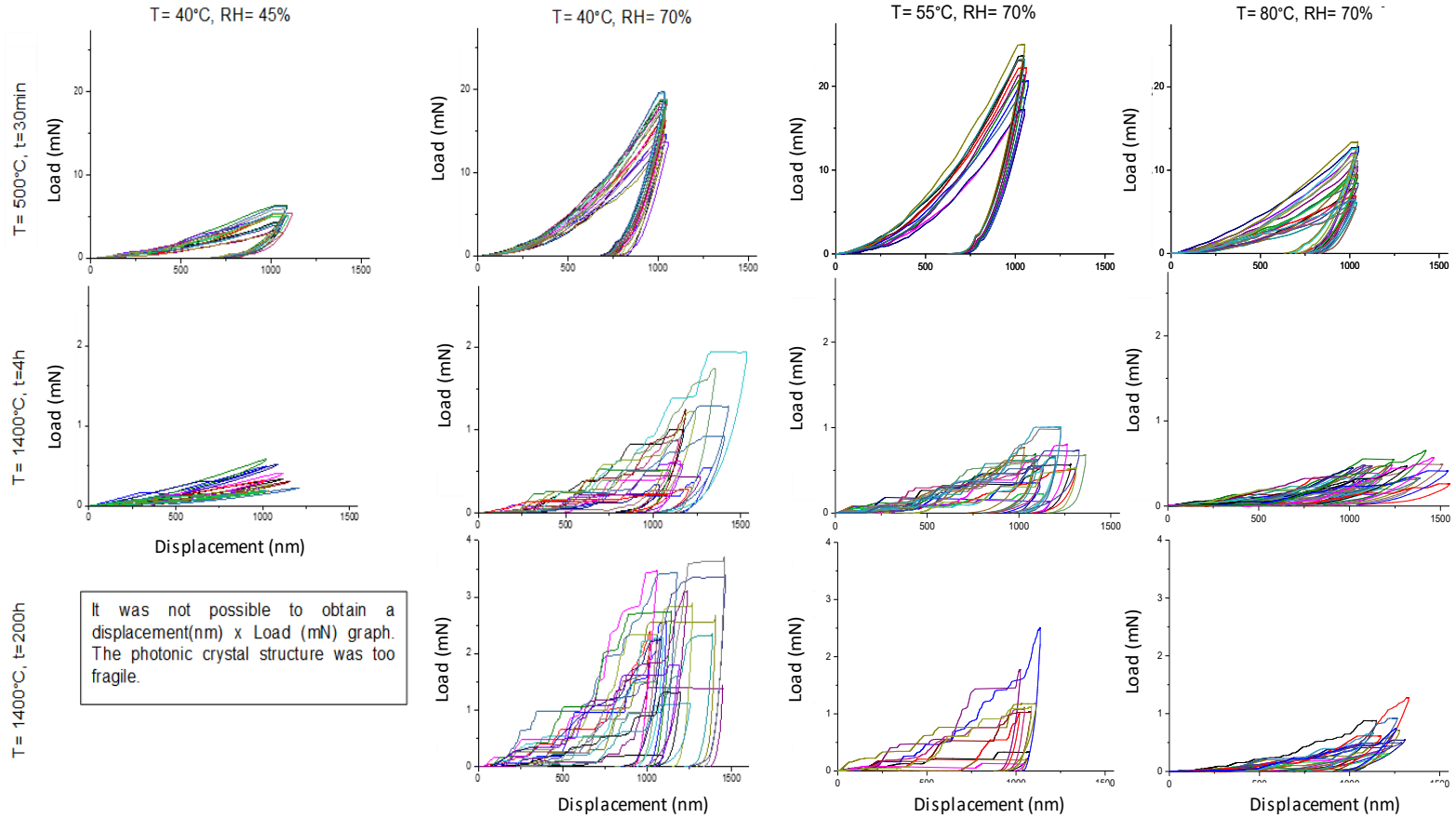

Figure 49. Load x Displacement curves of the produced inverse alumina opal photonic crystals.

5 CONCLUSIONS AND PERSPECTIVES

5.1 Conclusions

Photonic crystals of polystyrene particles were self-assembled on sapphire substrates by vertical deposition through liquid evaporation. The number of defects in the direct photonic crystals increased with PS concentration and evaporation temperature and decreased with relative humidity up to a limit value in which self-assembly failed. Thickness was also affected by these parameters in different trends and synergic way, though. The resulting reflectance capability of both direct and inverse opal photonic crystals was primarily affected by the self-assembly parameters. Although ALD and polymeric template burn-out performed at 500 °C introduced some defects in the structures, the main key factor influencing the resulting photonic band gap and reflectance capability was the self-assembly process. Concerning the performance of the ceramic inverse opal photonic crystals, the optimum parameters for self-assembly related to both lower defects density and substrate adhesion were 40 °C, 70% RH and 1.5 mg/ml of suspension concentration.

The produced photonic crystals were heat treated to 1400°C for 4 and 200 h, and a correlation between the self-assembly parameters' combinations and the resultant 3D structures thermal stability was found. Although the sintering process had introduced some defects such as cracks, vacancies and distortions, processing parameters showed to have more influence on the photonic crystals' thermal stability.

A different response to the sintering process was shown on the surface and in the center of the structures. A heat gradient in the structure was found as a possible cause for this behavior. Besides, the structures fabricated at 40 °C, 70% RH and 1.5 mg/ml of suspension concentration had a peculiar result, when compared to the other structures produced with different processing parameters combination. An organizational issue was sustained as a thinkable explanation.

The sintering dwell time influence was also evaluated and seemed to contribute to a higher grain growth, which also activated the collapse of the photonic crystals' structures. The 3D structures remained stable until 1400°C for 4 h, but not after 200 h. The crystallinity and the grains orientation do not seem to be affected by either self-assembly or tested sintering dwell time or temperature.

A novel method to evaluate the mechanical stability of the produced photonic crystals was proposed. Nanoindentation tests were performed creating load-displacement curves that allowed the comparison of the 3D photonic structures mechanical stability. The mechanical behavior of the inverse alumina 3D structures permitted a correlation between the influence of the self-assembly parameters and the mechanical behavior of the heat-treated photonic crystals. We can say that the same effect of the processing parameters on the direct photonic crystals remained on the inverse alumina 3D structures. The photonic crystals produced at 40°C, 70% and 1.5 mg/ml (evaporation temperature, relative humidity and polystyrene concentration) seemed to be the most stable, and the one fabricated at 40°C, 45% and 1. 5 mg/ml, the most unstable structure.

5.2 Perspectives

The processing parameters combination showed to have a great influence on photonic crystals ordering. Thus, the manipulation of self-assembly parameters could be used to produce not only photonic crystals, but also photonic glasses, which are also attractive materials, because of their potential applications.

The study of thermal stability at high temperatures was performed for inverse alumina opal photonic crystals. For a short period of time (4 h) the structures remained stable, but not for a long period (200h). In the aim to have 3D photonic crystals with a higher thermal stability, new materials should be tested. For instance, composites with alumina and ceria or titania, due to their mechanical properties, should be some options. In addition, higher temperatures could be tested so that a wider number of applications for these materials can be foreseen.

Finally, considering the potentiality showed by nanoindentation results, it is suggested to evaluate the mechanical stability of the inverse 3D structures and correlate it with processing parameters. A further mathematical modeling would enable to have theoretical results for such properties. Parameters should be investigated to provide more precise results and to allow designing 3D structures with a tailored mechanical behavior.

6 REFERENCES

(1) Shklover, V.; Braginsky, L.; Witz, G.; Mishrikey, M.; Hafner, C. High-Temperature Photonic Structures. Thermal Barrier Coatings, Infrared Sources and Other Applications. *Jnl of Comp & Theo Nano* **2008**, *5*, 862–893.

(2) Dyachenko, P. N.; do Rosário, J. J.; Leib, E. W.; Petrov, A. Y.; Kubrin, R.; Schneider, G. A.; Weller, H.; Vossmeyer, T.; Eich, M. Ceramic Photonic Glass for Broadband Omnidirectional Reflection. *ACS Photonics* **2014**, *1*, 1127–1133.

(3) Marichy, C.; Muller, N.; Froufe-Pérez, L. S.; Scheffold, F. High-quality photonic crystals with a nearly complete band gap obtained by direct inversion of woodpile templates with titanium dioxide. *Scientific reports* **2016**, *6*, 21818 EP -.

(4) Kuai, S.-L.; Hu, X.-F.; Haché, A.; Truong, V.-V. High-quality colloidal photonic crystals obtained by optimizing growth parameters in a vertical deposition technique. *Journal of Crystal Growth* **2004**, *267*, 317–324.

(5) Furlan, K. P.; Pasquarelli, R. M.; Krekeler, T.; Ritter, M.; Zierold, R.; Nielsch, K.; Schneider, G. A.; Janssen, R. Highly porous α-Al 2 O 3 ceramics obtained by sintering atomic layer deposited inverse opals. *Ceramics International* **2017**, *43*, 11260–11264.

(6) Zhang, J.; Sun, Z.; Yang, B. Self-assembly of photonic crystals from polymer colloids. *Current Opinion in Colloid & Interface Science* **2009**, *14*, 103–114.

(7) Anthony Smallwood. 35 Years on a new look at sythetic opal. *Australian Gemmlogist,* 2003, 438–447.

(8) Joannopoulos, J. D.; Villeneuve, P. R.; Fan, S. Photonic crystals: putting a new twist on light. *Nature* **1997**, *386*, 143 EP -.

(9) Shao, J.; Liu, G.; Zhou, L. Biomimetic nanocoatings for structural coloration of textiles. *Active Coatings for Smart Textiles*; Elsevier, 2016; pp 269–299.

(10) Wang, Z.; Guo, Z. Biomimetic photonic structures with tunable structural colours: From natural to biomimetic to applications. *Journal of Bionic Engineering* **2018**, *15*, 1–33.

(11) Yablonovitch, E. Photonic Crystals. *Journal of Modern Optics* **1994**, *41*, 173–194.

(12) Stcvcn G. Johnson and J.D.Joannopoulos. Introduction to Photonic Crystals: Bloch's Theorem, Band Diagrams, and Gaps (But No Defects), 2003, 1–16.

(13) K.M. Ho, C.T.Chan, C.M Soukoulis, R. Biswas and M. Sigalas. Photonic Band Gaps In Three

Dimensions : New Layer-by-Layer Periodic Structures, 1994, 413–416.

(14) Fan, S. Manipulating light with photonic crystals. In *AIP Conference Proceedings*; AIP, 2000; pp 57–76.

(15) Aoki, K.; Miyazaki, H. T.; Hirayama, H.; Inoshita, K.; Baba, T.; Sakoda, K.; Shinya, N.; Aoyagi, Y. Microassembly of semiconductor three-dimensional photonic crystals. *Nature Materials* **2003**, *2*, 117 EP -.

(16) Chen, J.; Jiang, W.; Chen, X.; Wang, L.; Zhang, S.; Chen, R. T. 3D holographic polymer photonic crystal for superprism application. In ; Adibi, A., Lin, S.-Y., Scherer, A., Eds.; SPIE, 2007; p 648013.

(17) Toshihiko Baba. Photonic Crystals - An Introduction, 1–4.

(18) Celanovic, I.; O'Sullivan, F.; Jovanovic, N.; Qi, M.; Kassakian, J. G. 1D and 2D photonic crystals for thermophotovoltaic applications. In ; La Rue, R. M. D., Viktorovitch, P., Sotomayor Torres, C. M., Midrio, M., Eds.; SPIE, 2004; p 416.

(19) Cai, Z.; Smith, N. L.; Zhang, J.-T.; Asher, S. A. Two-dimensional photonic crystal chemical and biomolecular sensors. *Analytical chemistry* **2015**, *87*, 5013–5025.

(20) Shen, H.; Wang, Z.; Wu, Y.; Yang, B. One-dimensional photonic crystals: fabrication, responsiveness and emerging applications in 3D construction. *RSC Adv.* **2016**, *6*, 4505–4520.

(21) Yablonovitch; Gmitter; Leung. Photonic band structure: The face-centered-cubic case employing nonspherical atoms. *Physical review letters* **1991**, *67*, 2295–2298.

(22) Arpin, K. A.; Losego, M. D.; Cloud, A. N.; Ning, H.; Mallek, J.; Sergeant, N. P.; Zhu, L.; Yu, Z.; Kalanyan, B.; Parsons, G. N.*; et al.* Three-dimensional self-assembled photonic crystals with high temperature stability for thermal emission modification. *Nature communications* **2013**, *4*, 2630.

(23) Sung Park, S. in; Tae Ho Lee, Jin Ho Ahn, Seoul:Rana BisWas, Ames; Kristen; Kai-Ming; Jae-HWang Lee; Brookline. Manufacturing Method of Photonic Crystal.

(24) Bormashenko, E.; Pogreb, R.; Musin, A.; Stanevsky, O.; Bormashenko, Y.; Whyman, G.; Gendelman, O.; Barkay, Z. Self-assembly in evaporated polymer solutions: influence of the solution concentration. *Journal of colloid and interface science* **2006**, *297*, 534–540.

(25) Meijer, J.-M.; Hagemans, F.; Rossi, L.; Byelov, D. V.; Castillo, S. I. R.; Snigirev, A.; Snigireva, I.; Philipse, A. P.; Petukhov, A. V. Self-assembly of colloidal cubes via vertical deposition. *Langmuir : the ACS journal of surfaces and colloids* **2012**, *28*, 7631–7638.

(26) Weiss, D.; Kreger, K.; Schmidt, H.-W. Self-Assembly of Alkoxy-Substituted 1,3,5-Benzenetrisamides Under Controlled Conditions. *Macromol. Mater. Eng.* **2017**, *302*, 1600390.

(27) Rengarajan, R.; Mittleman, D.; Rich, C.; Colvin, V. Effect of disorder on the optical properties of colloidal crystals. *Physical review. E, Statistical, nonlinear, and soft matter physics* **2005**, *71*,

16615.

(28) Y. K. Koh; L. K. Teh; C. C. Wong. *Defects in Self Assembled Colloidal Crystals*, 11/18/2004.

(29) J. Hilhorst; V.V. Abramova; A. Sinitskii; N.A. Sapoletova; K.S. Napolskii; A.A. Eliseev; D.V. Byelov; N.A. Grigoryeva; A.V. Vasilieva; W.G. Bouwman*; et al.* Stacking faults in colloidal photonic crystals revealed by microradian X-ray diffraction.

(30) Meseguer, F.; Blanco, A.; Míguez, H.; García-Santamaría, F.; Ibisate, M.; López, C. Synthesis of inverse opals. *Colloids and Surfaces A: Physicochemical and Engineering Aspects* **2002**, *202*, 281–290.

(31) Armstrong, E.; O'Dwyer, C. Artificial opal photonic crystals and inverse opal structures – fundamentals and applications from optics to energy storage. *J. Mater. Chem. C* **2015**, *3*, 6109–6143.

(32) Waterhouse, G. I.N.; Waterland, M. R. Opal and inverse opal photonic crystals: Fabrication and characterization. *Polyhedron* **2007**, *26*, 356–368.

(33) Gaillot, D. P.; Summers, C. J. Photonic band gaps in non-close-packed inverse opals. *J. Opt. Soc. Am. B* **2006**, *100*, 113118.

(34) Míguez, H.; Chomski, E.; García-Santamaría, F.; Ibisate, M.; John, S.; López, C.; Meseguer, F.; Mondia, J. P.; Ozin, G. A.; Toader, O.*; et al.* Photonic Bandgap Engineering in Germanium Inverse Opals by Chemical Vapor Deposition. *Adv. Mater.* **2001**, *13*, 1634–1637.

(35) Seitaro Matsuo and Mikiho Kiuchi. Low Temperature Chemical Vapor Deposition Method Utilizing an Electron Cyclotron Resonance Plasma. *Japanese Journal of Applied Physics* **1983**, *22*, L210.

(36) Kirihara, S.; Miyamoto, Y.; Kajiyama, K. Fabrication of Ceramic-Polymer Photonic Crystals by Stereolithography and Their Microwave Properties. *J American Ceramic Society* **2002**, *85*, 1369–1371.

(37) Graugnard, E.; King, J. S.; Gaillot, D. P.; Summers, C. J. Sacrificial-Layer Atomic Layer Deposition for Fabrication of Non-Close-Packed Inverse-Opal Photonic Crystals. *Adv. Funct. Mater.* **2006**, *16*, 1187–1196.

(38) Kubrin, R.; Pasquarelli, R. M.; Waleczek, M.; Lee, H. S.; Zierold, R.; do Rosário, J. J.; Dyachenko, P. N.; Montero Moreno, J. M.; Petrov, A. Y.; Janssen, R.*; et al.* Bottom-up Fabrication of Multilayer Stacks of 3D Photonic Crystals from Titanium Dioxide. *ACS applied materials & interfaces* **2016**, *8*, 10466–10476.

(39) Ghadarghadr, S.; Fucetola, C. P.; Lee Cheong, L.; E. Moon, E.; I. Smith, H. 3D nanostructures by stacking pre-patterned fluid-supported single-crystal Si membranes. *Journal of Vacuum Science*

& Technology B, Nanotechnology and Microelectronics: Materials, Processing, Measurement, and Phenomena **2011**, *29*, 06F401.

(40) Mihi, A.; Ocaña, M.; Míguez, H. Oriented Colloidal-Crystal Thin Films by Spin-Coating Microspheres Dispersed in Volatile Media. *Adv. Mater.* **2006**, *18*, 2244–2249.

(41) Mijovic, J. S.; Koutsky, J. A. Etching of Polymeric Surfaces: A Review. *Polymer-Plastics Technology and Engineering* **1977**, *9*, 139–179.

(42) Leskelä, M.; Ritala, M. Atomic layer deposition (ALD): from precursors to thin film structures. *Thin Solid Films* **2002**, *409*, 138–146.

(43) Besler, R.; Rossetti da Silva, M.; do Rosario, J. J.; Dosta, M.; Heinrich, S.; Janssen, R. Sintering Simulation of Periodic Macro Porous Alumina. *J American Ceramic Society* **2015**, *98*, 3496–3502.

(44) Margarete Therese Schloßer. Vapor Transport Sintering of Calcium Phosphate Ceramics.

(45) German, R. M.; Munir, Z. A. A Kinetic Model for the Reduction in Surface Area during Initial Stage Sintering. In *Sintering and Catalysis*; Kuczynski, G. C., Ed.; Springer US: Boston, MA, 1975; pp 249–257.

(46) Song, J.; Gelin, J. C.; Barrière, T.; Liu, B. Experiments and numerical modelling of solid state sintering for 316L stainless steel components. *Journal of Materials Processing Technology* **2006**, *177*, 352–355.

(47) AIP Conference Proceedings; AIP, 2000.

(48) Lau, K.-T.; Cheung, H.-Y.; Lu, J.; Yin, Y.-S.; Hui, D.; Li, H.-L. Carbon Nanotubes for Space and Bio-Engineering Applications. *Jnl of Comp & Theo Nano* **2008**, *5*, 23–35.

(49) Scardi, P.; Galvanetto, E.; Tomasi, A.; Bertamini, L. Thermal stability of stabilized zirconia thermal barrier coatings prepared by atmosphere- and temperature-controlled spraying. *Surface and Coatings Technology* **1994**, *68-69*, 106–112.

(50) PANWAR, S. S.; PATRO, T. U.; BALASUBRAMANIAN, K.; VENKATARAMAN, B. High-temperature stability of yttria-stabilized zirconia thermal barrier coating on niobium alloy—C-103. *Bull Mater Sci* **2016**, *39*, 321–329.

(51) Padture, N. P.; Gell, M.; Jordan, E. H. Thermal barrier coatings for gas-turbine engine applications. *Science (New York, N.Y.)* **2002**, *296*, 280–284.

(52) Carter, M.; Shieh, J. Microscopy. *Guide to Research Techniques in Neuroscience*; Elsevier, 2015; pp 117–144.

(53) Guide to Research Techniques in Neuroscience; Elsevier, 2015.

(54) Jeremy Burgess. Electron Microscopy.

(55) Leonard, D. N.; Chandler, G. W.; Seraphin, S. Scanning Electron Microscopy. In *Characterization of Materials*; Kaufmann, E. N., Ed.; John Wiley & Sons, Inc: Hoboken, NJ, USA, 2002; p 819.

(56) Michael Agthe. Rare Earth Oxide Nanopowder (RE = Nd, Eu, Gd, Ho, Y, Yb) by Combustion Synthesis, Sulfation and Calcination.

(57) Kaufmann, E. N., Ed. *Characterization of Materials*; John Wiley & Sons, Inc: Hoboken, NJ, USA, 2002.

(58) Timmermann, J. Scannning Electron Microscopy. TUHH, Hamburg, 2020.

(59) Fabio Ciuffreda. Synthesis and characterization of Pt/polyoxometalates composite catalysts for PEM fuel cells.

(60) Wilson, W. A.; Roach, P. J.; Montero, M.; Baroja-Fernández, E.; Muñoz, F. J.; Eydallin, G.; Viale, A. M.; Pozueta-Romero, J. Regulation of glycogen metabolism in yeast and bacteria. *FEMS microbiology reviews* **2010**, *34*, 952–985.

(61) Muniz, F. T. L.; Miranda, M. A. R.; Morilla Dos Santos, C.; Sasaki, J. M. The Scherrer equation and the dynamical theory of X-ray diffraction. *Acta crystallographica. Section A, Foundations and advances* **2016**, *72*, 385–390.

(62) Brucker. https://www.bruker.com/pt/products/x-ray-diffraction-and-elemental-analysis/x-ray-diffraction/d8-advance/overview.html.

(63) Joachim Hedberg. Conduction Band Mediated Charge Transfer for Highly Reduced, Catalytically Active State: A Comparison Between Thin Films and Colloidal Solutions.

(64) Müller, M.; Zentel, R.; Maka, T.; Romanov, S. G.; Sotomayor Torres, C. M. Dye-Containing Polymer Beads as Photonic Crystals. *Chem. Mater.* **2000**, *12*, 2508–2512.

(65) Gu, Z.-Z.; Fujishima, A.; Sato, O. Fabrication of High-Quality Opal Films with Controllable Thickness. *Chem. Mater.* **2002**, *14*, 760–765.

(66) PerkinElmer. http://www.perkinelmer.com/product/lambda-1050-uv-vis-nir-spectrophotometer-l1050.

(67) Oleksandr Polonskyi. Preparation of nanocomposites of metal oxides in plasma polymer and study of their properties.

(68) Tihomir Gugov. Transmission electron microscopy characterization of long wavelength dilute nitrides.

(69) Wirth, R. Focused Ion Beam (FIB) combined with SEM and TEM: Advanced analytical tools

for studies of chemical composition, microstructure and crystal structure in geomaterials on a nanometre scale. *Chemical Geology* **2009**, *261*, 217–229.

(70) Central facility in electron microscopy. https://cime.epfl.ch/FIB-techniques.

(71) Šandera, P.; Pokluda, J.; Schöberl, T.; Horníková, J.; Černý, M. Modeling Load-displacement Curve and Pop-in Effect in Nanoindentation Tests. *Procedia Materials Science* **2014**, *3*, 1111–1116.

(72) Chen, X.; Xiang, Y.; Vlassak, J. J. Novel technique for measuring the mechanical properties of porous materials by nanoindentation. *J. Mater. Res.* **2006**, *21*, 715–724.

(73) do Rosário, J. J.; Berger, J. B.; Lilleodden, E. T.; McMeeking, R. M.; Schneider, G. A. The stiffness and strength of metamaterials based on the inverse opal architecture. *Extreme Mechanics Letters* **2017**, *12*, 86–96.

(74) Marqués-Hueso, J.; Schöpe, H. J. Regular Horizontal Patterning on Colloidal Crystals Produced by Vertical Deposition. In *Surface and Interfacial Forces – From Fundamentals to Applications*; Auernhammer, G. K., Butt, H.-J., Vollmer, D., Eds.; Springer Berlin Heidelberg: Berlin, Heidelberg, 2008; pp 48–56.

(75) Yoldi, M.; Arcos, C.; Paulke, B.-R.; Sirera, R.; González-Viñas, W.; Görnitz, E. On the parameters influencing the deposition of polystyrene colloidal crystals. *Materials Science and Engineering: C* **2008**, *28*, 1038–1043.

(76) Yan, Q.; Zhou, Z.; Zhao, X. S. Inward-growing self-assembly of colloidal crystal films on horizontal substrates. *Langmuir : the ACS journal of surfaces and colloids* **2005**, *21*, 3158–3164.

(77) McLachlan, M. A.; Johnson, N. P.; La Rue, R. M. D.; McComb, D. W. Thin film photonic crystals: synthesis and characterisation. *J. Mater. Chem.* **2004**, *14*, 144.

(78) Liu, G. Q.; Wang, Z. S.; Ji, Y. H. Influence of growth parameters on the fabrication of high-quality colloidal crystals via a controlled evaporation self-assembly method. *Thin Solid Films* **2010**, *518*, 5083–5090.

(79) Vogel, N.; Retsch, M.; Fustin, C.-A.; Del Campo, A.; Jonas, U. Advances in colloidal assembly: the design of structure and hierarchy in two and three dimensions. *Chemical reviews* **2015**, *115*, 6265–6311.

(80) Fang, Y.; Lee, W. C.; Canciani, G. E.; Draper, T. C.; Al-Bawi, Z. F.; Bedi, J. S.; Perry, C. C.; Chen, Q. Thickness control in electrophoretic deposition of WO3 nanofiber thin films for solar water splitting. *Materials Science and Engineering: B* **2015**, *202*, 39–45.

(81) Liau, L. C.-K.; Huang, Y.-K. Effects of influential factors on sedimentation self-assembly processing of photonic band gap crystals by relative humidity-controlled environments. *Chemical Engineering and Processing: Process Intensification* **2008**, *47*, 1578–1584.

(82) Zhou, L.; Wu, Y.; Chai, L.; Liu, G.; Fan, Q.; Shao, J. Study on the formation of three-dimensionally ordered SiO 2 photonic crystals on polyester fabrics by vertical deposition self-

assembly. *Textile Research Journal* **2016**, *86*, 1973–1987.

(83) Liu, T.-T.; Tian, W.; Song, Y.-L.; Bai, Y.; Wei, P.-L.; Yao, H.; Yan, H.-X. Reversible Self-Assembly of Backbone-Thermoresponsive Long Chain Hyperbranched Poly(N-Isopropyl Acrylamide). *Polymers* **2016**, *8*, 33.

(84) Im, S. H.; Park, O. O. Effect of Evaporation Temperature on the Quality of Colloidal Crystals at the Water−Air Interface. *Langmuir : the ACS journal of surfaces and colloids* **2002**, *18*, 9642–9646.

(85) Min, Y.; Akbulut, M.; Kristiansen, K.; Golan, Y.; Israelachvili, J. The role of interparticle and external forces in nanoparticle assembly. *Nature Materials* **2008**, *7*, 527–538.

(86) Mastai, Y.; Lidor-Shalev, O.; Aviv, H. Assembly of Ordered Polystyrene Nanoparticles on Self- Assembled Monolayers. *J. Res. Updates Polym. Sci.* **2016**, *4*, 202–209.

(87) Teh, L. K.; Tan, N. K.; Wong, C. C.; Li, S. Growth imperfections in three-dimensional colloidal self-assembly. *Appl. Phys. A* **2005**, *81*, 1399–1404.

(88) Bogue, R. Self-assembly: a review of recent developments. *Assembly Automation* **2008**, *28*, 211–215.

(89) Ahmed, A. M.; Shaban, M.; Aly, A. H. Electro-optical tenability properties of defective one-dimensional photonic crystal. *Optik - International Journal for Light and Electron Optics* **2017**, *145*, 121–129.

(90) Xavier, J.; Dasgupta, R.; Ahlawat, S.; Joseph, J.; Gupta, P. K. Controlled formation and manipulation of colloidal lattices by dynamically reconfigurable three dimensional interferometric optical traps. *Appl. Phys. Lett.* **2012**, *101*, 201101.

(91) Chhasatia, V. H.; Joshi, A. S.; Sun, Y. Effect of relative humidity on contact angle and particle deposition morphology of an evaporating colloidal drop. *Appl. Phys. Lett.* **2010**, *97*, 231909.

(92) Chung, Y.-W.; Leu, I.-C.; Lee, J.-H.; Hon, M.-H. Influence of humidity on the fabrication of high-quality colloidal crystals via a capillary-enhanced process. *Langmuir : the ACS journal of surfaces and colloids* **2006**, *22*, 6454–6460.

(93) García, P. D.; Sapienza, R.; López, C. Photonic glasses: a step beyond white paint. *Advanced materials (Deerfield Beach, Fla.)* **2010**, *22*, 12–19.

(94) Lee, H. S.; Kubrin, R.; Zierold, R.; Petrov, A. Y.; Nielsch, K.; Schneider, G. A.; Eich, M. Thermal radiation transmission and reflection properties of ceramic 3D photonic crystals. *J. Opt. Soc. Am. B* **2012**, *29*, 450.

(95) John, S.; Busch, K. Photonic bandgap formation and tunability in certain self-organizing

systems. *J. Lightwave Technol.* **1999**, *17*, 1931–1943.

(96) Zhang, X.; Blanchard, G. J. Polymer sol-gel composite inverse opal structures. *ACS applied materials & interfaces* **2015**, *7*, 6054–6061.

(97) Ridder, R. M. de; Hopman, W. C.L.; Ay, F. Focused-Ion-Beam Processing for Photonics. In *2007 9th International Conference on Transparent Optical Networks*; IEEE, 6/30/2007 - 2007; pp 212–215.

(98) Huyang, G.; Canning, J.; Gibson, B. C.; Khoury, T.; Sum, T. J.; Neto, C.; Crossley, M. J. Focused ion beam processing and engineering of devices in self-assembled supramolecular structures. *Nanotechnology* **2009**, *20*, 485301.

(99) Cryan, M. J.; Hill, M.; Sanz, D. C.; Ivanov, P. S.; Heard, P. J.; Tian, L.; Yu, S.; Rorison, J. M. Focused ion beam-based fabrication of nanostructured photonic devices. *IEEE J. Select. Topics Quantum Electron.* **2005**, *11*, 1266–1277.

(100) O. Olea-Mejía. FIB-SEM Combination Technique for Characterization of Polymer Composites. *Current Microscopy Contributions to Advances in Science and Technology* **2012**, 1060–1065.

(101) Yang, C.; Kneiß, M.; Schein, F.-L.; Lorenz, M.; Grundmann, M. Room-temperature Domain-epitaxy of Copper Iodide Thin Films for Transparent CuI/ZnO Heterojunctions with High Rectification Ratios Larger than 10(9). *Scientific reports* **2016**, *6*, 21937.

(102) Singh, V.; Agrawal, H. M. Qualitative soil mineral analysis by EDXRF, XRD and AAS probes. *Radiation Physics and Chemistry* **2012**, *81*, 1796–1803.

(103) Rossignol, S.; Kappenstein, C. Effect of doping elements on the thermal stability of transition alumina. *International Journal of Inorganic Materials* **2001**, *3*, 51–58.

(104) Boumaza, A.; Favaro, L.; Lédion, J.; Sattonnay, G.; Brubach, J. B.; Berthet, P.; Huntz, A. M.; Roy, P.; Tétot, R. Transition alumina phases induced by heat treatment of boehmite: An X-ray diffraction and infrared spectroscopy study. *Journal of Solid State Chemistry* **2009**, *182*, 1171–1176.

(105) KUMAGAI, M.; MESSING, G. L. Controlled Transformation and Sintering of a Boehmite Sol-Gel by alpha-Alumina Seeding. *J American Ceramic Society* **1985**, *68*, 500–505.

(106) Ye, Y.-H.; LeBlanc, F.; Haché, A.; Truong, V.-V. Self-assembling three-dimensional colloidal photonic crystal structure with high crystalline quality. *Appl. Phys. Lett.* **2001**, *78*, 52–54.

(107) Lin, H.-T.; Hemrick, J. *Advanced and Refractory Ceramics for Energy Conservation and Efficiency*; John Wiley & Sons, Inc: Hoboken, NJ, USA, 2016.

(108) Russell, H. W. PRINCIPLES OF HEAT FLOW IN POROUS INSULATORS. *J American Ceramic Society* **1935**, *18*, 1–5.

(109) Ling, F. F.; Kaviany, M. *Principles of Heat Transfer in Porous Media*; Springer US: New

York, NY, 1991.

(110) Clyne, T. W.; Golosnoy, I. O.; Tan, J. C.; Markaki, A. E. Porous materials for thermal management under extreme conditions. *Philosophical transactions. Series A, Mathematical, physical, and engineering sciences* **2006**, *364*, 125–146.

(111) Lamouri, S.; Hamidouche, M.; Bouaouadja, N.; Belhouchet, H.; Garnier, V.; Fantozzi, G.; Trelkat, J. F. Control of the γ-alumina to α-alumina phase transformation for an optimized alumina densification. *Boletín de la Sociedad Española de Cerámica y Vidrio* **2017**, *56*, 47–54.

(112) Mondini, S.; Ferretti, A. M.; Puglisi, A.; Ponti, A. Pebbles and PebbleJuggler: software for accurate, unbiased, and fast measurement and analysis of nanoparticle morphology from transmission electron microscopy (TEM) micrographs. *Nanoscale* **2012**, *4*, 5356–5372.

(113) Borchert, H.; Shevchenko, E. V.; Robert, A.; Mekis, I.; Kornowski, A.; Grübel, G.; Weller, H. Determination of nanocrystal sizes: a comparison of TEM, SAXS, and XRD studies of highly monodisperse CoPt3 particles. *Langmuir : the ACS journal of surfaces and colloids* **2005**, *21*, 1931–1936.

(114) Kril, C. E.; Birringer, R. Estimating grain-size distributions in nanocrystalline materials from X-ray diffraction profile analysis. *Philosophical Magazine A* **1998**, *77*, 621–640.

(115) Uvarov, V.; Popov, I. Metrological characterization of X-ray diffraction methods for determination of crystallite size in nano-scale materials. *Materials Characterization* **2007**, *58*, 883–891.

(116) Biju, V.; Sugathan, N.; Vrinda, V.; Salini, S. L. Estimation of lattice strain in nanocrystalline silver from X-ray diffraction line broadening. *J Mater Sci* **2008**, *43*, 1175–1179.

(117) Dinnebier; Etter; Müller; Hanfland. Possibilities and limitations of parametric Rietveld refinement on high pressure data: The case study of LaFeO3. *Zeitschrift für Kristallographie – Crystalline Materials* **2014**, *229*.

(118) Rogojan, R.; Andronescu, E.; Ghitulica, C.; Vasile, B. Synthesis and characterization of alumina nano-powder obtained by sol-gel method. *UPB Scientific Bulletin, Series B: Chemistry and Materials Science* **2011**, *73*.

(119) Aryasomayajula, A.; Canovic, S.; Bhat, D.; Gordon, M. H.; Halvarsson, M. Transmission electron microscopy and X-ray diffraction analysis of alumina coating by alternate-current inverted magnetron-sputtering technique. *Thin Solid Films* **2007**, *516*, 397–401.

(120) George, S. M. Atomic layer deposition: an overview. *Chemical reviews* **2010**, *110*, 111–131.

(121) Knez, M.; Nielsch, K.; Niinistö, L. Synthesis and Surface Engineering of Complex

Nanostructures by Atomic Layer Deposition. *Adv. Mater.* **2007**, *19*, 3425–3438.

(122) Palmstrom, A. F.; Santra, P. K.; Bent, S. F. Atomic layer deposition in nanostructured photovoltaics: tuning optical, electronic and surface properties. *Nanoscale* **2015**, *7*, 12266–12283.

(123) Mastai, Y., Ed. *Materials Science - Advanced Topics*; InTech, 2013.

(124) Moshe, H.; Mastai, Y. Atomic Layer Deposition on Self-Assembled-Monolayers. In *Materials Science - Advanced Topics*; Mastai, Y., Ed.; InTech, 2013.

(125) Quantum Optics with Semiconductor Nanostructures; Elsevier, 2012.

(126) Hendrickson, J.; Homyk, A.; Scherer, A.; Alasaarela, T.; Säynätjoki, A.; Honkanen, S.; Richards, B. C.; Kim, J.-Y.; Lee, Y.-H.; Gibson, R.*; et al.* One-dimensional photonic crystal nanobeam cavities. *Quantum Optics with Semiconductor Nanostructures*; Elsevier, 2012; pp 421–446.

(127) Johnson, R. W.; Hultqvist, A.; Bent, S. F. A brief review of atomic layer deposition: from fundamentals to applications. *Materials Today* **2014**, *17*, 236–246.

(128) Ponraj, J. S.; Attolini, G.; Bosi, M. Review on Atomic Layer Deposition and Applications of Oxide Thin Films. *Critical Reviews in Solid State and Materials Sciences* **2013**, *38*, 203–233.

(129) Sundberg, P.; Karppinen, M. Organic and inorganic-organic thin film structures by molecular layer deposition: A review. *Beilstein journal of nanotechnology* **2014**, *5*, 1104–1136.

(130) Tripathi, T. S.; Karppinen, M. Atomic Layer Deposition of p-Type Semiconducting Thin Films: a Review. *Adv. Mater. Interfaces* **2017**, *4*, 1700300.

(131) Berger, V. Nonlinear Photonic Crystals. *Phys. Rev. Lett.* **1998**, *81*, 4136–4139.

(132) Campbell; Sharp; Harrison; Denning; Turberfield. Fabrication of photonic crystals for the visible spectrum by holographic lithography. *Nature* **2000**, *404*, 53–56.

(133) Kitzerow, H. Tunable photonic crystals. *Liquid Crystals Today* **2002**, *11*, 3–7.

(134) Kondo, T.; Matsuo, S.; Juodkazis, S.; Misawa, H. Femtosecond laser interference technique with diffractive beam splitter for fabrication of three-dimensional photonic crystals. *Appl. Phys. Lett.* **2001**, *79*, 725–727.

(135) King, J. S.; Graugnard, E.; Summers, C. J. TiO2 Inverse Opals Fabricated Using Low-Temperature Atomic Layer Deposition. *Adv. Mater.* **2005**, *17*, 1010–1013.

(136) Povey, I. M.; Bardosova, M.; Chalvet, F.; Pemble, M. E.; Yates, H. M. Atomic layer deposition for the fabrication of 3D photonic crystals structures: Growth of Al2O3 and VO2 photonic crystal systems. *Surface and Coatings Technology* **2007**, *201*, 9345–9348.

(137) Gaillot, D. P.; Deparis, O.; Welch, V.; Wagner, B. K.; Vigneron, J. P.; Summers, C. J.

Composite organic-inorganic butterfly scales: production of photonic structures with atomic layer deposition. *Physical review. E, Statistical, nonlinear, and soft matter physics* **2008**, *78*, 31922.

(138) Im, H.; Lindquist, N. C.; Lesuffleur, A.; Oh, S.-H. Atomic layer deposition of dielectric overlayers for enhancing the optical properties and chemical stability of plasmonic nanoholes. *ACS nano* **2010**, *4*, 947–954.

(139) Saleem, M. R.; Honkanen, S.; Turunen, J. Thermal properties of TiO 2 films fabricated by atomic layer deposition. *IOP Conf. Ser.: Mater. Sci. Eng.* **2014**, *60*, 12008.

(140) Sechrist, Z. A.; Schwartz, B. T.; Lee, J. H.; McCormick, J. A.; Piestun, R.; Park, W.; George, S. M. Modification of Opal Photonic Crystals Using Al 2 O 3 Atomic Layer Deposition. *Chem. Mater.* **2006**, *18*, 3562–3570.

(141) Peng, Q.; Sun, X.-Y.; Spagnola, J. C.; Hyde, G. K.; Spontak, R. J.; Parsons, G. N. Atomic layer deposition on electrospun polymer fibers as a direct route to AL2O3 microtubes with precise wall thickness control. *Nano letters* **2007**, *7*, 719–722.

(142) Botzakaki, M. A.; Skoulatakis, G.; Xanthopoulos, N.; Gianneta, V.; Travlos, A.; Kennou, S.; Ladas, S.; Tsamis, C.; Makarona, E.; Georga, S. N.*; et al.* Influence of the atomic layer deposition temperature on the structural and electrical properties of Al/Al 2 O 3 /p-Ge MOS structures. *Journal of Vacuum Science & Technology A: Vacuum, Surfaces, and Films* **2018**, *36*, 01A120.

(143) Maindron, T.; Jullien, T.; André, A. Defect analysis in low temperature atomic layer deposited Al 2 O 3 and physical vapor deposited SiO barrier films and combination of both to achieve high quality moisture barriers. *Journal of Vacuum Science & Technology A: Vacuum, Surfaces, and Films* **2016**, *34*, 31513.

(144) Ge, J.; Yin, Y. Responsive photonic crystals. *Angewandte Chemie (International ed. in English)* **2011**, *50*, 1492–1522.

(145) Grüner, C.; Liedtke, S.; Bauer, J.; Mayr, S. G.; Rauschenbach, B. Morphology of Thin Films Formed by Oblique Physical Vapor Deposition. *ACS Appl. Nano Mater.* **2018**, *1*, 1370–1376.

(146) Wang, Z.; West, P. R.; Meng, X.; Kinsey, N.; Shalaev, V. M.; Boltasseva, A. Angled physical vapor deposition techniques for non-conformal thin films and three-dimensional structures. *MRC* **2016**, *6*, 17–22.

(147) Sechrist, Z. A.; Fabreguette, F. H.; Heintz, O.; Phung, T. M.; Johnson, D. C.; George, S. M. Optimization and Structural Characterization of W/Al 2 O 3 Nanolaminates Grown Using Atomic Layer Deposition Techniques. *Chem. Mater.* **2005**, *17*, 3475–3485.

(148) Ritala, M.; Leskelä, M.; Nykänen, E.; Soininen, P.; Niinistö, L. Growth of titanium dioxide thin films by atomic layer epitaxy. *Thin Solid Films* **1993**, *225*, 288–295.

(149) An, J.-K.; Chung, N.-K.; Kim, J.-T.; Hahm, S.-H.; Lee, G.; Lee, S. B.; Lee, T.; Park, I.-S.; Yun, J.-Y. Effect of Growth Temperature on the Structural and Electrical Properties of ZrO_2 Films Fabricated by Atomic Layer Deposition Using a $CpZrN(CH_3)_{23}/C_7H_8$ Cocktail Precursor. *Materials (Basel, Switzerland)* **2018**, *11*.

(150) Ali, K.; Choi, K.-H. Low-temperature roll-to-roll atmospheric atomic layer deposition of Al_2O_3 thin films. *Langmuir : the ACS journal of surfaces and colloids* **2014**, *30*, 14195–14203.

(151) Groner, M. D.; Fabreguette, F. H.; Elam, J. W.; George, S. M. Low-Temperature Al 2 O 3 Atomic Layer Deposition. *Chem. Mater.* **2004**, *16*, 639–645.

(152) Kowalik, I. A.; Guziewicz, E.; Kopalko, K.; Yatsunenko, S.; Godlewski, M.; Wójcik, A.; Osinniy, V.; Krajewski, T.; Story, T.; Łusakowska, E.*; et al.* Extra-Low Temperature Growth of ZnO by Atomic Layer Deposition with Diethylzinc Precursor. *Acta Phys. Pol. A* **2007**, *112*, 401–406.

(153) Gierałtowska, S.; Sztenkiel, D.; Guziewicz, E.; Godlewski, M.; Łuka, G.; Witkowski, B. S.; Wachnicki, Ł.; Łusakowska, E.; Dietl, T.; Sawicki, M. Properties and Characterization of ALD Grown Dielectric Oxides for MIS Structures. *Acta Phys. Pol. A* **2011**, *119*, 692–695.

(154) Barbos, C.; Blanc-Pelissier, D.; Fave, A.; Blanquet, E.; Crisci, A.; Fourmond, E.; Albertini, D.; Sabac, A.; Ayadi, K.; Girard, P.*; et al.* Characterization of Al2O3 Thin Films Prepared by Thermal ALD. *Energy Procedia* **2015**, *77*, 558–564.

(155) Saleem, M. R.; Ali, R.; Khan, M. B.; Honkanen, S.; Turunen, J. Impact of Atomic Layer Deposition to Nanophotonic Structures and Devices. *Front. Mater.* **2014**, *1*, 270.

(156) Photonic crystals: Principles and applications Editors: Qihuang Gong and Xiaoyong Hu. *MRS Bull.* **2014**, *39*, 824–825.

(157) Chen, H.; Lou, R.; Chen, Y.; Chen, L.; Lu, J.; Dong, Q. Photonic crystal materials and their application in biomedicine. *Drug delivery* **2017**, *24*, 775–780.

(158) Bhattacharya, P. K. Photonic Crystal Devices. *IOP Conf. Ser.: Mater. Sci. Eng.* **2007**, *40*.

(159) Collins, G.; Armstrong, E.; McNulty, D.; O'Hanlon, S.; Geaney, H.; O'Dwyer, C. 2D and 3D photonic crystal materials for photocatalysis and electrochemical energy storage and conversion. *Science and technology of advanced materials* **2016**, *17*, 563–582.

(160) Li, Y. Y.; Cunin, F.; Link, J. R.; Gao, T.; Betts, R. E.; Reiver, S. H.; Chin, V.; Bhatia, S. N.; Sailor, M. J. Polymer replicas of photonic porous silicon for sensing and drug delivery applications. *Science (New York, N.Y.)* **2003**, *299*, 2045–2047.

(161) Skoog, S. A.; Elam, J. W.; Narayan, R. J. Atomic layer deposition: medical and biological applications. *International Materials Reviews* **2013**, *58*, 113–129.

(162) Li, P.; Ohtsuki, C.; Kokubo, T.; Nakanishi, K.; Soga, N.; Groot, K. de. The role of hydrated silica, titania, and alumina in inducing apatite on implants. *Journal of biomedical materials research* **1994**, *28*, 7–15.

(163) Xiao, F.-X.; Miao, J.; Liu, B. Layer-by-layer self-assembly of CdS quantum dots/graphene nanosheets hybrid films for photoelectrochemical and photocatalytic applications. *Journal of the American Chemical Society.* **2014**, *136*, 1559–1569.

(164) Marqués-Hueso, J.; Schöpe, H. J. Regular Horizontal Patterning on Colloidal Crystals Produced by Vertical Deposition. In *Surface and Interfacial Forces – From Fundamentals to Applications*; Auernhammer, G. K., Butt, H.-J., Vollmer, D., Eds.; Springer Berlin Heidelberg: Berlin, Heidelberg, 2008; pp 48–56.

(165) Yoldi, M.; Arcos, C.; Paulke, B.-R.; Sirera, R.; González-Viñas, W.; Görnitz, E. On the parameters influencing the deposition of polystyrene colloidal crystals. *Materials Science and Engineering: C.* **2008**, *28*, 1038–1043.

(166) Xia, H.; Wu, S.; Su, X.; Zhang, S. Monodisperse TiO2 Spheres with High Charge Density and Their Self-Assembly. *Chemistry, an Asian Journal.* **2017**, *12*, 95–100.

(167) Wu, Y.; Chen, C.; Liu, Y.; Xu, X.; Yang, Z.; Zhang, H.; Liu, L.; Zhang, Y. Fast fabrication of a self-cleaning coating constructed with scallion-like ZnO using a perfect colloidal monolayer enabled by a predictive self-assembly method. *Journal of Materials Chemistry A.* **2017**, *5*, 5943–5951.

(168) Zhang, H.; Liu, X. Preparation and self-assembly of photonic crystals on polyester fabrics. *Iranian Polymer Journal.* **2017**, *26*, 107–114.

(169) Meijer, J.-M.; Hagemans, F.; Rossi, L.; Byelov, D. V.; Castillo, S. I. R.; Snigirev, A.; Snigireva, I.; Philipse, A. P.; Petukhov, A. V. Self-assembly of colloidal cubes via vertical deposition. *Langmuir : The ACS Journal of Surfaces and Colloids.* **2012**, *28*, 7631–7638.

(170) Guo, P.; Fan, J.; Cheng, Y.; Wang, J.; Wang, C. Characterization of the Self-Assembly of Glutathione Stabilized Cadmium Selenide–Zinc Sulfide Quantum Dots with a Cyanine5-Labeled Peptide by Capillary Electrophoresis and Fluorescence. *Analytical Letters.* **2017**, *50*, 197–206.

(171) Barros Filho, D. A.; Hisano, C.; Bertholdo, R.; Schiavetto, M. G.; Santilli, C.; Ribeiro, S. J. L.; Messaddeq, Y. Effects of self-assembly process of latex spheres on the final topology of macroporous silica. *Journal of Colloids and Interface Science.* **2005**, *291*, 448–464.

(172) Liang, X.; Zhao, Z.; Zhu, M.; Liu, F.; Wang, L.; Yin, H.; Qiu, G.; Cao, F.; Liu, X.; Feng, X. Self-assembly of birnessite nanoflowers by staged three-dimensional oriented attachment. *Environmental Science: Nano.* **2017**, *4*, 1656–1669.

(173) Hanafusa, T.; Mino, Y.; Watanabe, S.; Miyahara, M. T. Controlling self-assembled structure of Au nanoparticles by convective self-assembly with liquid-level manipulation. *Advanced Powder Technology.* **2014**, *25*, 811–815.

(174) Bormashenko, E.; Whyman, G.; Pogreb, R.; Stanevsky, O.; Hakham-Itzhaq, M.; Gendelman, O. Self-Assembly in Evaporated Polymer Solutions: Patterning on Two Scales. *Israel Journal of Chemistry.* **2007**, *47*, 319–328.

(175) Zhang, J.; Sun, Z.; Yang, B. Self-assembly of photonic crystals from polymer colloids. *Current Opinion in Colloid & Interface Science.* **2009**, *14*, 103–114.

(176) Kuai, S.-L.; Hu, X.-F.; Haché, A.; Truong, V.-V. High-quality colloidal photonic crystals obtained by optimizing growth parameters in a vertical deposition technique. *Journal of Crystal Growth* **2004**, *267*, 317–324.

(177) Weiss, D.; Kreger, K.; Schmidt, H.-W. Self-Assembly of Alkoxy-Substituted 1,3,5-Benzenetrisamides Under Controlled Conditions. *Macromolecular Materials and Engineering.* **2017**, *302*, 1600390.

(178) Voïtchovsky, K.; Giofrè, D.; José Segura, J.; Stellacci, F.; Ceriotti, M. Thermally-nucleated self-assembly of water and alcohol into stable structures at hydrophobic interfaces. *Nature Communications.* **2016**, *7*, 13064.

(179) Kuai, S.-L.; Hu, X.-F.; Haché, A.; Truong, V.-V. High-quality colloidal photonic crystals obtained by optimizing growth parameters in a vertical deposition technique. *Journal of Crystal Growth* **2004**, *267*, 317–324.

(180) Furlan, K. P.; Pasquarelli, R. M.; Krekeler, T.; Ritter, M.; Zierold, R.; Nielsch, K.; Schneider, G. A.; Janssen, R. Highly porous α-Al 2 O 3 ceramics obtained by sintering atomic layer deposited inverse opals. *Ceramics International* **2017**, *43*, 11260–11264.

(181) Nandiyanto, A. B. D.; Suhendi, A.; Arutanti, O.; Ogi, T.; Okuyama, K. Influences of Surface Charge, Size, and Concentration of Colloidal Nanoparticles on Fabrication of Self-Organized Porous Silica in Film and Particle Forms. *Langmuir : the ACS journal of surfaces and colloids* **2013**, *29*, 6262–6270.

(182) Hilhorst, J.; van Schooneveld, M. M.; Wang, J.; Smit, E. de; Tyliszczak, T.; Raabe, J.; Hitchcock, A. P.; Obst, M.; Groot, F. M. F. de; Petukhov, A. V. Three-dimensional structure and defects in colloidal photonic crystals revealed by tomographic scanning transmission X-ray microscopy. *Langmuir : the ACS journal of surfaces and colloids* **2012**, *28*, 3614–3620.

(183) Wang, J.; Yang, L.; Lin, D.; Luo, Y.; Li, D.; Meng, Q. Optical studies of random disorder of colloidal photonic crystals and its evolution in evaporation induced self-assembly. *The Journal of Chemical Physics.* **2012**, *137*, 234111.

(184) Furlan, K. P.; Pasquarelli, R. M.; Krekeler, T.; Ritter, M.; Zierold, R.; Nielsch, K.; Schneider, G. A.; Janssen, R. Highly porous α-Al 2 O 3 ceramics obtained by sintering atomic layer deposited inverse opals. *Ceramics International.* **2017**, *43*, 11260–11264.

(185) Zhang, X.; Blanchard, G. J. Polymer sol-gel composite inverse opal structures. *ACS Applied Materials & Interfaces.* **2015**, *7*, 6054–6061.